ABSOLUTE YIELDS OF DELAYED NEUTRONS IN THE FAST FISSION OF U-235 AND U-238

A Thesis submitted for the award of
the degree of Doctor of Philosophy of
the University of London

by

D.A. CLIFFORD, B.Sc.

Nuclear Power Section
Department of Mechanical Engineering
Imperial College of Science and Technology

February, 1972

ABSTRACT

Absolute yields of delayed neutrons in the fast fission of U-235 and U-238, and the time dependence of the delayed neutron decay, have been measured at A.W.R.E., using the fast pulsed reactor VIPER. A sample of fissile material was irradiated in the reactor and transferred to a neutron detector, by means of a rabbit tube, in about 50 msec. Fission measurements were made by gamma-counting foils of the sample material irradiated in the rabbit.

The delayed neutron yields were found to be:

U-235 0.0174 ± 0.0008 d.n. per fission

U-238 0.0492 ± 0.0025 d.n. per fission

the value obtained for U-238 being significantly higher than the commonly accepted value.

ACKNOWLEDGEMENTS

I should like to express my gratitude to Dr. C.B. Besant for his supervision and advice throughout the period of this work, and also the other members of the Nuclear Power Section at Imperial College, especially Professor P.J. Grant.

I am also indebted to Mr. M.H. McTaggart, and all the VIPER reactor staff at A.W.R.E., Aldermaston for their help and practical advice, and to the U.K.A.E.A. for financial support.

CONTENTS

LIST OF FIGURES

Page

LIST OF TABLES

1. INTRODUCTION

1.1. General

Of the neutrons emitted during the fission process, a small fraction (about 1%) are not emitted directly during fission, but are emitted after the radioactive decay of some of the fission products. These neutrons (delayed neutrons) are emitted at times very long (on a nuclear time-scale) after fission, being emitted when the product nuclide from a previous β - transition is left in a state of sufficiently high excitation (Section 7). The half-lives associated with these beta transitions lie, in general, in the region of 0.2 to 55 secs., and thus, although they only represent about 1% of the total number of neutrons emitted in fission delayed neutrons have a very great effect on the mean neutron lifetime in a reactor. If it were not for the existence of these delayed neutrons, reactors could not safely be operated in other than subcritical conditions, as mechanical forms of control could not operate at speeds comparable to the prompt neutron lifetime in a reactor.

1.2. The Importance of Delayed Neutron Yield Data for Reactor Kinetics Calculations

The dynamic behaviour of a reactor during normal operation is determined largely by the delayed neutrons, and knowledge of the delayed neutron yields of the reactor constituents and their energies is thus very important in determining the "margin of safety" associated with a particular reactor. Uncertainties in these quantities involving the safety of a reactor necessitate the design of reactors with a high safety margin, with consequent increase in cost.

Although from the point of view of thermal reactor design, these quantities are well understood, through direct measurement and operating experience, the advent of fast reactors and breeder reactors, where little operating experience has been gained, has made the re-evaluation of delayed neutron parameters an important task.

The delayed neutron yield data in current use is that of Keepin et al [Keepin 1965], which is summarised in Tables 1.1. These measurements were

made at Los Alamos using the fast pulsed reactor GODIVA, and until recently had not been questioned. However, the use of plutonium-uranium cores, where the delayed neutron contribution of U-238 can be very important, has suggested that the Los Alamos results for U-238 might be in error. Reactivity worth measurements performed on ZEBRA at A.E.E. Winfrith also suggest that the delayed neutron yields in current use may be incorrect. Codd [Codd] has suggested that an increase of up to 30% in the delayed neutron yield of U-238 may be necessary to account for the discrepancies between calculated and experimental results for some core types.

In view of the unsatisfactory information available on delayed neutron yields, a programme was initiated at A.W.R.E. Aldermaston for the measurement of gross decay parameters and yields in fast fission of the isotopes of principal interest in fast reactors.

Group	Decay Constant Sec^{-1}	Relative Abundance	Group Yield D.N. Per Fission
1	$0.0127 \pm .0002$	0.038 ± 0.003	$6.3 \pm 0.5 \times 10^{-4}$
2	$0.0317 \pm .0008$	0.213 ± 0.005	$3.51 \pm 0.11 \times 10^{-3}$
3	$0.115 \pm .003$	0.188 ± 0.016	$3.10 \pm 0.28 \times 10^{-3}$
4	$0.311 \pm .008$	0.407 ± 0.007	$6.72 \pm 0.23 \times 10^{-3}$
5	$1.40 \pm .081$	0.128 ± 0.008	$2.11 \pm 0.15 \times 10^{-3}$
6	$3.87 \pm .369$	0.026 ± 0.003	$4.30 \pm 0.5 \times 10^{-4}$
TOTAL YIELD (Delayed Neutrons per Fission)			$1.65 \pm 0.05 \times 10^{-2}$

Table 1.1(a)

Delayed Neutron Absolute Yields and Decay Constants in the Fast Fission of U-235 [Keepin 1965]

Group	Decay Constant Sec^{-1}	Relative Abundance	Group Yield D.N. Per Fission
1	0.0132 ± 0.0003	0.013 ± 0.001	$5.4 \pm 0.5 \times 10^{-4}$
2	0.0321 ± 0.0006	0.137 ± 0.002	$5.64 \pm 0.25 \times 10^{-3}$
3	0.139 ± 0.005	0.162 ± 0.020	$6.67 \pm 0.87 \times 10^{-3}$
4	0.358 ± 0.014	0.388 ± 0.012	$1.599 \pm 0.08 \times 10^{-2}$
5	1.41 ± 0.067	0.225 ± 0.013	$9.27 \pm 0.60 \times 10^{-3}$
6	4.02 ± 0.214	0.075 ± 0.005	$3.09 \pm 0.24 \times 10^{-3}$
TOTAL YIELD (Delayed Neutrons Per Fission)			$4.12 \pm 0.17 \times 10^{-2}$

Table 1.1(b)

Delayed Neutron Absolute Yields and Decay Constants in the Fast Fission of U-238 [Keepin 1965]

1.3. Previous Delayed Neutron Yield Measurements

The existence of delayed neutrons in fission was first demonstrated by Roberts, Meyer and Wang in 1939 [Roberts 1939], who reported an activity of period 12.5 ± 3 sec. The first detailed measurements of delayed neutron periods were made by Snell [Snell 1942], using a BF_3 counter surrounded by paraffin to monitor the decay of delayed neutrons from a large block of U-235 after its bombardment with neutrons from an accelerator. Five delayed neutron groups were found, with half-lives in the range 0.4 to 56 sec.

Hughes, Dabbs, Cahn and Hall [Hughes 1948] made measurements of the delayed neutron yields and decay constants in the thermal fission of U-235 using the Argonne heavy water reactor, and a sample shuttle system. Yields were measured relative to the total fission neutron emission, and six groups of delayed neutrons were found. The results of Hughes et al. are shown in Table 1.2.

Smith, Rose, McVicar and Thorne [Smith 1957] measured delayed neutron yields using the fast reactor ZEPHYR at Harwell. The statistics obtained from the delayed neutron counting were not good enough to allow the determination of the delayed neutron periods, the results being analysed in terms of the group periods reported by Hughes et al. The Harwell measurements are summarised in Table 1.3.

The measurements made at Los Alamos by Keepin, Wimett and Zeigler [Keepin 1957] were the most detailed measurements of this period. Delayed neutrons were counted using a modified "long counter" from samples irradiated in the fast pulsed reactor GODIVA. Because of the low efficiency of the "long counter", a large number of irradiations was used to accumulate counts. Fission measurements were made by radiochemical separation and subsequent ^{99}Mo beta counting. The delayed neutron yields and periods measured by Keepin et al. are given in Table 1.1. These results were found to predict

Half Life (sec)	Energy (KeV)	Yield* (%)
55.6	250	0.025
22.0	560	0.166
4.51	430	0.213
1.52	620	0.241
0.43	420	0.085
0.05		0.025
TOTAL YIELD		0.755

Table 1.2

U-235 Delayed Neutron Yields and Average Energies [Hughes 1948] (Thermal Fission)

* Relative to total neutron emission

Half Life (sec)	U-235 Relative Abundance	U-238 Relative Abundance
55.6	0.035 ± 0.001	0.012 ± 0.001
22.0	0.224 ± 0.007	0.154 ± 0.005
4.51	0.340 ± 0.017	0.266 ± 0.017
1.52	0.320 ± 0.021	0.401 ± 0.032
0.43	0.081 ± 0.027	0.167 ± 0.033
Absolute Yield	1.74 ± 0.14	3.7 ± 0.4

Table 1.3

Delayed Neutron Relative Abundances and Absolute Yields (delayed neutrons per fission) in Fast Fission [Smith 1957]

the kinetic behaviour of simple systems, such as GODIVA, very well, and have been in general use for a number of years.

Since the 1950's, most of the effort devoted to delayed neutron studies has been towards the determination of the variation in delayed neutron yields, with increasing energy of the neutrons causing fission. Early work in this field suggested that the delayed neutron yield of a fissile material nearly doubled when the energy of the neutrons inducing fission was changed from thermal to 14 MeV [Maksiutenko 1963] [Shpakov 1962]. This is contrary to the theoretical predictions, based on the known precursors and the mass distributions in fission at various energies, which indicated that the delayed neutron yield should be lower at high energies than at thermal energies. More recently Masters, Thorpe and Smith [Masters 1968] have made measurements which indicate that the yields do in fact decrease with increasing fission energy.

1.4. The Energies of Delayed Neutrons

The parameters of principal interest to the reactor designer are not the absolute delayed neutron yields of a particular fissile material, but the effective delayed neutron fraction, i.e. the likelihood of a fission being caused by a delayed neutron relative to that of a fission being caused by a prompt neutron. A knowledge of delayed neutron energies is therefore necessary, and information on these is scarce.

One of the earliest detailed measurements of delayed neutron energies was made by Hughes et al. [Hughes 1948]. The average group energies were measured by comparing the slowing down curves of the neutrons of the various groups with similar curves for monoenergetic neutron sources. These average energies are shown in Table 1.2.

Measurements of delayed neutron energies by observation of proton recoils in a hydrogen-filled cloud-chamber were made by Burgy et al. [Burgy 1946] and Bonner et al. [Bonner 1956].

The most detailed measurements of delayed neutron energies to date were made by Batchelor and Hyder [Batchelor 1956], using a He^3 neutron spectrometer. A sample of natural uranium was irradiated in the BEPO reactor, and transferred to the spectrometer by a sample shuttle. Various combinations of irradiation times and delay times were used before counting, in order to emphasise the different groups. Spectra were obtained for the four longest-lived groups with an estimated accuracy of about $\pm$ 10%. These spectra are shown in Figure 1.1.

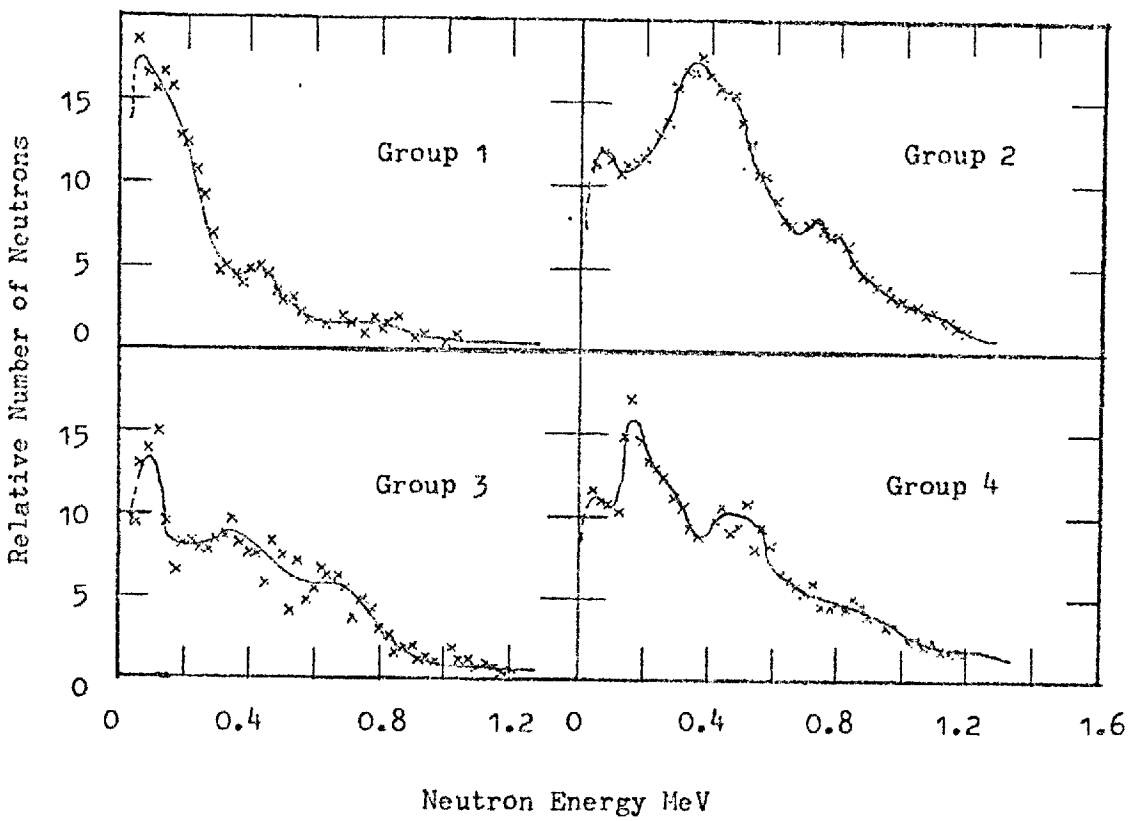

Figure 1.1

Delayed Neutron Group Spectra [Batchelor 1956b]

1.5. References

Batchelor 1956 - Batchelor, R.; Hyder, H.R.McK.
J. Nuclear Energy 3 7 (1956).

Bonner 1956 - Bonner, T.W.; Bame, S.J.; Evans, J.E.
Phys. Rev. 101 1514 (1956).

Burgy 1946 - Burgy, Purdue, Willard and Wollam.
Phys. Rev. 70, 104 (1946).

Codd - Codd, J.
Unpublished.

Hughes 1948 - Hughes, D.J.; Dabbs, J.; Cahn, A. and Hall, D.
Phys. Rev. 73, 111 (1948).

Keepin 1965 - Keepin, G.R.
Physics of Nuclear Kinetics.
Addison Wesley 1965.

Keepin 1957 - Keepin, G.R.; Wimett, T.F.; Zeigler, R.K.
J. Nuclear Energy 6, 1 (1957).

Maksiutenko 1963 - Maksiutenko, B.P.
Atomnaya Energiya 15, 321 (1963).

Masters 1968 - Masters, C.F.; Thorpe, M.M.; Smith, D.B.
Am. Nucl. Soc. Trans. 11, 1 (1968).

Roberts 1939 - Roberts, R.; Meyer, R.; Wang, P.
Phys. Rev. 55, 510 (1939a).

Shpakov 1962 - Shpakov, Petrzhak, Bak, Kavalenko and Kostochkin.
Soviet J. Atomic Energy 11 1190 (1962).

Smith 1957 - Smith, Rose, McVicar and Thorne.
J. Nuclear Energy 4, 133 (1957).

Snell 1942 - Snell, A.H.; Netzel, V.A.; Ibsen, H.W.;
Heringer, J.S.; Wilkinson, R.G.; Sampson, M.B.
Phys. Rev. 72, 541 (1947b).

2. GENERAL REQUIREMENTS FOR THE MEASUREMENT OF DELAYED NEUTRON YIELDS

2.1. General

One of the most straightforward methods for the measurement of absolute delayed neutron yields is the irradiation and subsequent neutron counting of a small sample of the material in question. Such experiments usually make use of a reactor for the irradiation, since it is desirable to produce a large number of fissions in the sample, and a sample shuttle tube (rabbit tube) for the transfer of the sample to a shielded counting position. Although other methods have been used for the measurement of delayed neutron yields (see Section 1), the procedure to be described is well suited to the examination of the time-dependence of the delayed-neutron decay after irradiation, because of the relatively high delayed neutron counting rates involved.

2.2. Experimental Requirements

The principal requirements for a delayed neutron yield measurement of the type outlined above are:

1. A means of producing an intense irradiation.
2. A fast sample-transfer system.
3. A neutron detector.
4. A means of measuring the number of fissions which occur in the sample.

2.2(1) Irradiation

In order to minimise the self-multiplication of fissions in the sample, and to keep the sample to a reasonable size for a rabbit tube system, it is desirable that the sample mass be restricted to about 10 gm. In order to obtain sufficient statistical accuracy on the delayed neutron count, the number of fissions produced in the sample must be large, and it is desirable that the irradiation be performed in a time short compared with the shortest delayed-neutron group period. Such considerations favour the use of a pulsed reactor for the irradiation.

The fast pulsed reactor VIPER [Weale 1968] at A.W.R.E. Aldermaston produces an extremely intense neutron burst with a typical pulse width of 400 μ sec (F.W.H.M.). In the large irradiation cavity up to about 10^{12} fissions per gramme of U-235 may be produced in a pulse. It is therefore an ideal irradiation facility for the type of experiment proposed.

The VIPER reactor (Figure 2.1) comprises a copper-reflected core of uranium rods enriched to 37.5% U-235. The core contains epoxy resin which provides a degree of neutron moderation, and the spectrum of VIPER (Figure 2.2) is thus much more similar to that of a steady-state fast reactor than such reactors as GODIVA [Peterson 1956] which have been used in the past for delayed neutron yield measurements in fast fission.

2.2(2) Sample Transfer System

The sample shuttle should be capable of transferring the irradiated sample to the neutron detector in a time short compared with the shortest-lived delayed neutron group period. The value obtained by Keepin et al [Keepin 1956] for the shortest delayed neutron group period from U-235 was 179 ± 17 msec. A search for short-lived groups was made by Gibbs and Thomson [Gibbs 1939], who found no activities with periods in the range 10^{-3} to 10^{-1} sec. No delayed neutron precursors have been identified with periods of less than 0.2 sec [I.A.E.A. Panel, 1967].

It is therefore reasonable to assume that a shuttle with a transit time of about 100 msec is satisfactory for such an experiment. It is desirable, however, that the neutron detector be well separated from the reactor, in order to overcome problems from reactor background. This was achieved in the present experiment by housing the neutron detector outside the reactor cell, and using the rabbit tube to transfer the sample through the 6-foot thick biological shield.

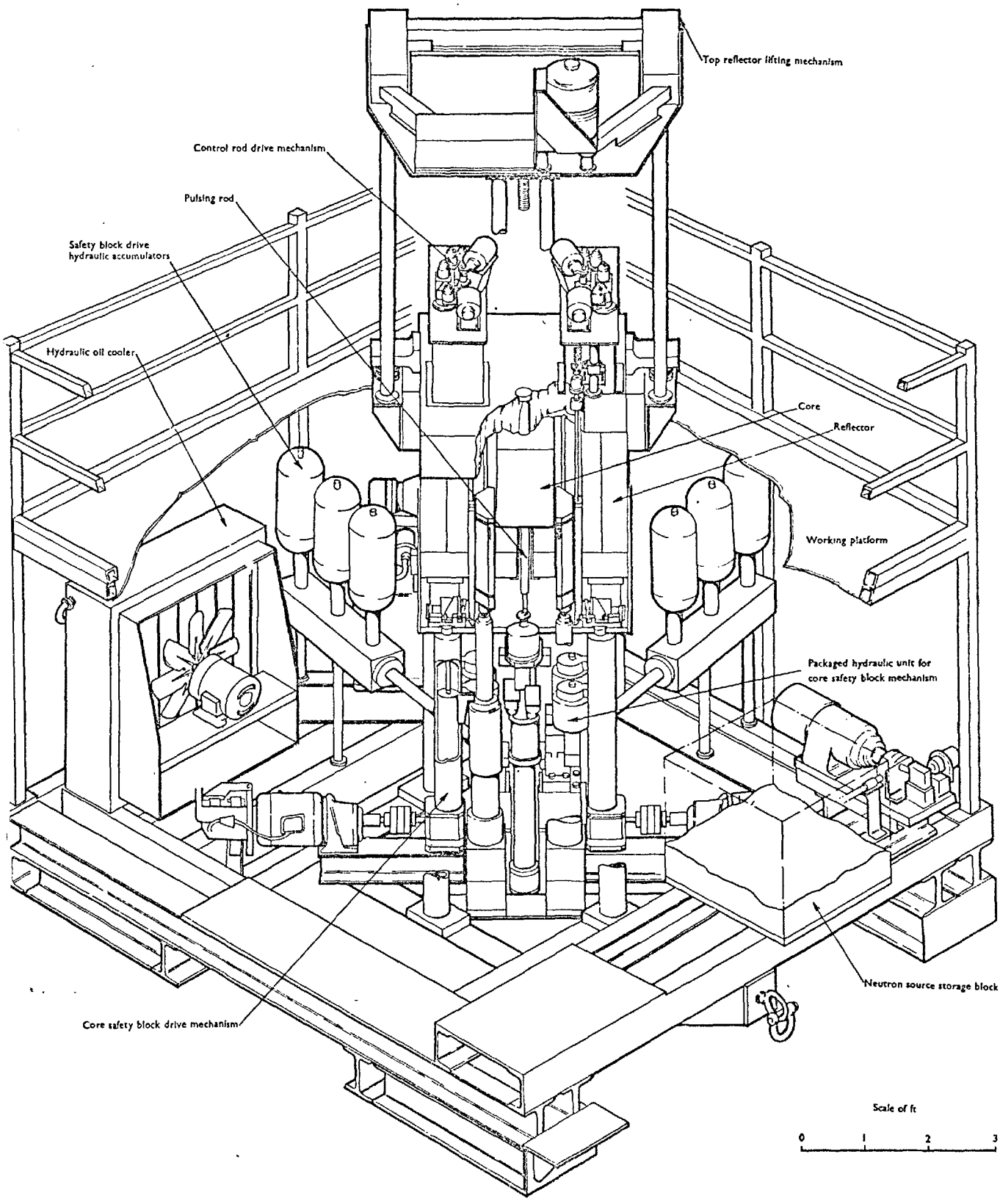

Figure 2.1

General View of VIPER

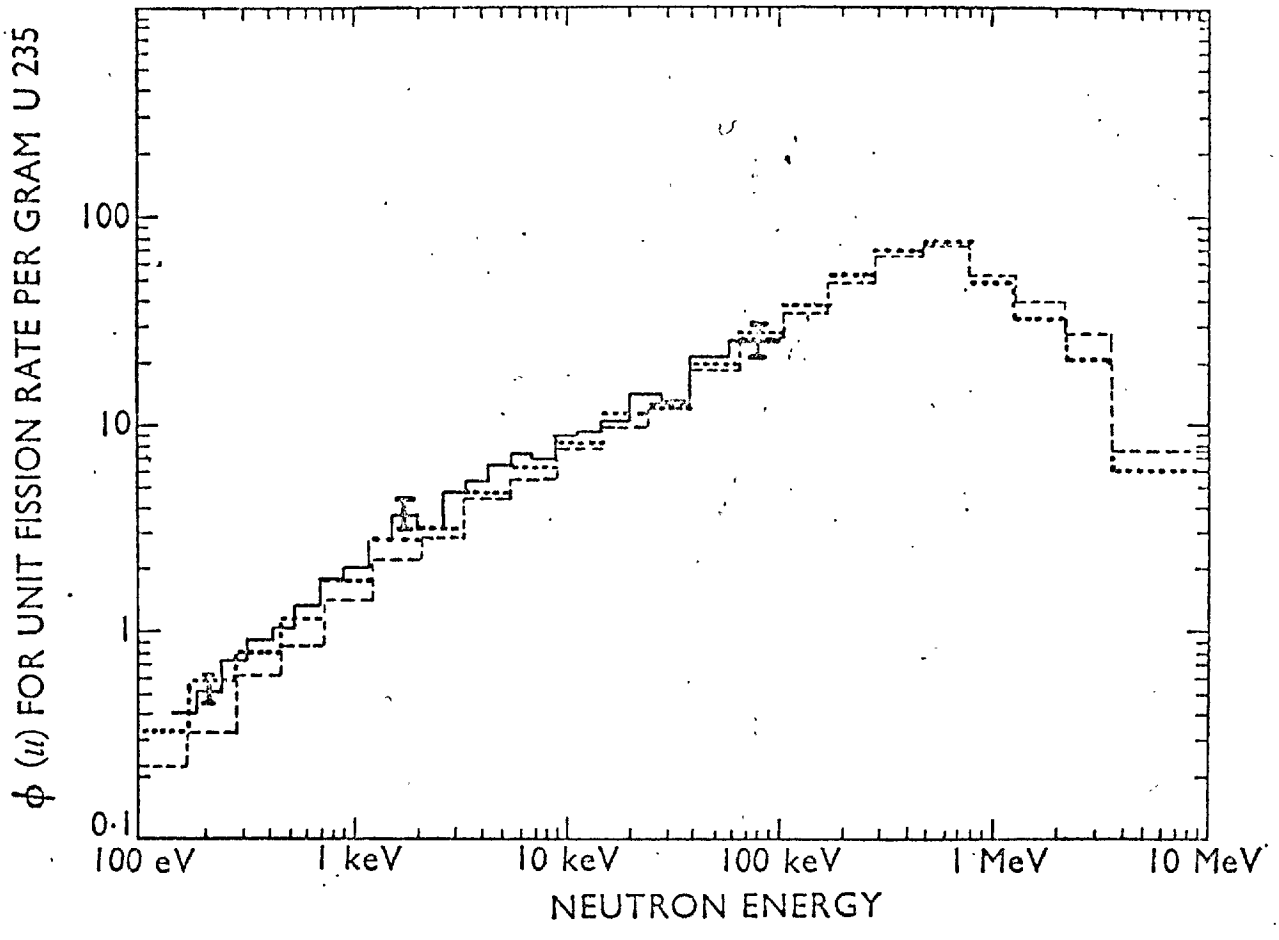

—— Time of flight results normalized at 337 eV using Mn foils, calibrated in VERA 5A, showing 1 standard deviation errors
- - - Two dimensional S_4 TURTLE calculation using FD2 data (critical)
. . . . SWAN calculation using effective group cross sections from heterogeneous GENEX/SDR Doppler calculation

Figure 2.2

VIPER Neutron Spectrum

Figure 2.3
View of Demounted Rabbit

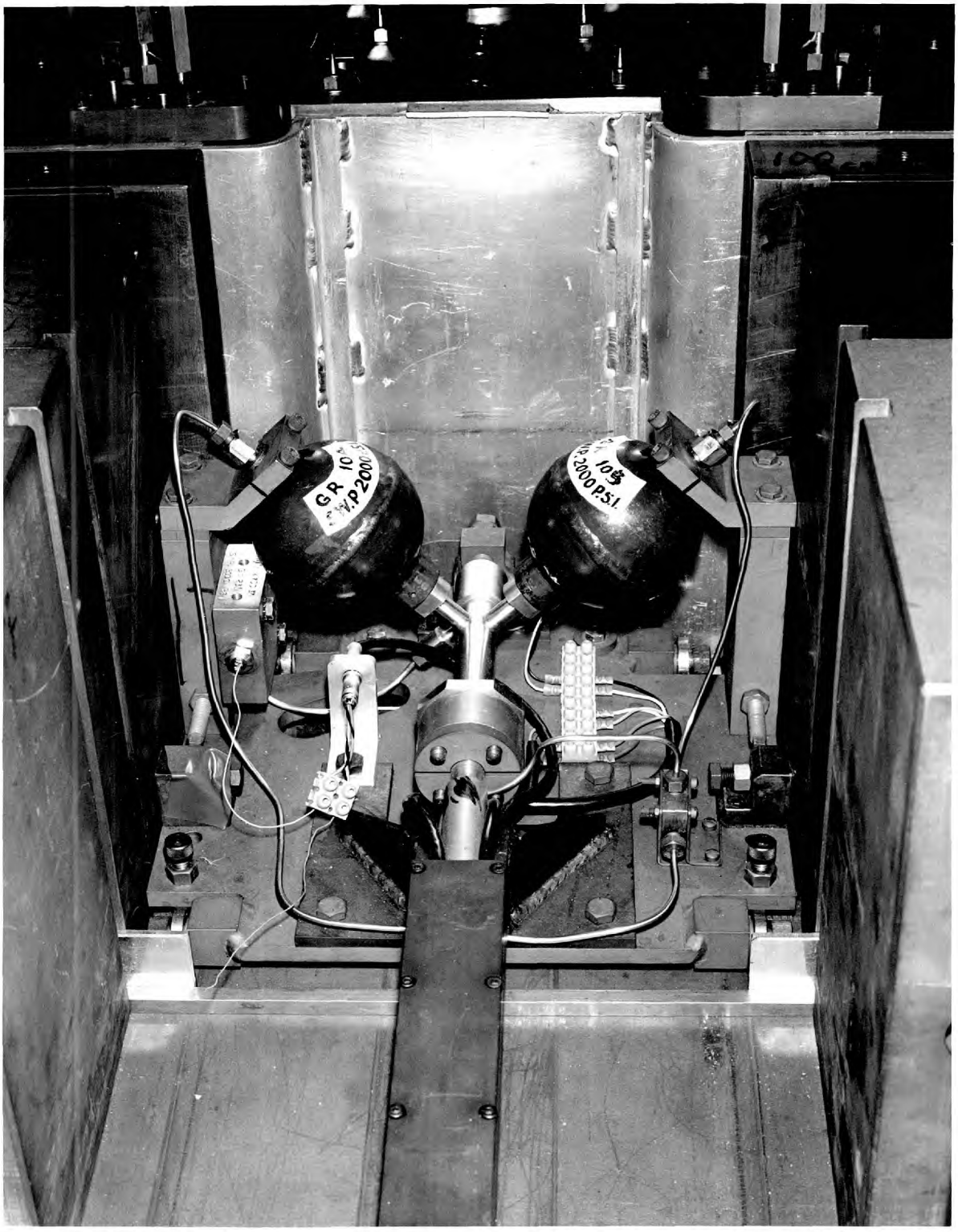

Figure 2.4

Rabbit Tube Breech Assembly

A pneumatic sample transfer system was designed by WD/4 at A.W.R.E. [Broome 1968]. It is capable of transferring samples of up to 20 gm wt. from the large irradiation cavity in the reactor to the neutron detector in about 35 msec. As the rabbit tube design has affected the design of the neutron detector, it will be described briefly.

Figures 2.3 and 2.4 show the rabbit and the reactor end of the shuttle system respectively. The rear of the rabbit is provided with two 'O'-ring seals which mate with part of the breech assembly. Argon gas may be admitted to the breech assembly at a point between these two seals at pressures up to 2000 p.s.i.g., the rabbit thus experiencing no net force. On pulsing the reactor a squib, situated behind the rabbit, is fired, disturbing the equilibrium, and causing the rabbit to be shot down the tube by the force associated with the gas pressure (Figure 2.5).

The rabbit is arrested at the detector end of the tube in a cylinder of polyurethane foam, its rest position for a given rabbit mass and firing position being uncertain by about $\pm$ 2 cm.

2.2(3) Neutron Detector

The decay of delayed neutrons from an irradiated sample is very rapid, the count rate decreasing by three orders of magnitude in about 100 sec [Keepin 1956]. Thus, in order to make the greatest use of an irradiation, the neutron detector must be capable of accepting a wide range of count rates, i.e. it should have a low dead time and high efficiency.

Since the irradiated sample will be highly γ-active, the neutron detector must be insensitive to γ rays. The neutron - and gamma - emission rates from an irradiated U-235 sample are compared at various times after irradiation in Table 2.1 [LAMS - 2642]. In order to keep the correction for gamma count below 1% at all times, the detector must have a ratio of neutron efficiency to gamma efficiency in excess of 10^5.

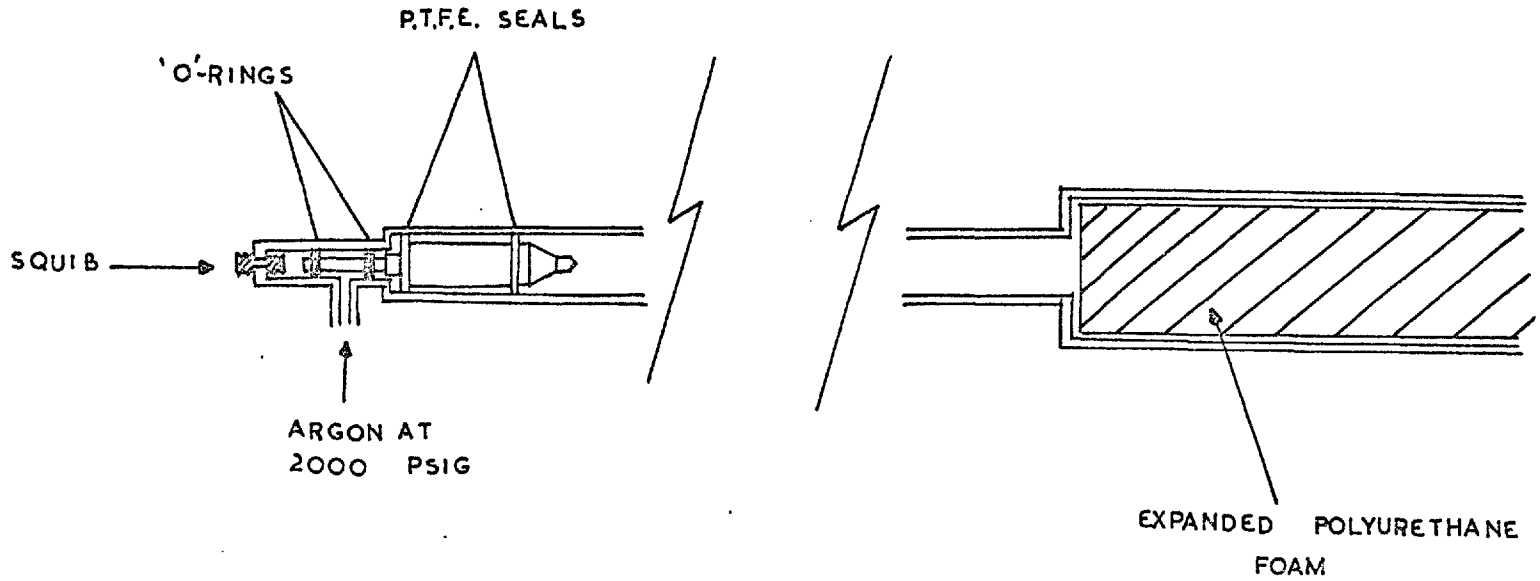

FIGURE 2.5

RABBIT TUBE OPERATION

Time Interval (sec)	Gamma emission (γ sec^{-1})	Neutron emission (n sec^{-1})	$\frac{N(n)}{N(\gamma)}$
0.2 - 0.5	3.0×10^{11}	1.0×10^{10}	0.03
1.0 - 2.0	1.6×10^{11}	4.0×10^{9}	0.02
4.0 - 5.5	8.0×10^{10}	1.0×10^{9}	0.01
10.0 - 13.0	4.0×10^{10}	4.5×10^{8}	0.01
35.0 - 45.0	1.2×10^{10}	8.0×10^{7}	0.007
500			0.001*

Table 2.1

Neutron - and Gamma - emission rates from a one-gramme metallic sample of U-235 irradiated in a full-size VIPER pulse.

* Gamma emission fitted to $t^{-1.2}$ at 40 sec.

The energies of delayed neutrons are not well known. Only one detailed measurement has been made of the spectra of the four longest lived groups in the thermal fission of U-235 [Batchelor 1956]. These spectra are accurate to about ± 10%, and thus it is desirable to minimise the correction required for the variation in detector response with neutron energy.

Owing to the uncertainty in sample rest position, the detector efficiency must not vary greatly with small displacements in source position.

The development of the neutron detector is discussed in detail in Section 3.

2.2(4) Fission Measurements

Very few of the measurements reviewed in Section 1 were absolute measurements. The majority of workers measured delayed neutron yields relative to the delayed neutron yield of U-235 in thermal fission. Keepin et al [Keepin 1956] used radio chemical separation and subsequent Mo^{99} beta counting for the measurement of fission rates using the known cumulative yield of Mo^{99} in fast fission. Such a method could not accurately be applied to the present work, since the yield of Mo^{99} in a "fast reactor" type spectrum is not well known. The method used by the Harwell workers [Smith 1957], that of using a calibrated fission chamber in the pile could not be applied to a pulsed reactor.

It was therefore decided to measure the fissions produced in the sample by gamma-counting foils of the sample material which are housed in the rabbit during irradiation. These measurements were made relative to a calibration against a fission chamber in a steady-state VIPER irradiation, in which foils similar to those used in the rabbit irradiations were irradiated in a calibrated fission chamber, and subsequently counted for gamma activity, thus eliminating the need for accurate radio-chemical yield values.

The fission measurements are discussed in detail in Section 4.

2.3. Experimental Procedure

For an experiment of the type proposed two types of irradiation are applicable, namely burst irradiations in which the time of irradiation is short compared with the shortest-lived delayed neutron group period, and saturation irradiations in which the irradiation is long compared with the longest-lived delayed neutron group period.

If there are no appreciable growth - and decay effects the delayed neutron emission from a sample which has received a burst irradiation is given by:

$$N(t) = F.Y. \sum_i a_i \lambda_i \exp(-\lambda_i t) \qquad (2.1)$$

and that following a saturation irradiation by:

$$N(t) = F.Y. \sum_i a_i \exp(-\lambda_i t) \qquad (2.2)$$

The number of delayed neutron groups to be used in such an expression as (2.1) or (2.2) is open to question. Keepin et al [Keepin 1956] showed that the statistically best fit to the Los Alamos data used six groups, but that a fit using the periods of the nine, then identified, delayed neutron precursors was no worse. Over twenty precursors have now been identified [I.A.E.A. 1967] and these are shown in Table 2.2, with their associated half-lives. Considering the large uncertainties in these half-lives, and the large number of precursors with periods in the range 0.5 to 2.0 sec., it could not be expected that a gross decay measurement be amenable to analysis into a unique scheme containing groups identifiable with all these precursors. For reactor kinetics measurements, however, such a detailed scheme would not be warranted in terms of the accuracy of predictions obtainable.

Precursor	Half-Life (sec)
As - 85	2.10 ± 0.12
Br - 87	55.67 ± 0.20
Br - 88	15.85 ± 0.10
Br - 89	4.46 ± 0.31
Br - 90	1.6 ± 0.6
Kr - 91	8.36 ± 0.15
Kr - 92	1.92 ± 0.07
Kr - 93	1.18 ± 0.04
Rb - 93	5.89 ± 0.04
Rb - 94	2.67 ± 0.04
Rb - 95	0.36 ± 0.02
Rb - 96	0.23 ± 0.02
Sb - 134	10
Sb - 135	1.9 ± 0.9
I - 137	24.4 ± 0.4
I - 138	6.3 ± 0.7
I - 139	2.0 ± 0.5
I - 140	0.8
Xe - 141	1.70 ± 0.05
Cs - 142	2.3 ± 0.2
Cs - 143	1.60 ± 0.14

Table 2.2

Experimentally Identified Delayed Neutron Precursors and their Half-Lives

2.3(1) Absolute Yield Measurements

Two methods for the determination of absolute delayed neutron yield are applicable to the proposed experiment, namely extrapolation to zero time following a saturation irradiation, and the measurement of the integral count following either a burst or a saturation irradiation.

The delayed neutron activity following a saturation irradiation is given by equation 2.2. and the initial emission rate is therefore:

$$N\ (t = 0) = F \cdot Y \cdot \sum_i a_i \qquad (2.3)$$

and therefore:

$$Y = \frac{N\ (t = 0)}{F} \qquad (2.4)$$

since:

$$\sum_i a_i = 1 \qquad (2.5)$$

This method allows the determination of absolute delayed neutron yields without knowledge of the group periods and abundances. However, the method is not satisfactory because of the large uncertainty in the extrapolated count rate.

In practice, a measurement of the delayed neutrons emitted from a sample entails the observation of the delayed neutron count rate between two fixed times, the lower limit being set by the speed with which the sample may be transferred to the counting station, and the upper limit by the relative magnitudes of delayed neutron and background counts. Thus the total number of neutrons observed in a typical experiment is given by:

$$N^1 = \int_{t_1}^{t_2} N\ (t)\ dt \qquad (2.6)$$

and therefore some knowledge of the group structure is necessary for the determination of absolute delayed neutron yield.

2.4. Symbols

a_i	The relative abundance of the i'th delayed neutron group.
F	The number of fissions produced in the sample.
N (t)	The delayed neutron emission rate as a function of time.
N^1	The total number of delayed neutrons observed after an irradiation.
Y	The absolute delayed neutron yield of the sample material in delayed neutrons per fission.
λ_i	The decay constant of the i'th delayed neutron group.

2.5. References

Batchelor 1956 - Batchelor, R. and Hyder, H.R. McK.
The Energy of Delayed Neutrons from Fission.
J. Nuclear Energy 3, 7 (1956).

Broome 1968 - N. Broome (A.W.R.E.) unpublished.

Gibbs 1939 - Gibbs, D.F. and Thomson, G.P.
Nature, 144, 202 (1939).

Keepin 1956 - Keepin, G.R., Wimett, T.F. and Zeigler, R.K.
Delayed Neutrons from Fissionable Isotopes of Uranium, Plutonium and Thorium.
J. Nuclear Energy 6, 1 (1957).

I.A.E.A. 1967 - Delayed Fission Neutrons.
Proceedings of a Panel, Vienna, 1967.

LAMS 2642 - Engle, L.B. and Fisher, P.C.
Energy and Time Dependence of Delayed Gammas from Fission.

Peterson 1956 - Peterson, R.E. and Newby, G.A.
Nuclear Science and Engng. 1, 112 (1956).

Smith 1957 - Smith, R.D., Rose, H., McVicar, D.D. amd Thorne, E.A.
Delayed Neutron Investigations with the Zephyr Fast Reactor.
J. Nuclear Energy, 4, 133 (1957).

Weale 1968 - Weale, J.W., Goodfellow, H., McTaggart, M.H. and Warnke, E.G.
The Fast Pulsed Reactor VIPER.
J.B.N.E.S., 7, 313 (1968).

3. NEUTRON DETECTOR AND DATA ACQUISITION

3.1. General Requirements

It has been shown (Section 2.2(3)) that desirable features of the neutron detector are:

1. High neutron efficiency.
2. Low gamma efficiency.
3. Little variation in efficiency with neutron energy.
4. Little variation in efficiency with small displacements of the sample.
5. Short resolving time.

Previous delayed neutron measurements have almost always been made with a neutron detector comprising a number of BF_3 detectors embedded in a moderating medium. Only the Harwell workers [Smith 1957] appear to have made a detailed investigation of the response of such a detector as a function of neutron energy, which in their case varied by about 40% in efficiency over the range of delayed neutron energies. At Los Alamos [Keepin 1956] a long counter was used, but the efficiency of this type of detector is very low.

Because of the lack of information on delayed neutron energies it was decided to develop a detector for use with the rabbit tube with as flat a response as could be achieved over the range of delayed neutron energies.

3.2. Preliminary Detector Design

The requirement that the detector efficiency should not vary greatly with neutron energy over the range of a few KeV to about 1 MeV suggests the use of a thermal neutron detector combined with a moderator. Such an arrangement, where the rabbit comes to rest in a relatively large volume of moderator also satisfies the requirement that small displacements of the rabbit should not greatly affect the efficiency of the detector.

The restriction on gamma efficiency is a very stringent one (see 2.2(3)), and for this reason it was decided to use as a neutron detector a lithium-6 loaded zinc sulphide scintillator, in which the scintillating material is dispersed as small beads [Stedman 1960]. This type of detector comprises a large number of beads of ZnS (Ag) scintillator embedded in a lithium-6 loaded plastic. Thermal neutrons are detected by the reaction:

$$Li^6 (n, \alpha) t$$

which has a Q - value of 4.64 MeV. The charged particles formed in this reaction cause scintillations in the silver activated zinc sulphide phosphor. A charged particle will deposit all or most of its energy in one of the scintillator beads, because its range is small, but a gamma ray will deposit very little energy in the scintillator beads since the path length of a gamma ray through a bead is small, compared with its total range. The detector is therefore extremely insensitive to gamma rays.

It was decided to build a detector of the form of Figure 3.1, comprising a polythene annulus coaxial with the arrester end of the rabbit tube, and a scintillator of the type described above. In order to minimise the variation in efficiency as a function of neutron energy, the dimensions of the polythene would be adjusted.

3.3. Preliminary Detector Experiments

In order to evaluate the suitability of the proposed detector, a mock-up of the detector was constructed (Figure 3.1). A number of polythene cylinders were made with different outer radii, the inner radius being determined by the dimensions of the rabbit tube. The length of the polythene cylinders was chosen as 25 cm., being a compromise between ensuring that the cylinder was much longer than the sample to fulfil requirement 4 (3.1) and allowing the final

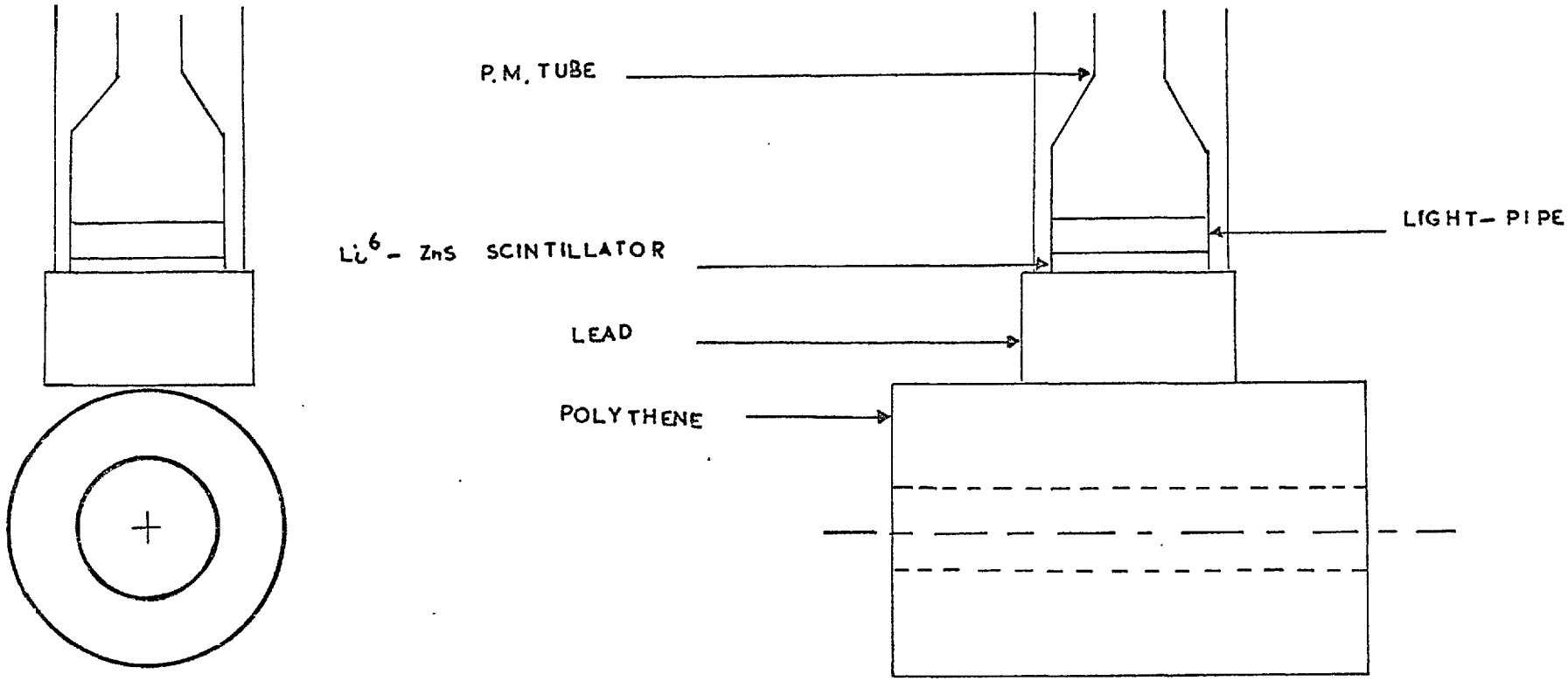

FIGURE 3.1

PRELIMINARY DETECTOR DESIGN

detector enough adjustment along the rabbit tube to cope with different sample rest positions. As may be seen from Figure 3.6, adjustment is limited by the rabbit tube construction.

A 4 inch diameter lithium loaded zinc sulphide scintillator was mounted on a 5 inch diameter photomultiplier tube by means of a perspex light guide, the whole being housed in a tinplate cylinder. A 5 cm. thickness of lead could be inserted between the polythene and the scintillator to reduce further the gamma efficiency of the detector.

3.3(1) Detector Efficiency

The efficiency of the mock-up detector was measured using calibrated neutron and gamma sources. Typical results for a polythene thickness of 5 cm., and with the lead shield in place were:

1. Neutron Efficiency Pu/Be neutrons

   $1.41 \pm .05 \times 10^{-3}$ counts per neutron

2. Gamma Efficiency Ra^{226} source

   $2.85 \pm .05 \times 10^{-8}$ counts per photon

Thus the ratio of neutron and gamma efficiencies was about 2.0×10^{5}, which was considered satisfactory since it represents a correction to the delayed neutron count rate of about 2% in the worst case. (See Section 2.2(3)).

3.3(2) Variation of Efficiency with Sample Position

An axial scan of the detector was made with a small antimony beryllium source. The count rate observed as a function of position is shown in Figure 3.2. At the peak efficiency, a variation of 1% in efficiency corresponds to a source movement of 2.2 cm., which was considered satisfactory as the rabbit stopping position is uncertain by only about 2 cm.

FIGURE 3.2

VARIATION OF DETECTOR EFFICIENCY WITH SOURCE POSITION.

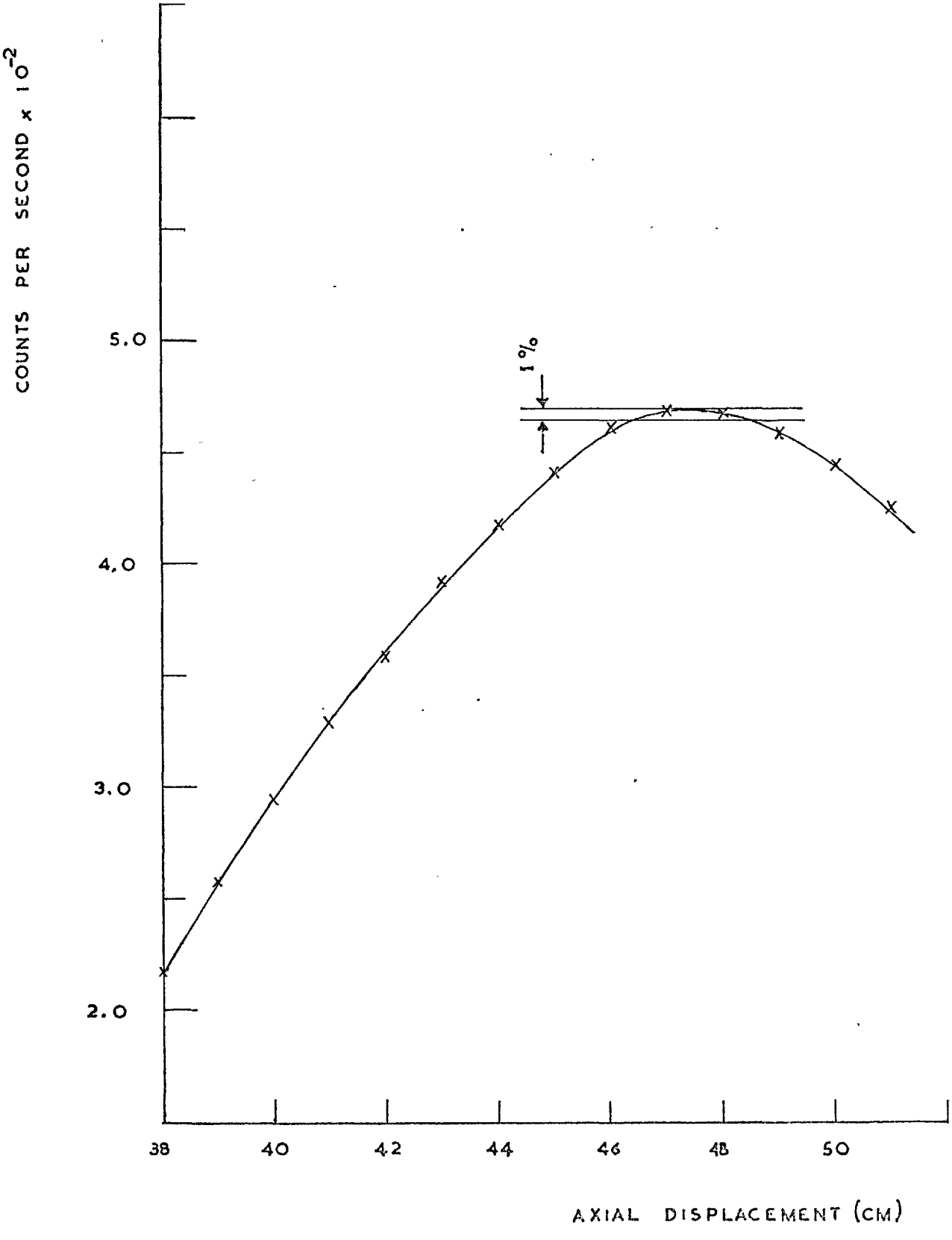

3.3(3) Variation of Efficiency with Neutron Energy

In order to determine the polythene geometry which gave the least variation in efficiency with neutron energy, the efficiency of the mock-up detector was compared with that of a long counter at various neutron energies, using each of the polythene cylinders. Monoenergetic neutrons were produced by a Van der Graaff accelerator using the reaction:

$$^{51}V\ (p,\ n)^{51}\ Cr$$

This reaction was chosen as the heavy target gives an almost isotopic distribution of monoenergetic neutrons, thus simulating the conditions of the delayed neutron measurements.

The experimental arrangement of Figure 3.3 was used, the vanadium target being situated at the centre of the detector. The long counter "viewed" the target through a borated wax collinator, in order to prevent neutrons scattered in the detector polythene from entering the long counter.

The count rates from the long counter and the detector mock-up were compared for neutron energies between a few KeV and 1 MeV, and the results are shown in Figure 3.4., where a correction has been made for the variation in long counter efficiency with energy [McTaggart 1959]. This correction varied from 0 to 15% of the observed efficiency ratio over the energy range 1 MeV to a few KeV.

It may be seen from Figure 3.4 that a polythene thickness of 5 cm. gave a satisfactory response curve, the variation in efficiency being only about 15% over the range measured.

3.4. Final Detector Design

The detector mock-up having performed satisfactorily, a detector was built to the design of Figure 3.5. A polythene cylinder of thickness 5 cm. was used, and two photomultipliers and scintillators incorporated, one of which was depleted in Li^6 and was used to monitor the gamma activity of the sample.

The final detector is shown in Figure 3.6.

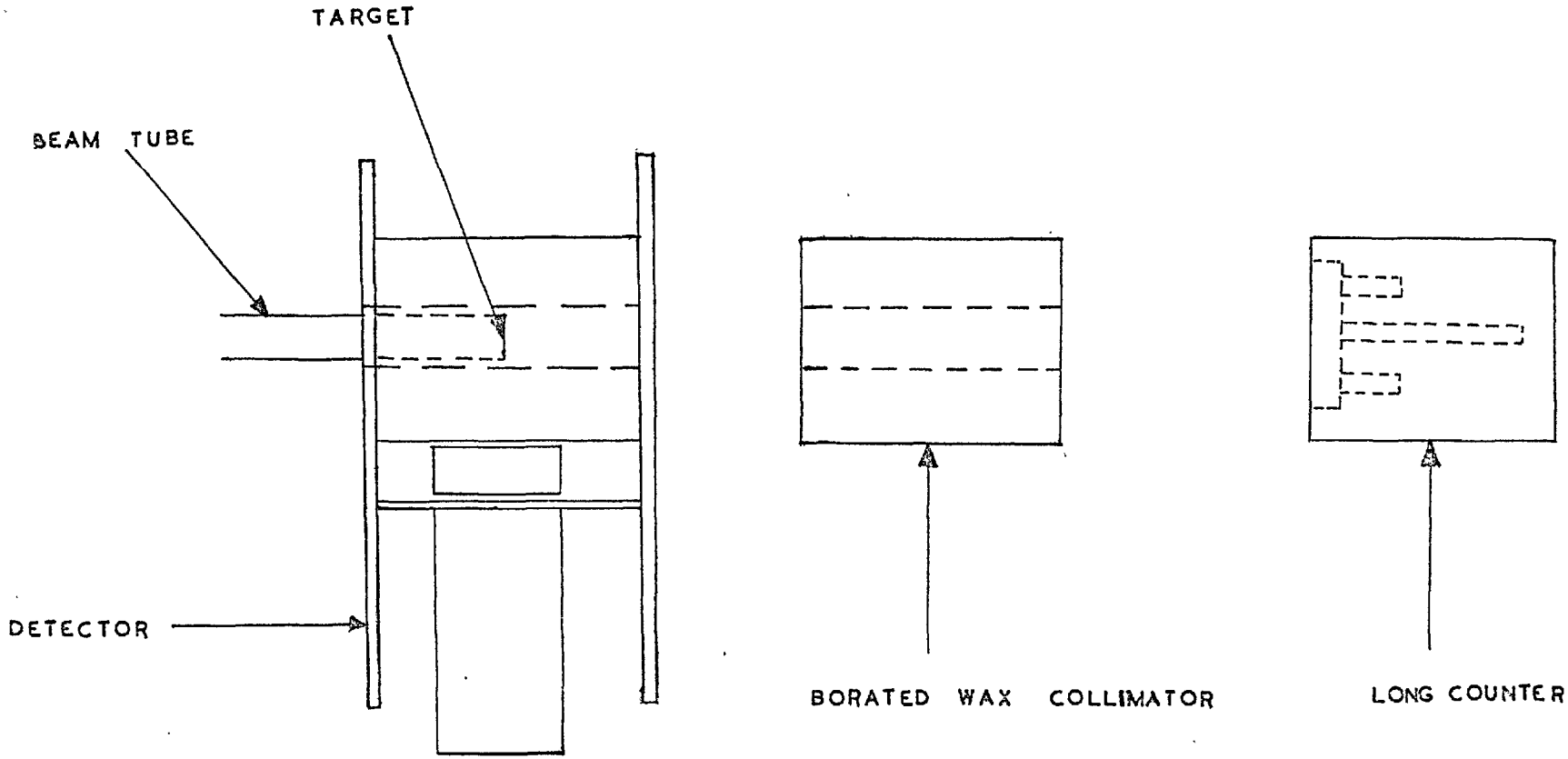

FIGURE 3.3

VAN DER GRAAFF MEASUREMENTS

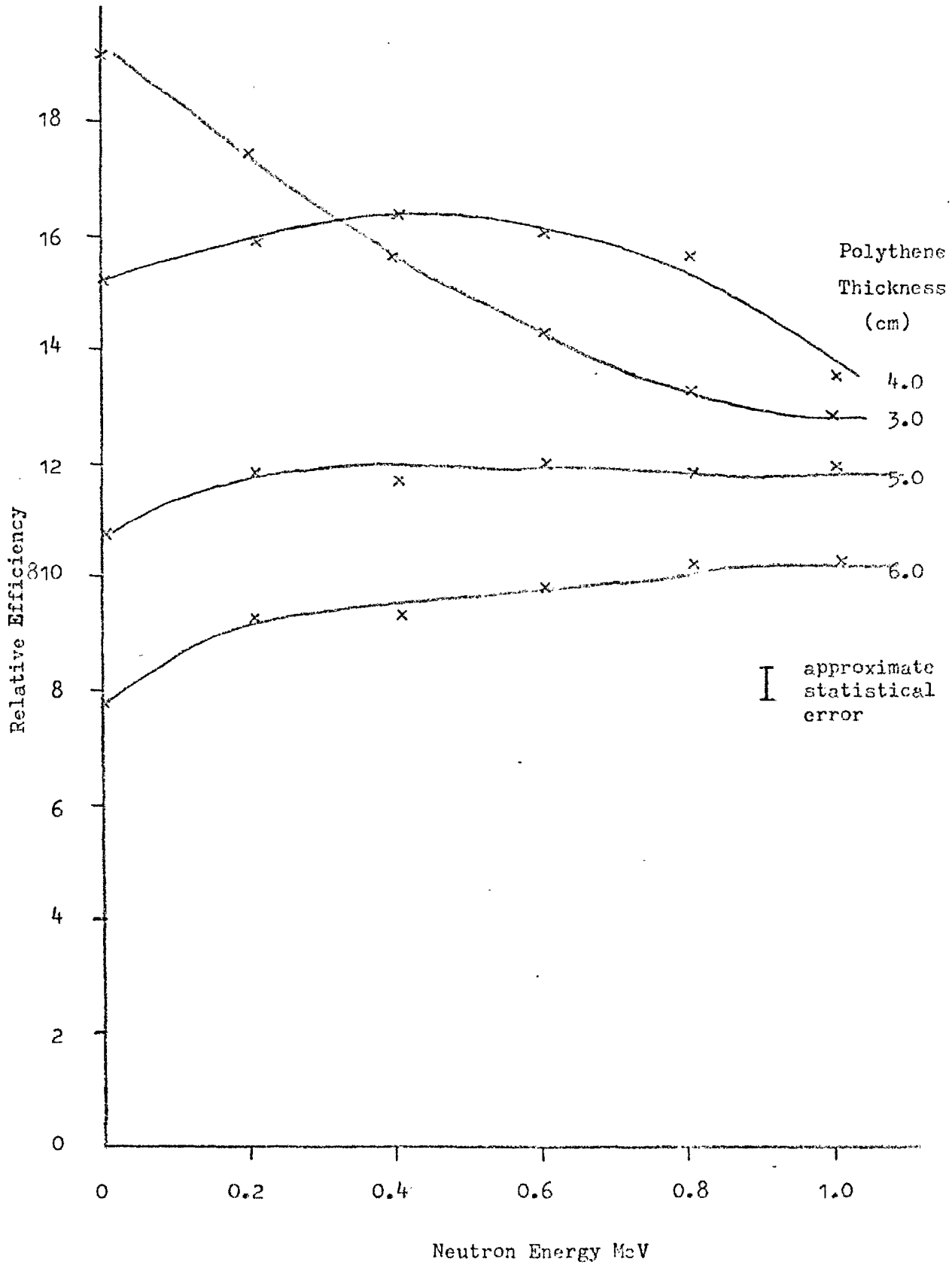

Figure 3.4

Variation of Efficiency with Incident Neutron Energy

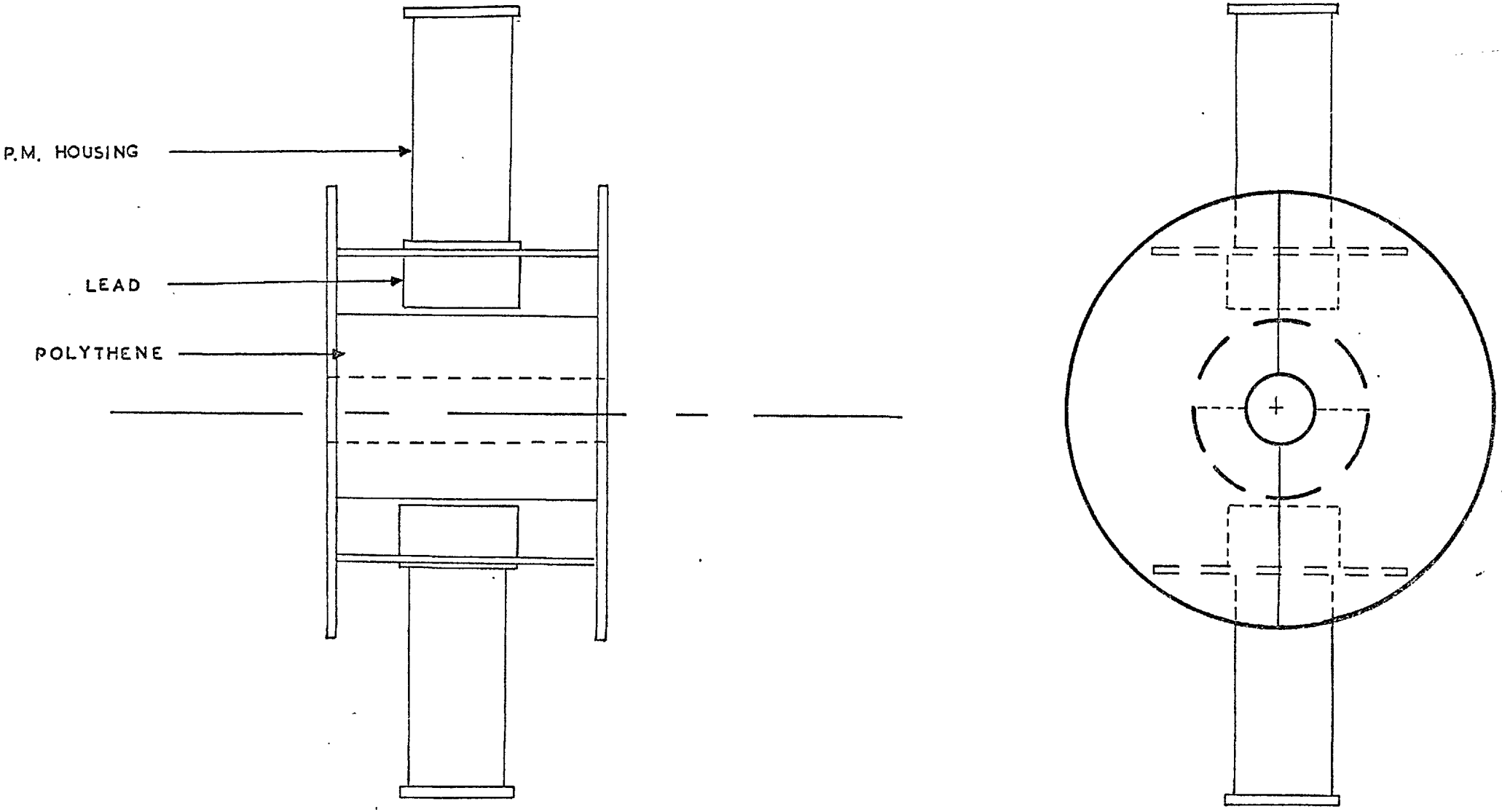

FIGURE 3.5

FINAL DETECTOR DESIGN

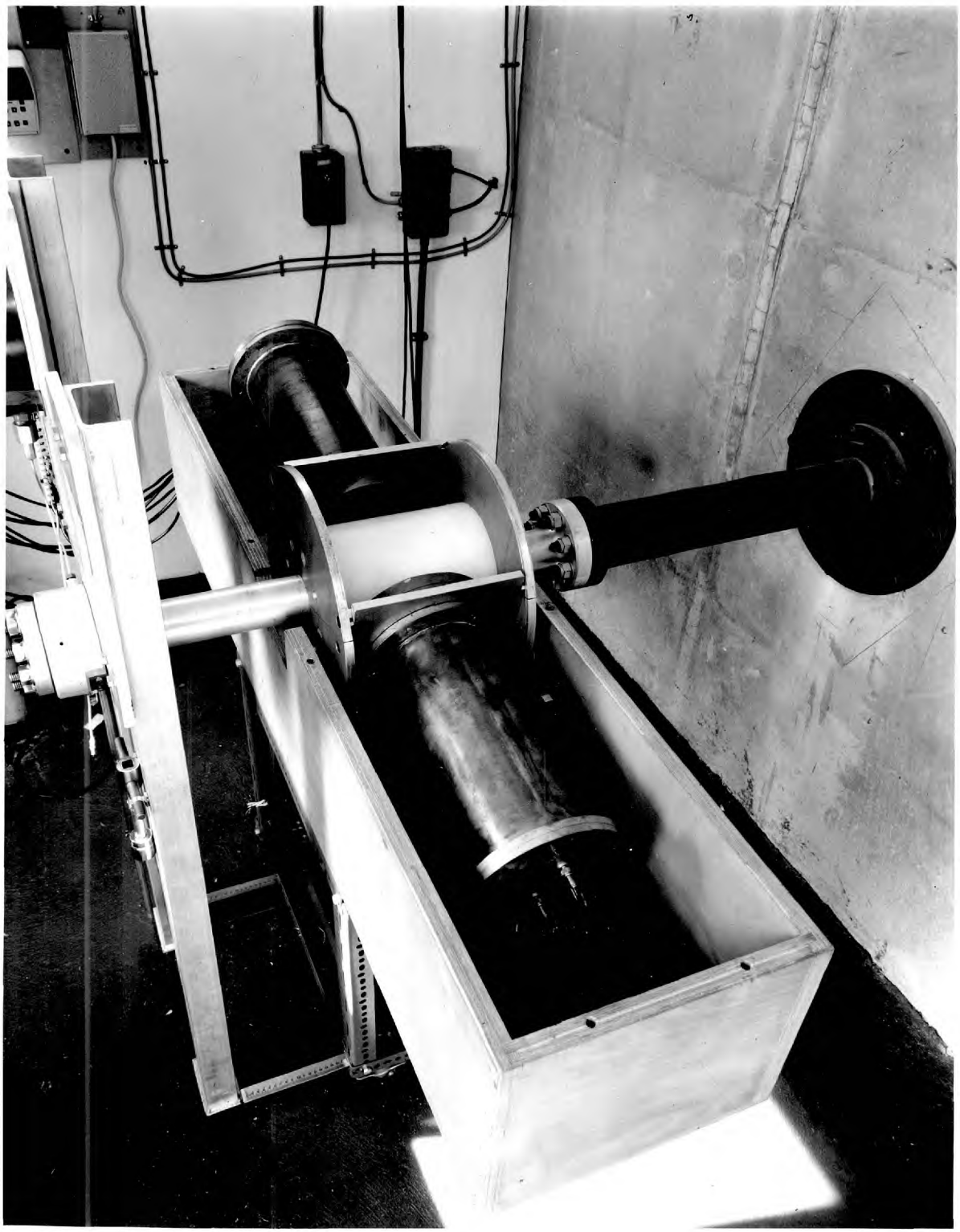

Figure 3.6

Final Detector Installed around Rabbit Tube

3.5. Detector Measurements

3.5(1) Electronics and Pulse Shaping

A block diagram of the electronics is shown in Figure 3.7. In order to be able to count at high rates shortly after irradiation, double delay line pulse shaping was used. The raw pulse from the photomultiplier was about 2 μsec long, and was not a clean pulse. This is a characteristic of the zinc sulphide scintillator, and in order to ensure that the noisy pulse was not counted as a multiple pulse, differentiating time constants very much shorter than the pulse length could not be used. Shaping constants of 0.3 μsec for differentiation and 0.3 to 1 μsec for integration gave a satisfactory pulse with approximately equal areas above and below the baseline.

In order that the dynode potentials should not drop appreciably when counting at high rates, an E.H.T. chain was built to carry 3mA (the maximum which could be supplied by the E.H.T. units). Head amplifiers terminated by emitter followers were incorporated in the P.M. tube housings.

3.5(2) Discriminator Bias Setting

The differential bias curve for the type of detector used shows no peak in pulse height for monoenergetic neutrons, since the charged particles from the nuclear reaction may lose an indeterminate amount of energy before entering a scintillator head. An integral bias curve for Pu/Be neutrons is shown in Figure 3.8, where the background contribution, which arises mainly from the scintillator itself, is also shown. The signal to noise ratio thus determined is shown in Figure 3.9, and exhibits a peak at a discriminator setting of about 1.0. Consequently this value was used as the bias setting.

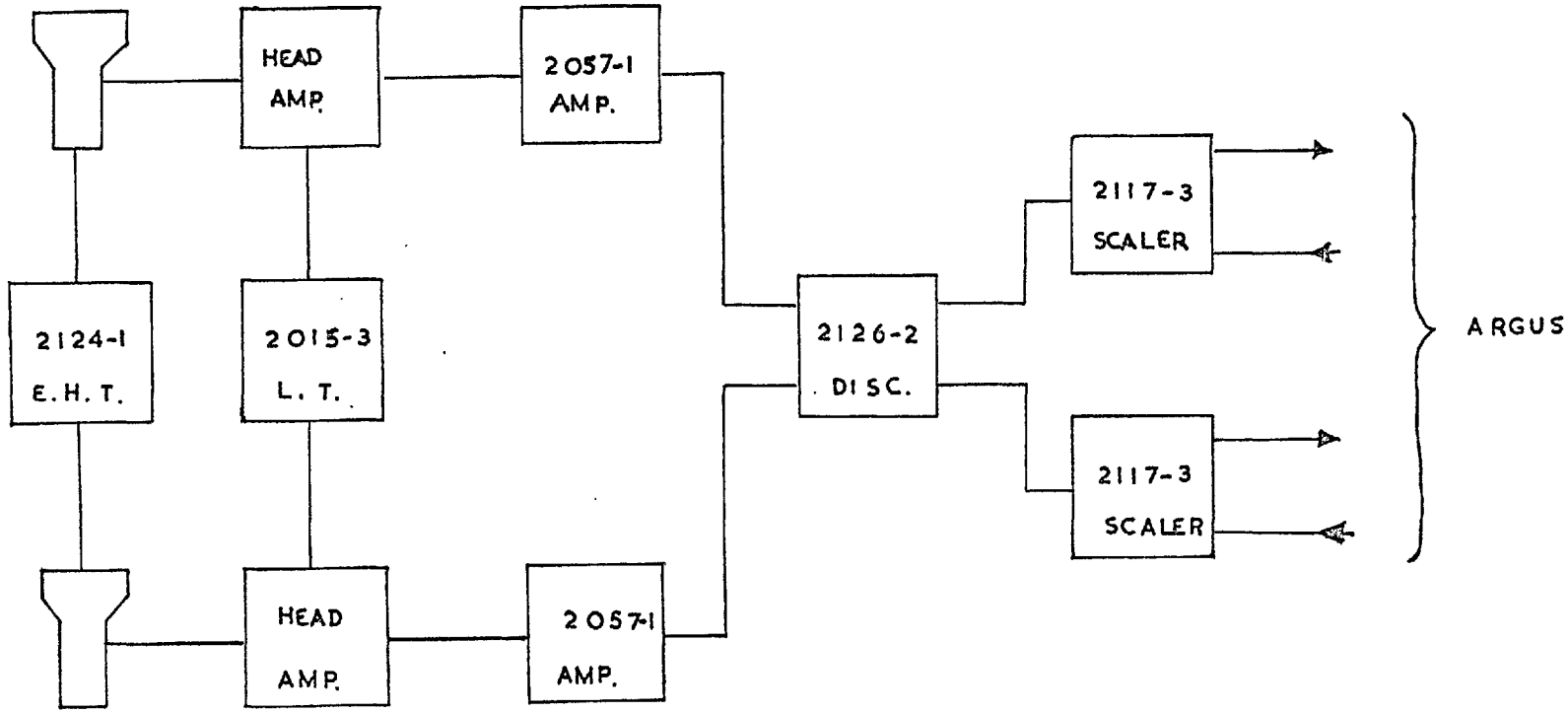

FIGURE 3.7

ELECTRONICS BLOCK DIAGRAM

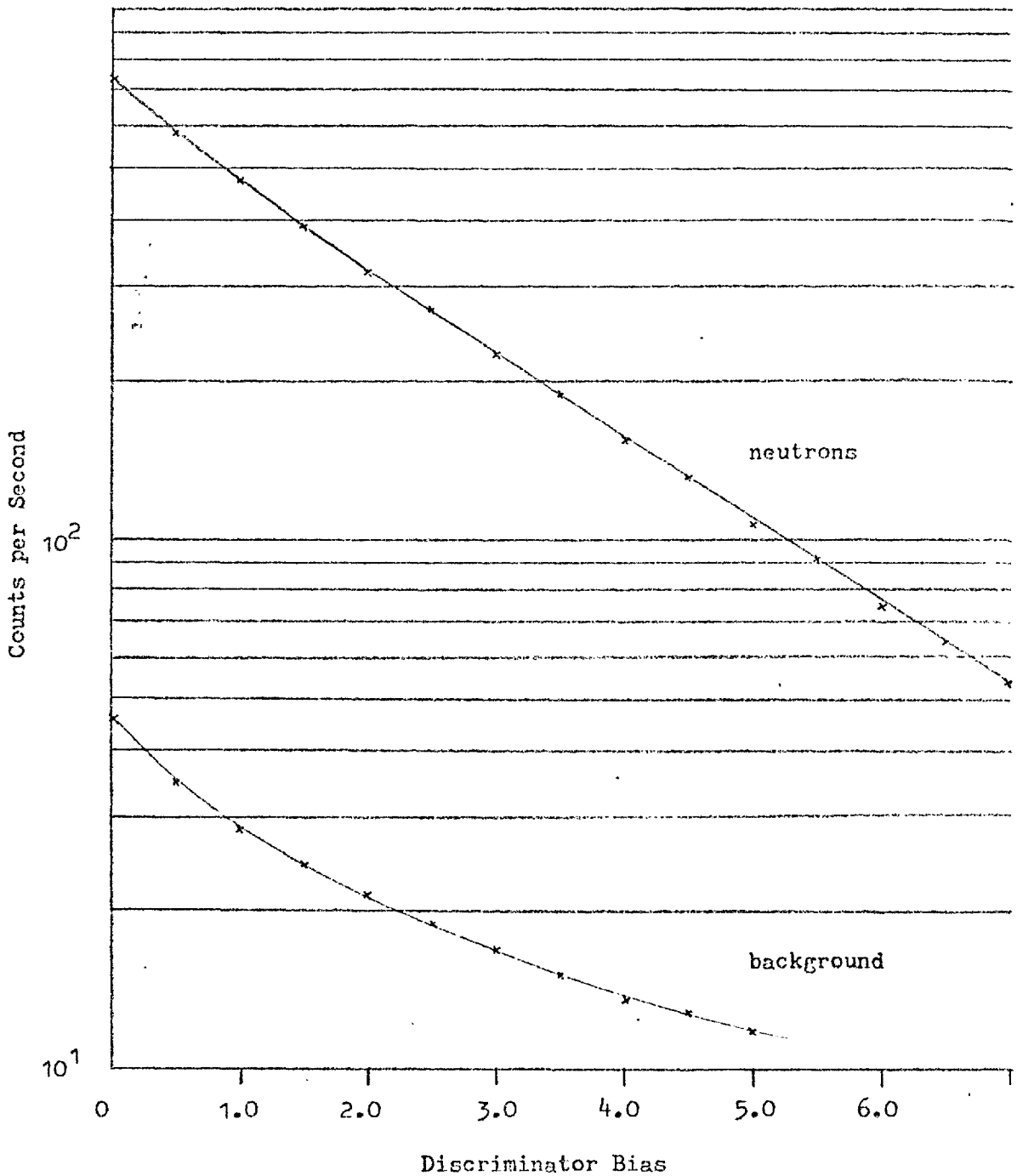

Figure 3.8

Detector Integral Bias Curve

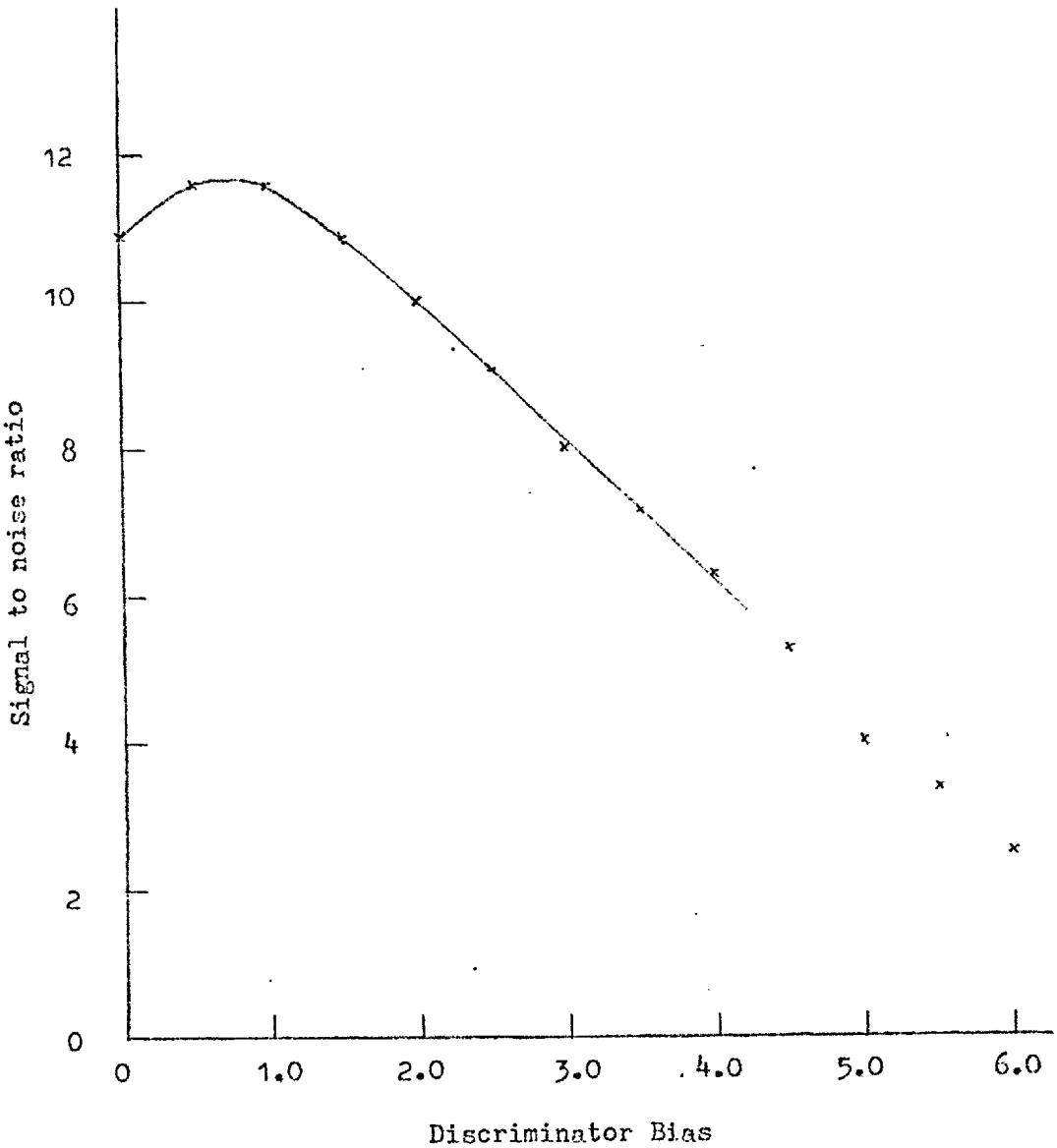

Figure 3.9

Signal to Noise Ratio

3.5(3) Detector Dead Time

As corrections for dead time counting loss were likely to be large at the high initial counting rates following an irradiation, it was necessary to measure the dead time of the counter accurately.

In order to do this, an intense source of neutrons from an accelerator using the t (d, n) α reaction was used. The count rate observed by the delayed neutron detector was compared with that from a less efficient detector at increasing neutron fluxes. The second detector was an associated particle detector, counting alpha-particles from the t (d, n) α reaction. The results obtained are listed in Table 3.1, along with the dead times calculated from the counting losses. The dead time of the alpha-particle detector was known to be about 1 μsec [D.L.E. Smith 1970], the maximum counting loss on this detector being therefore only 0.2%.

The mean dead time observed was 2.12 ± 0.22 μsec.

3.5(4) Stability

With scintillators of the type chosen stability of gain may prove to be a problem, since there is no minimum rate of change of count rate with bias setting. In order to overcome this problem it was decided to calibrate the detector with a standard source in a known position before each VIPER pulse. It was therefore necessary to ensure that the change in gain over a possible delay of a few hours between the detector calibration and the rabbit firing would be tolerably small.

Preliminary measurements indicated a change of observed count rate with temperature of about 2% per ^{o}C. It was therefore decided to house the detector in a constant temperature enclosure. The overall arrangement is shown in Figure 3.10 installed around the detector and rabbit tube.

With the constant temperature enclosure in operation, the detector stability was found to be satisfactory. A chart recording of detector count rate (Figure 3.11) over a period of 24 hours showed an acceptable (about 1%) drift in count rate.

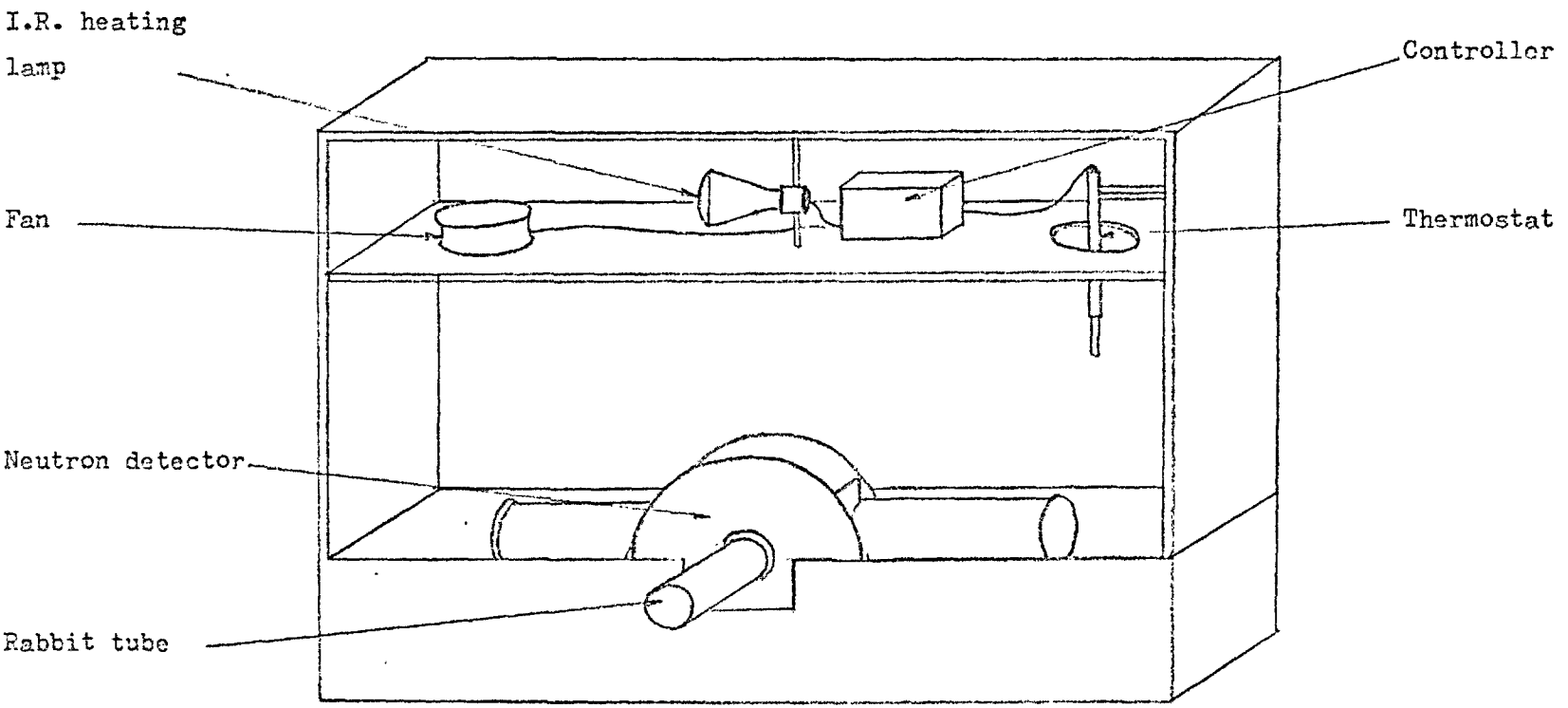

Figure 3.10

Constant Temperature Enclosure

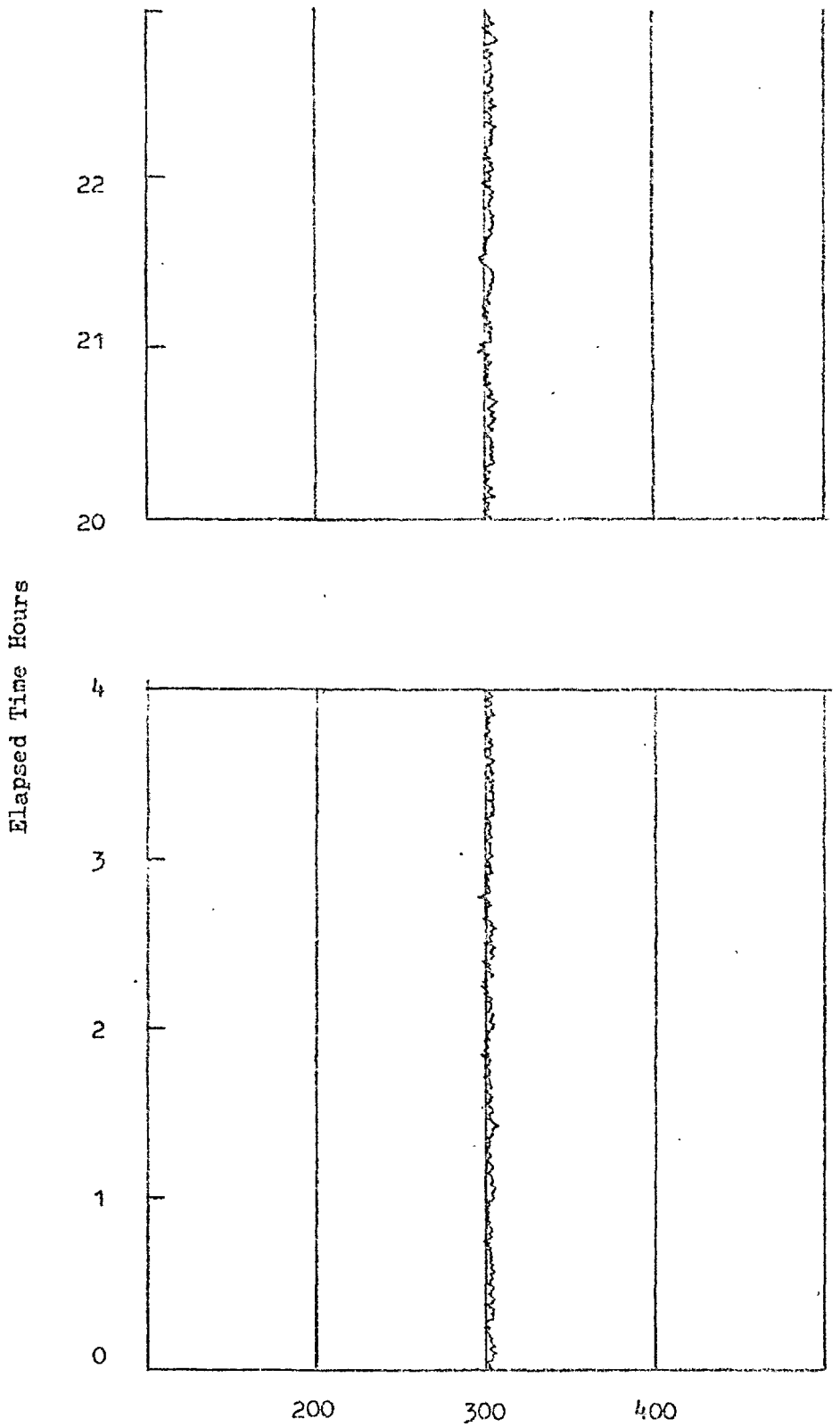

Figure 3.11

Detector Long-term Stability

Counts per 100 sec		Dead Time (μsec)	Standard Deviation
Neutron Detector	Alpha Detector		
749450	21376		
714073	20531		
718960	20508		
718830	20455		
3505333	108875	2.29	1.01
3308590	102820	2.44	1.07
3338461	102761	2.16	1.06
3367885	103838	2.19	1.05
6693211	221501	2.05	0.53
6641608	219874	2.07	0.54
6634907	219701	2.07	0.54
6577456	217736	2.09	0.54
6577342	218871	2.15	0.54
6571622	218438	2.14	0.54

Table 3.1

Detector Dead Time Measurements

3.5(5) Variation of Efficiency with Axial Displacement of Source

In order to provide a calibration curve of detector efficiency against rabbit arrival position, the variation in count rate along the detector axis was measured using a small Po/Be source. Results are tabulated in Table 3.2 and shown in Figure 3.12.

3.5(6) Variation of Efficiency with Neutron Energy

In order to estimate accurately the variation of efficiency with neutron energy for the final detector, the measurements described in Section 3.3(3) were repeated. The range of calibration was increased using the $^{57}Fe(p,n)^{57}Cr$ reaction. At each neutron energy the count rate observed from the delayed neutron detector was compared with that from a long counter. The results of this calibration are shown in Figure 3.13, where the results have been corrected for variations in long counter efficiency [McTaggart 1959]. The maximum correction applied was about 15%.

An estimate of the room-return contribution to the long counter counting rate was made by placing a block of borated wax between the source and the long counter. This contribution was found to be only a few percent.

3.5(7) Absolute Calibration of Detector Efficiency

The delayed neutron detector was calibrated using known neutron sources at various energies. For the purposes of calibration at low energies a number of (γ, n) sources were prepared. Figure 3.14 shows the sources, which comprise a gamma source, welded in stainless steel, and jackets of beryllium and heavy water. The gamma sources were activated in the HERALD reactor, and the (γ, n) sources calibrated in a vanadium bath.

For the purposes of calibration at higher energies Pu-240 spontaneous fission and americium-beryllium sources were used. The former had been in use at A.W.R.E. for a number of years, and its strength was well known. The americium-beryllium source had been calibrated at Amersham.

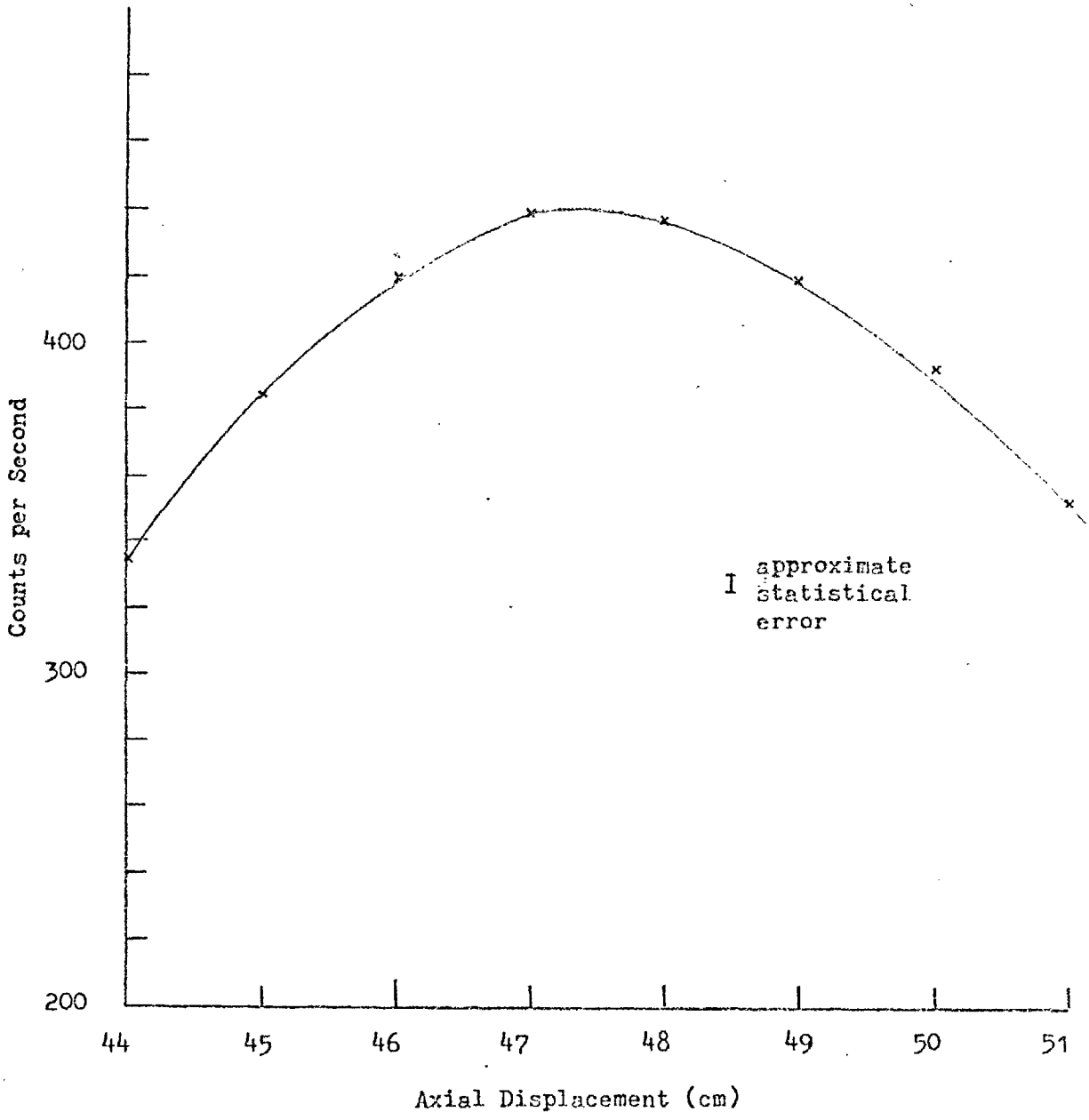

Figure 3.12

Variation of Efficiency with Axial Displacement of Source

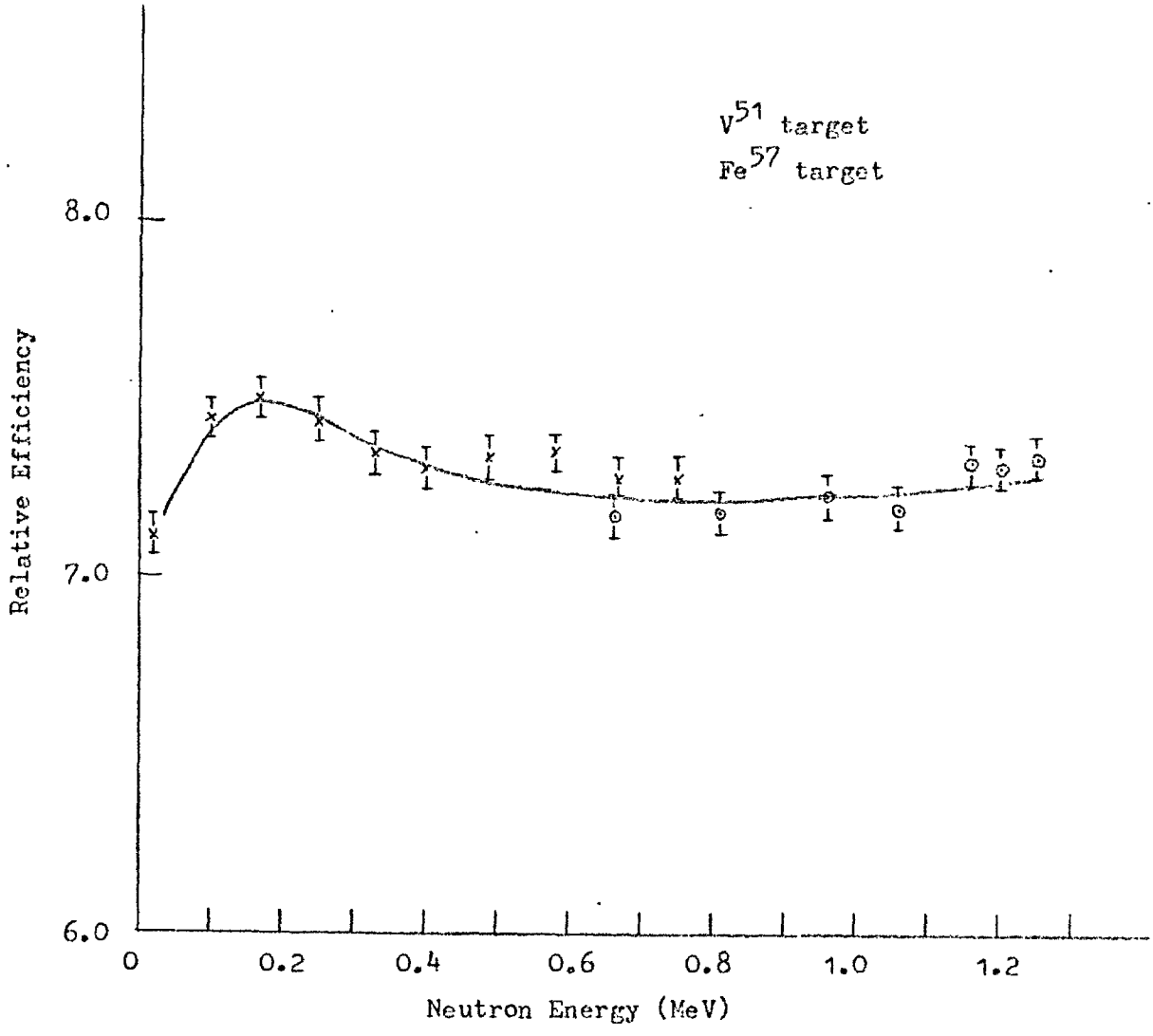

Figure 3.13

Variation in Efficiency with Incident Neutron Energy

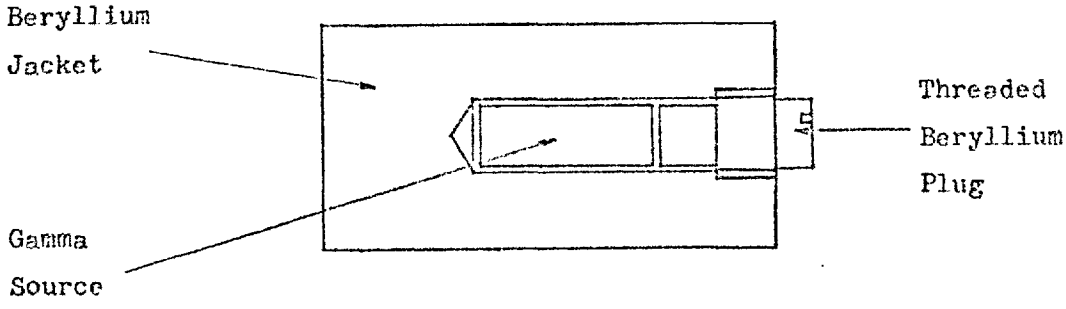

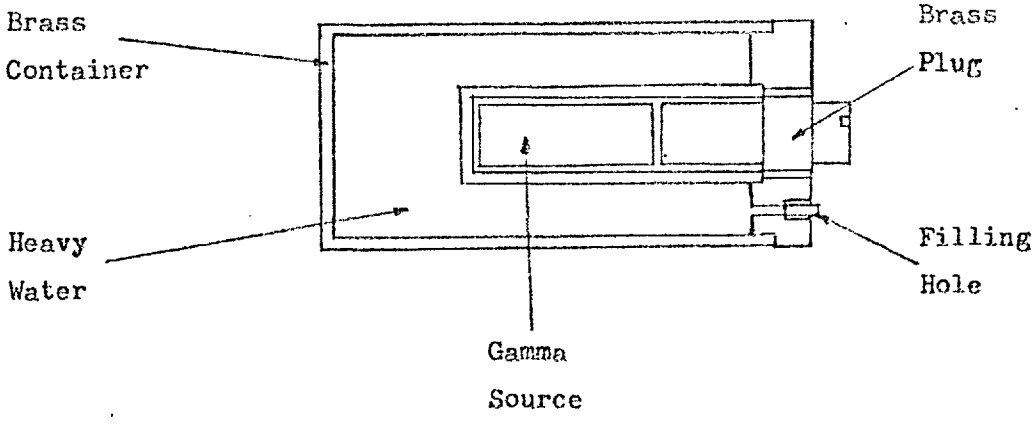

Figure 3.14

Photoneutron Sources

AXIAL DISPLACEMENT (cm)	MEAN COUNTS PER SEC BACKGROUND SUBTRACTED
44.0	335 ± 5
45.0	382
46.0	415
47.0	432
48.0	428
49.0	416
50.0	395
51.0	345

Table 3.2

Variation of Detector Efficiency with Axial Variation in Source Position (Po-Be Source 2.5 cm. long)

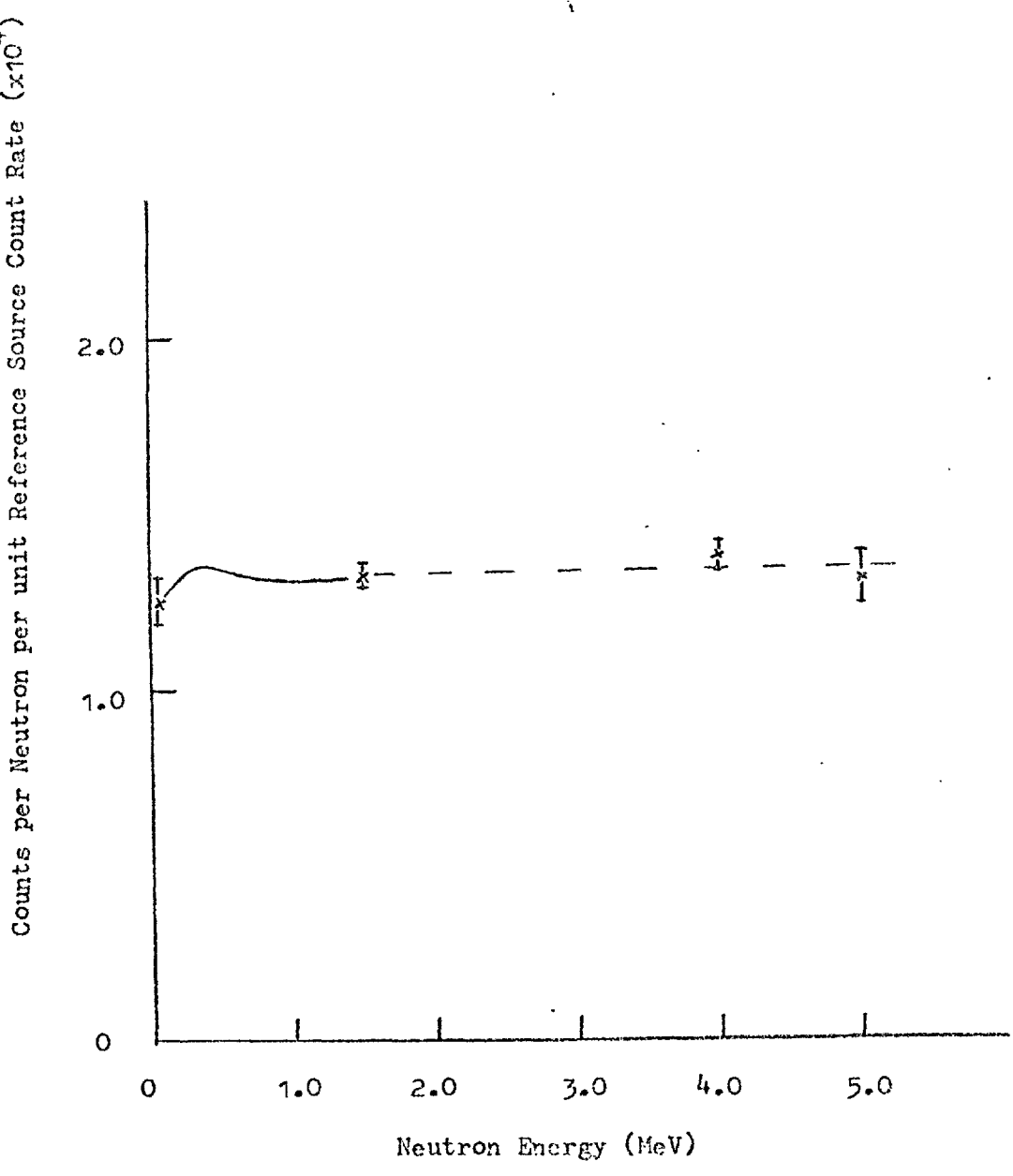

Figure 3.15

Absolute Detector Efficiency

The procedure adopted for the calibration of the detector with each of these sources was to perform an axial scan along the length of the detector, the peak efficiency being determined from these measurements. All calibrations were standardised by counting a reference source situated in a reproducible position before and after the calibration, thus accounting for any change in detector gain over the extended interval between calibration and delayed neutron measurements.

The peak efficiencies measured are shown in Table 3.3, and these values normalised to the response curve obtained by the Van der Graaff calibration are shown in Figure 3.15.

3.6. Data Acquisition

In order to obtain information on the time-dependence of the delayed neutron decay, the output from the delayed neutron detector was multiscaled using the ARGUS 500 computer. Software was provided which enabled time channels of 1, 10, 100 and 1000 msec to be obtained, the number of each of which could be chosen to suit the particular irradiation.

SOURCE	AVERAGE NEUTRON ENERGY (MeV)	DETECTOR* EFFICIENCY
Sb-Be	0.025	$1.25 \pm 0.05 \times 10^{-4}$
Pu^{240}(SP.Fiss)	1.5	$1.32 \pm 0.02 \times 10^{-4}$
Pu-Be	4.0	$1.38 \pm 0.03 \times 10^{-4}$
Am-Be	5.0	$1.31 \pm 0.06 \times 10^{-4}$

* Counts per neutron per unit reference source count rate.

Table 3.3

Absolute Detector Calibration

3.7. References

D.L.E. Smith 1970 - D.L.E. Smith (A.W.R.E.)
Private communication.

Keepin 1956 - Keepin, G.R., Wimett, T.F. and Zeigler, R.K.
J. Nuclear Energy, 6, 1 (1957)

McTaggart 1959 - McTaggart, M.H.
A study of the Neutron Long Counter.
A.W.R.E. Report NR/A-1/59.

Smith 1957 - Smith, Rose, McVicar and Thorne.
J. Nuclear Energy, 4, 133 (1957).

4. FISSION MEASUREMENTS

4.1. General

The number of fissions produced in a sample during a VIPER irradiation was measured by a foil activation technique. Foils composed of the same material as the sample were irradiated in the rabbit and subsequently counted for La-140 1.6 MeV gamma activity, using a 43-cc coaxial lithium-drifted germanium detector. These measurements were made relative to a steady-state calibration irradiation in VIPER, in which similar foils were irradiated in one half of a double fission chamber, while the other half was used as a fission counter.

4.2. Foils and Counting Arrangement

The foils used for the fission measurements were 0.3 inch diameter discs with a thickness of 0.002 - 0.003 ins.. This represented the minimum foil thickness which could readily be obtained, and was chosen to minimise self-absorption in the foils. The foil diameter was governed by the size of the rabbit body. The foils are shown with the rabbit in Figure 2.3.

After irradiation the foils were washed in acetone and inserted in aluminium foil holders. These holders fitted an automatic sample changer, which was used only to locate the foils in view of the long counting times necessary.

A block diagram of the counting system is given in Figure 4.1, and comprised a Canberra 43 cc. true coaxial detector with associated preamplifier and amplifier. Data acquisition was by a PDP-8/I computer reading a Northern 8192-channel analyser via a CAMAC interface.

The resolution of the detector was about 5KeV at 1.6 MeV (Figure 4.2).

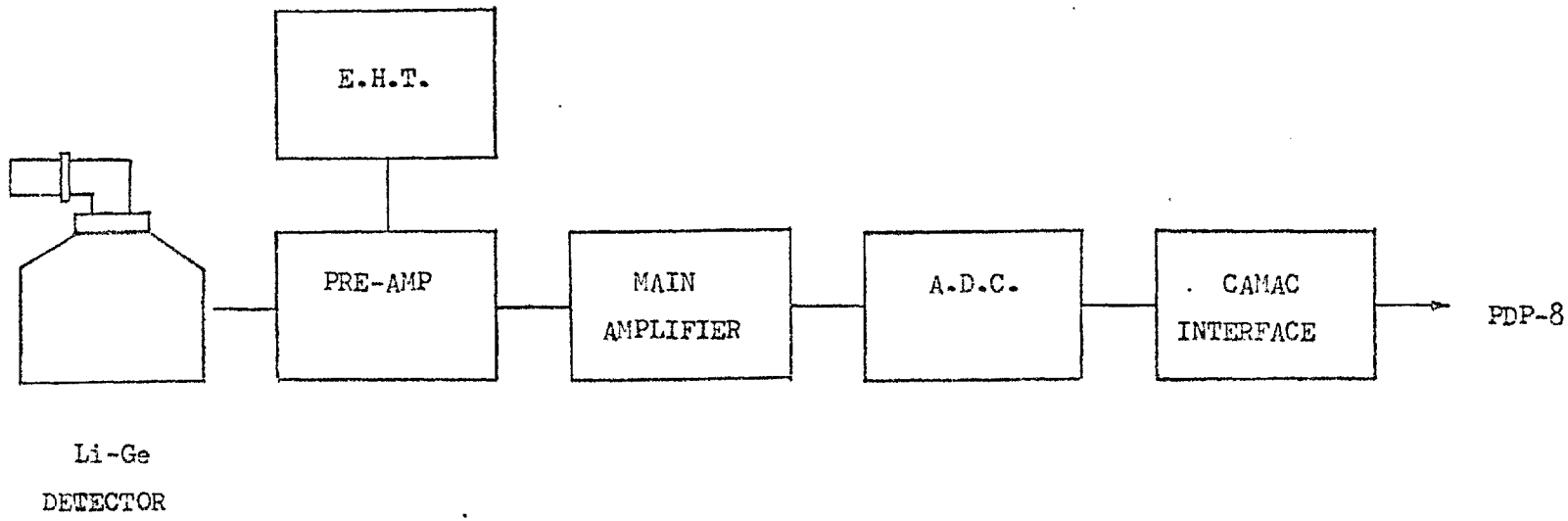

Figure 4.1

Gamma Counting System - Block Diagram

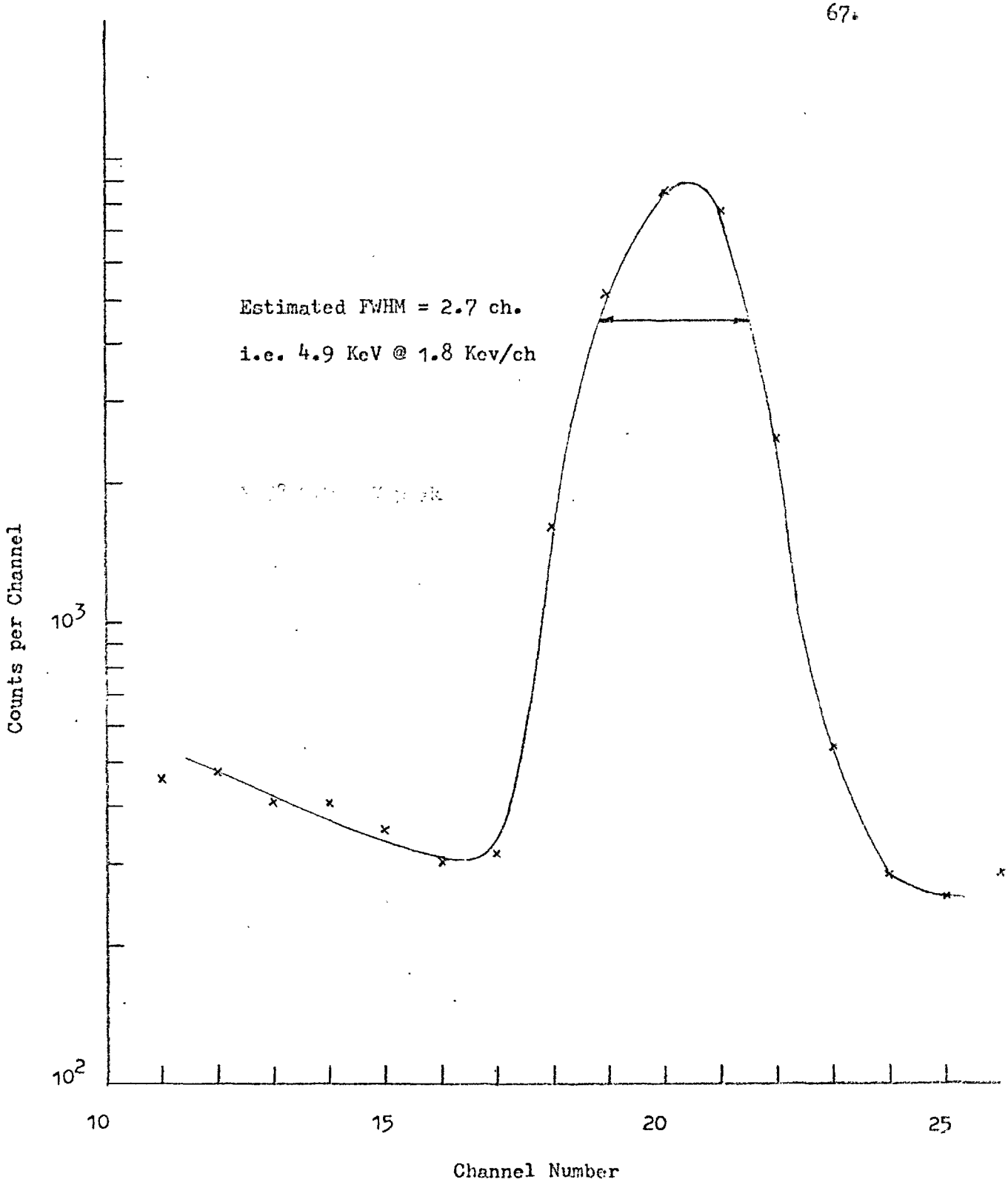

Figure 4.2

Detector Resolution

4.3. Counting Technique

Apart from being formed independently in fission, Ba-140 and La-140 are formed through the chain:

$$Xe^{140} \longrightarrow Cs^{140} \longrightarrow Ba^{140} \longrightarrow La^{140} \longrightarrow Ce^{140}$$

16 sec. 66 sec. 12.8 days 40.2 hours Stable

The beta decay of La^{140} to Ce^{140} is accompanied by a number of gamma rays, the most prominent being at 1.6 MeV. After the decay of the La^{140} formed directly in fission, this gamma ray appears to decay with the half life of Ba^{140}, namely 12.8 days, since this is much longer than the La^{140} half-life.

In practice, after a delay of about ten days from irradiation, the 1.6 MeV fission product gamma ray appears to decay with the characteristic Ba^{140} half-life. Foils were counted after a delay of about ten days over a period of a number of half-lives. Counting rates for inter-comparison were normalised to 300 hours after irradiation, this being a convenient point for interpolation.

4.4. Photopeak Analysis

As may be seen from Figure 4.2, the spectrum observed in the region of 1.6 MeV represents the photopeak superimposed on a general Compton background. Several methods were considered for the analysis of this peak:

1. Subtraction of a trapezoidal background (Figure 4.3a).
2. Least-squares fitting of a Gaussian plus polynomial background. (Figure 4.3b).
3. Covell's method. (Figure 4.3c).
4. Iterative method.

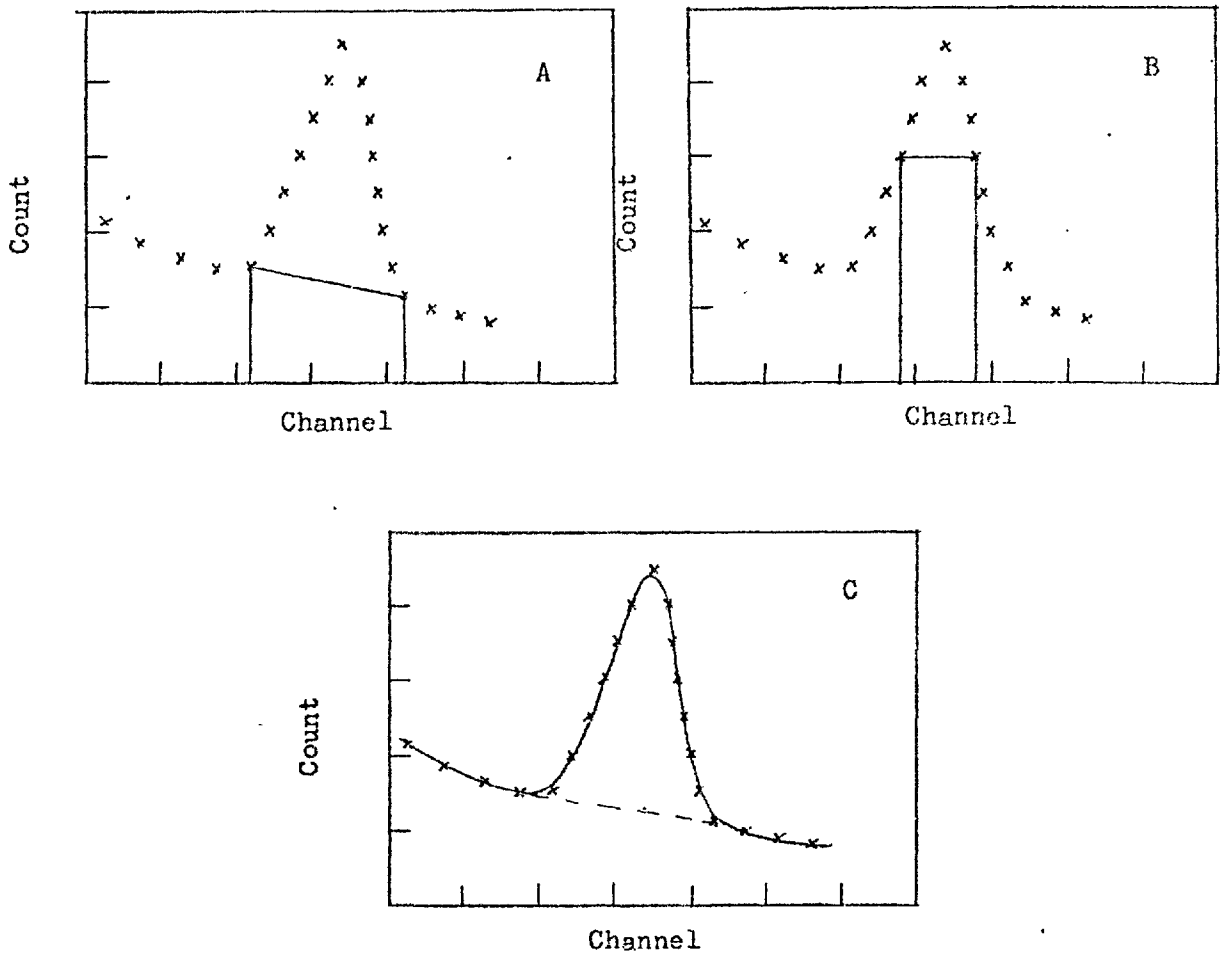

Figure 4.3

Photopeak Analysis Methods

4.4(1) Subtraction of Trapezoidal Background

This, the simplest method consists of subtracting a background found by averaging the background estimated at either minimum of the photopeak. This suffers from the fact that the minima are not well defined. Generally, it can be seen that the background is not well approximated by a straight line. Analysis of the photopeak by this method did not always result in the observation of the correct decay period.

4.4(2) Least Squares Fitting

This method was rejected on the grounds that a large number of parameters had to be fitted to a small number of points. The photopeak was generally only 2-3 channels wide (F.W.H.M.), and the statistical error on the individual points would have been unacceptably large had this been increased appreciably.

4.4(3) Covell's Method

The method due to Covell [Covell 1959] consists in using only counts in a limited region near the peak, and subtracting a trapezoidal background, which is clearly an overestimate. The method used is to take as limits for the count a window of a number of channels centred on the peak channel. It was felt that this technique could not usefully be used, since the number of channels in the peak was small, and any change in detector resolution or amplifier gain might radically change the count calculated by this method.

4.4(4) Iterative Method

The method finally adopted for the analysis of the photopeak was an iterative method [Yule 1969]. It consists of generating the background spectrum by replacing a given count by the average of the neighbouring counts if it does not exceed that average by a significant amount. A program was written to perform this analysis on the PDP-8/I computer.

4.5. Detector Stability

In order to estimate any drift in detector gain, the decay of the 0.9 MeV photopeak of Y-88 was followed for a period of a number of weeks. The results of 1000 second counts were normalised to account for the decay of the source, and the distribution of these counts is shown in Figure 4.4. The F.W.H.M. was estimated to be 1.4% of the observed count, the corresponding standard deviation, assuming Poison statistics being 0.5% of the observed count. It was therefore concluded that the detector was stable to within 1% in count rate.

In the long term the detector showed no appreciable drift in gain, as may be seen from Figure 4.5, where the observed count rate from the Y-88 source is plotted over a period of a number of weeks.

4.6. Calibration Irradiation

In order to correlate foil gamma activity with the number of fissions occurring in a sample, foils were irradiated in a demountable fission chamber along with a calibrated fission chamber deposit. The arrangement of foils in the chamber is shown in Figure 4.6.

In order to irradiate the foils to a level comparable with that achieved in a VIPER pulse, it was necessary to irradiate the chamber for a period of a number of hours at 600 W. The power could not be raised above this level as VIPER has no cooling system. In the case of U-235, these conditions necessitated the use of a calibrated fission chamber deposit with a total mass in the region of 100 μgm U-235, or serious dead time problems would have been encountered. The calibration of this foil is described in Section 5.

Two foils of the sample material were installed in the fission chamber together with the fission chamber deposit and the chamber filled with a mixture of 90% Argon, 10% Methane to a pressure of 2 atmospheres. The chamber was

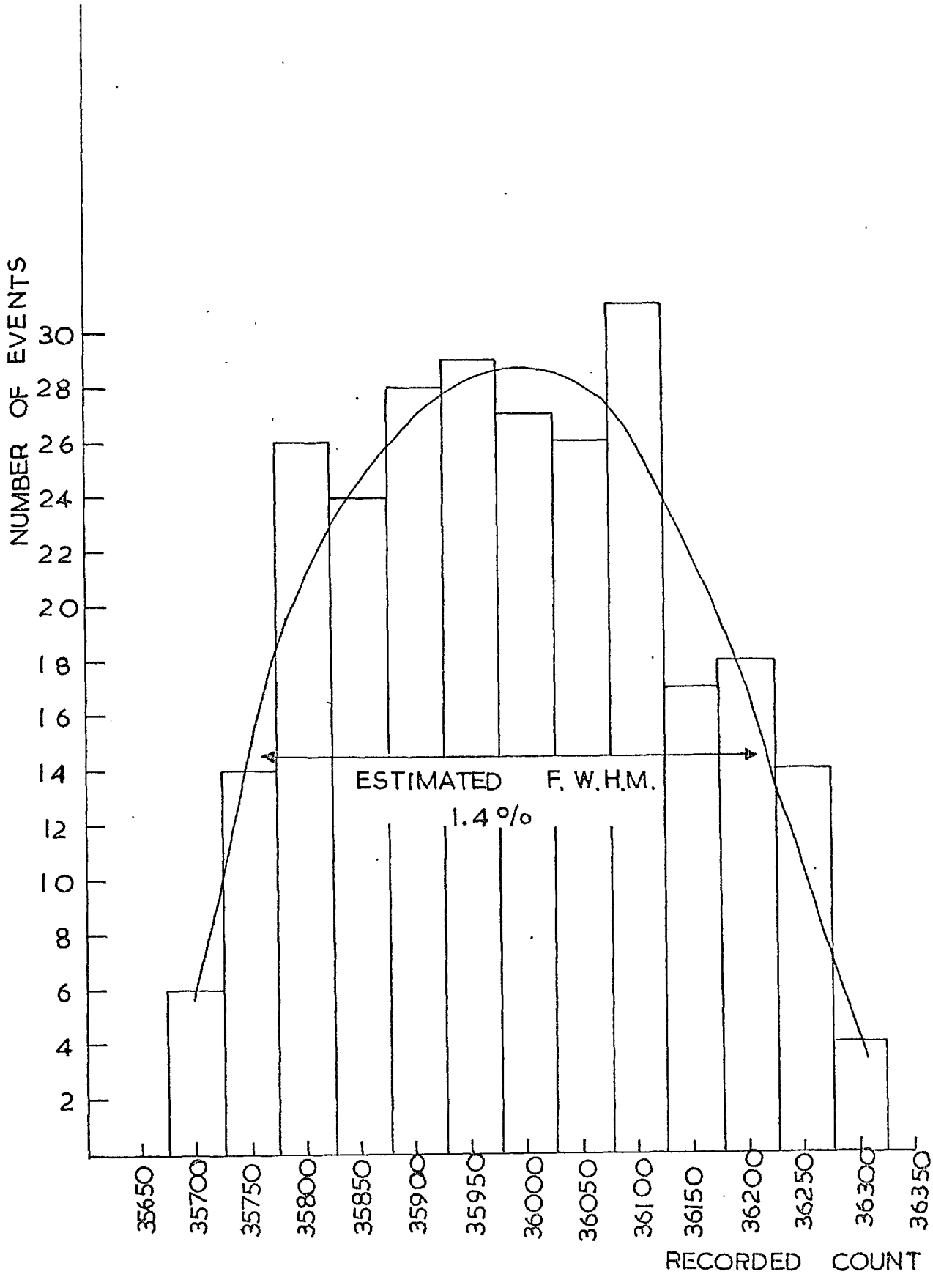

FIGURE 4.4

SHORT TERM DETECTOR STABILITY

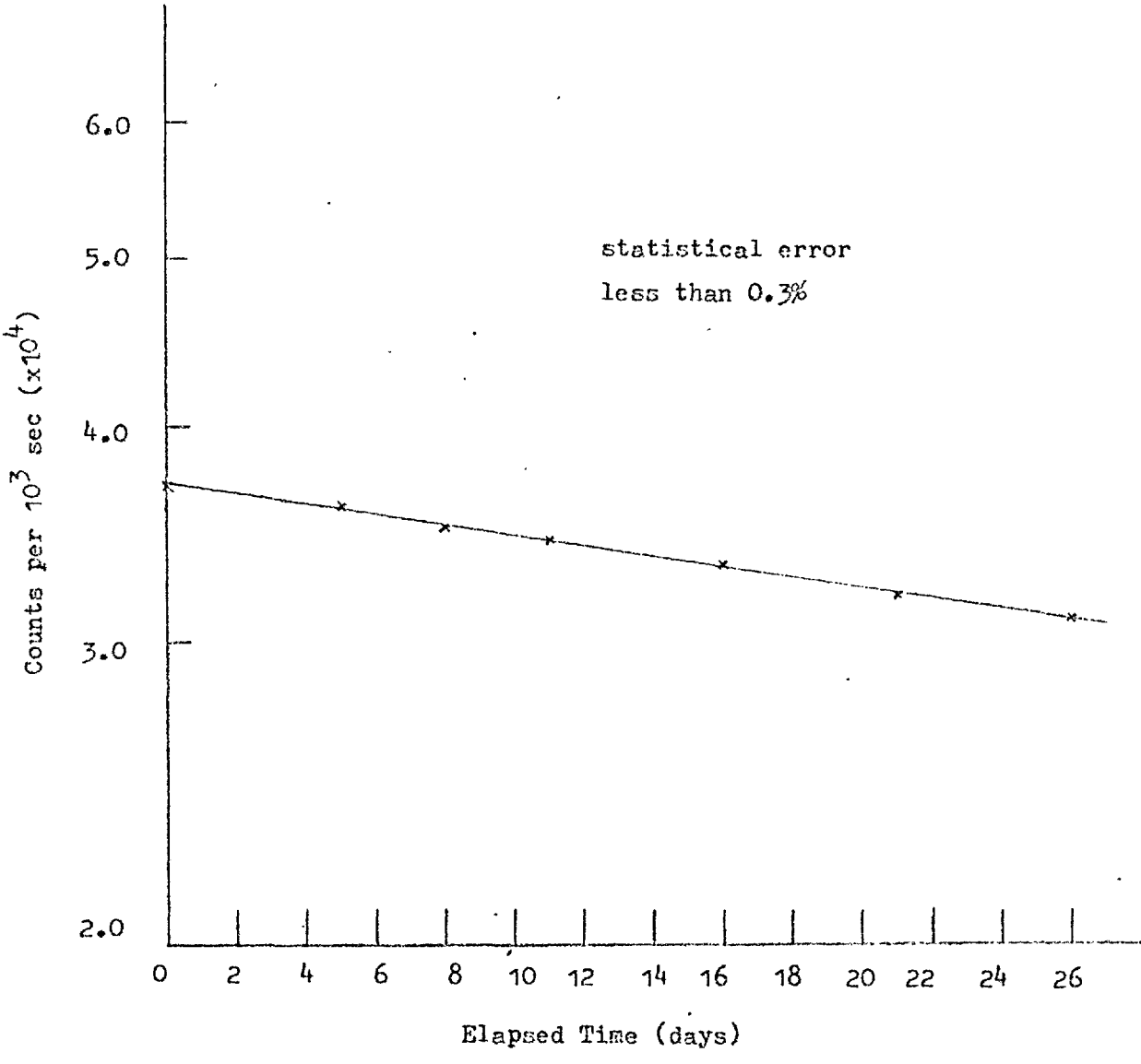

Figure 4.5

Long-term Detector Stability

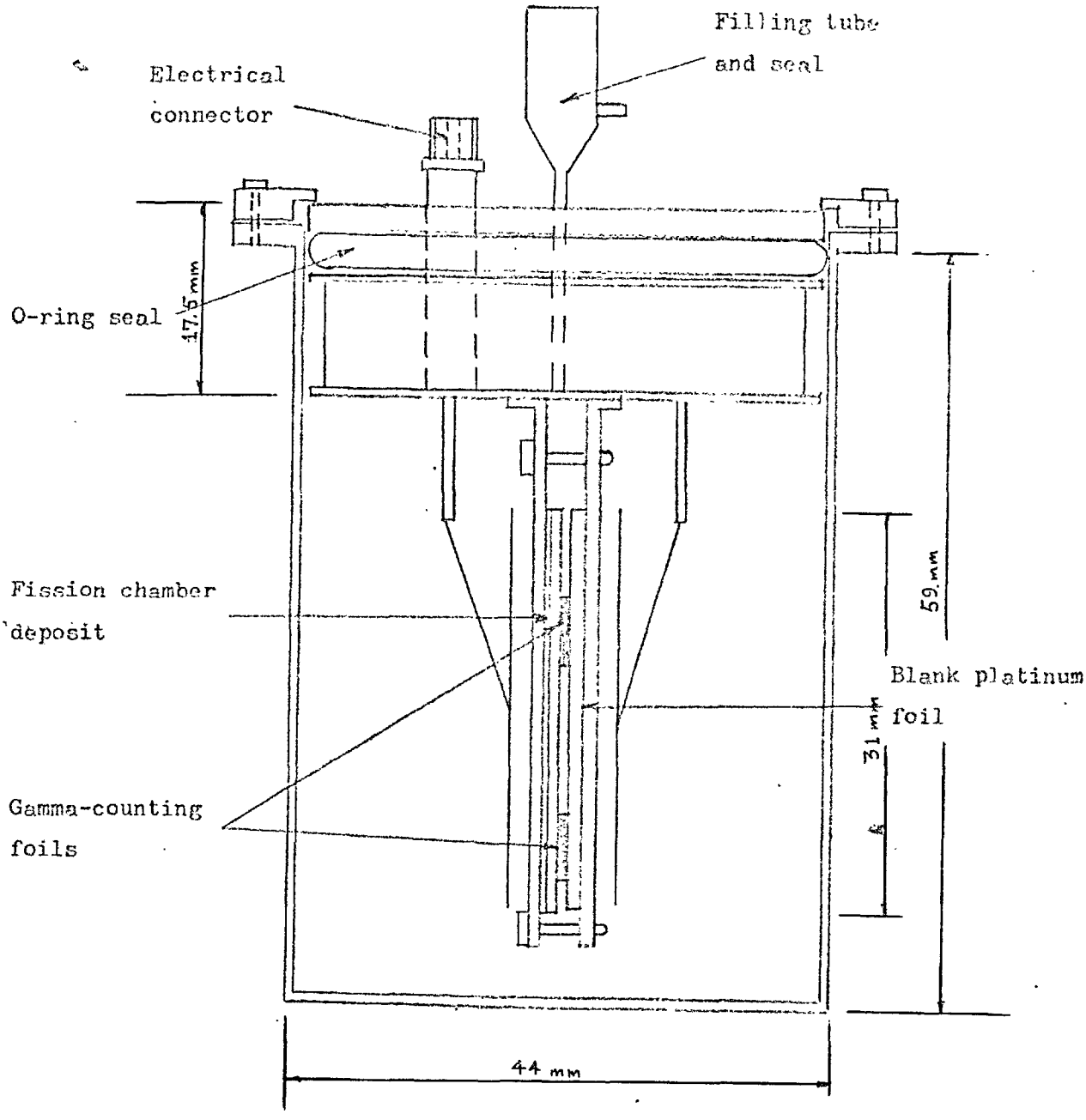

Figure 4.6

Arrangement of Foils in Double Fission Chamber

flushed with the gas several times before the final filling. The chamber was installed in the large VIPER irradiation cavity, and set up with the reactor running at a power of IOW. This procedure took only a few minutes, the power then being increased to 600 W for a number of hours.

After the irradiation the total fission chamber count was noted, and the foils counted after a delay of about 10 days. The results of the foil counting are shown in Figure 4.7.

4.7. Fission Rate Ratio Measurement

In order to correct for the isotopic composition of the foils it was necessary to measure the U-235/U-238 fission rate ratio in the VIPER irradiation cavity. This was performed using both fission chamber and foil activation methods. An irradiation was performed in a manner similar to that described in Section 4.6, using fission chamber deposits composed of U-235 and U-238 in a back-to-back fission chamber, foils of U-235 and U-238 being sandwiched between the two deposits. Foils were also irradiated independently during a VIPER pulse, in order to check that the presence of the fission chamber body produced no appreciable perturbation. The isotopic compositions of the foils and deposits used are shown in Table 4.1. Results of the fission chamber counting are shown in Table 4.2 along with the corrections. These corrections are discussed in detail in Section 5. The masses of the fission chamber deposits were:

1.12 (U-235) 78.84 $\pm$ .52 µgm [Section 5]

3.5 (U-238) 6354 $\pm$ 60 µgm [McCormick 1971]

This latter value was an effective mass (i.e. including the foil thickness correction) obtained by absolute calibration in a 14-MeV neutron beam.

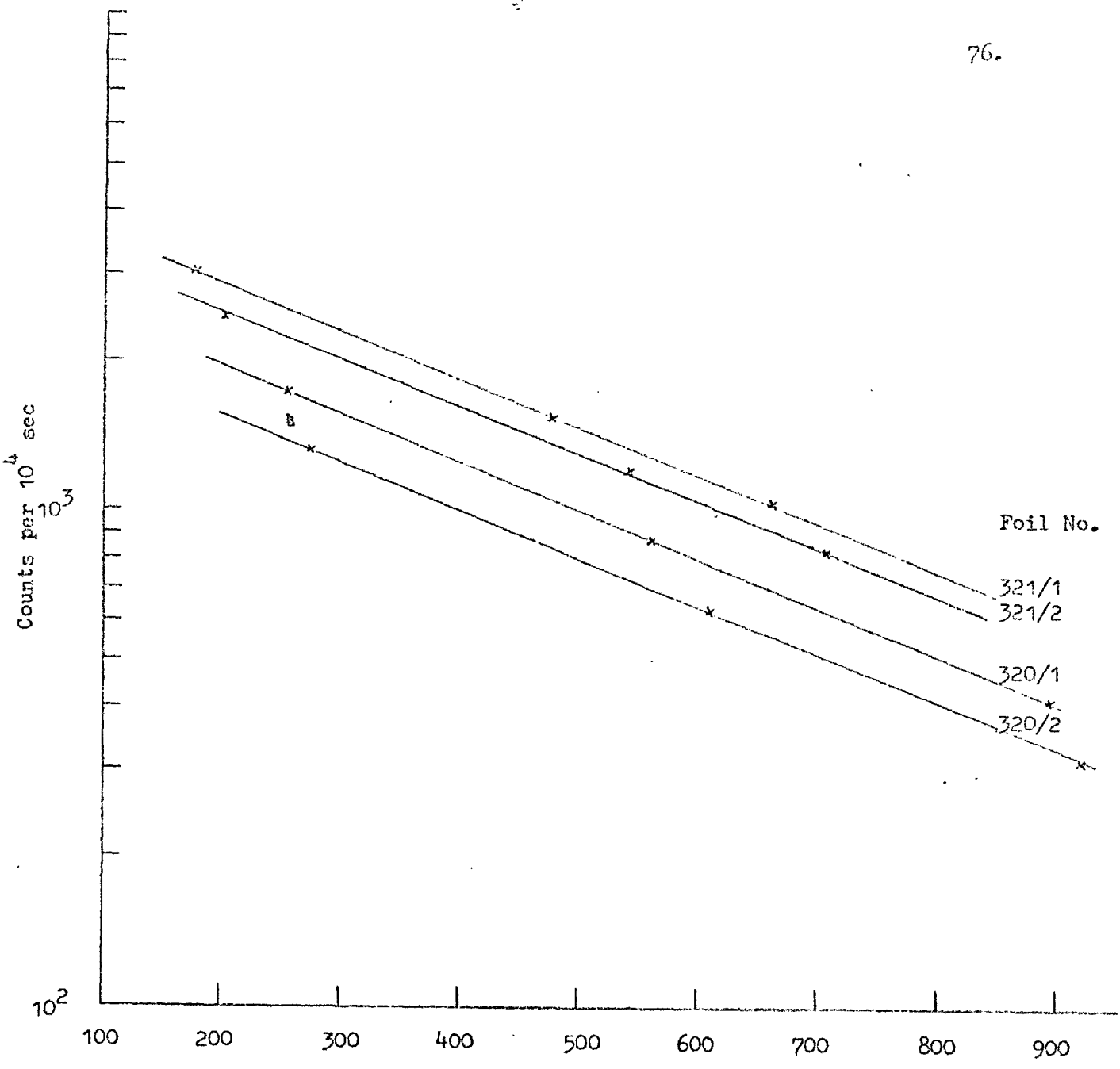

Figure 4.7

Typical Gamma Counting Results

Isotope	FOIL		FISSION CHAMBER DEPOSITS	
	U-235	U-238	U-235 1.12	U-238 3.5
U-234	1.20	-	1.19	-
U-235	95.54	0.39	92.95	0.03
U-236	0.17	-	0.18,	-
U-238	3.10	99.61	5.68	99.97

Table 4.1.

Composition of Foils and Fission Chamber Deposits (Atomic per cent)

Accuracy $\pm$ 0.7%

	FOIL 1.12 U-235	FOIL 3.5 U-238
OBSERVED COUNT	40 301 500	72 605 900
DEAD TIME CORRECTION	0.17%	0.29%
ZERO BIAS CORRECTION	1.61%	6.87%
FOIL THICKNESS CORRECTION	0.06%	-
CORRECTED COUNT	41 107 600	74 058 000

Table 4.2.

Fission Rate Ratio Measurement - Observed Counts and Corrections
(Fission Chamber Measurement)

SOURCE	CORRECTION	ESTIMATED ACCURACY OF CORRECTION	UNCERTAINTY
FOIL MASSES			1.5%
ZERO BIAS CORRECTION	9%	10%	1%
FOIL THICKNESS CORRECTION	0.06%	20%	.01%
DEAD TIME CORRECTION	0.5%	10%	.05%
STATISTICS			.02%
ISOTOPIC COMPOSITION OF FOILS			.7%
FISSIONS IN IMPURITY ISOTOPES			.5%
		TOTAL R.M.S. ERROR	2%

Table 4.3.

Fission Rate Ratio Measurements - Sources of Error
(Fission Chamber Measurement)

From the above masses and the corrected fission chamber counts, the fission rate ratio was calculated as:

$$\frac{U^{238}\ (n,\ f)}{U^{235}\ (n,\ f)} = 0.0227 \pm .0005$$

A summary of possible sources of error is given in Table 4.3.

The fission rate ratio was determined from the foil activation experiments using the radiochemical yield values given by Croall [Croall 1967]. Results of the La-140 1.6 MeV gamma counting normalised to 300 hours after irradiation are shown in Table 4.4.

The fission rate ratios calculated from the foil activation measurements were:

1. $$\frac{U^{238}\ (n,\ f)}{U^{235}\ (n,\ f)} = 0.0225 \pm .0009$$

(Foils irradiated inside fission chamber)

2. $$\frac{U^{238}\ (n,\ f)}{U^{235}\ (n,\ f)} = 0.0222 \pm .0009$$

(Foils irradiated during a VIPER pulse)

A summary of possible sources of error is given in Table 4.5.

The good agreement between the fission rate ratio measurements made in steady-state and pulse irradiations indicates that the VIPER spectrum during a pulse is essentially the same as that measured using steady-state techniques.

The value taken for the U-235/U-238 fission rate ratio was the weighted mean of these results, namely:

$$\frac{U^{238}\ (n,\ f)}{U^{235}\ (n,\ f)} = 0.0225 \pm .0004$$

FOIL		MASS (mgm)	COUNTS PER 10^4 SEC AT 300 HOURS**	COUNTS PER SEC PER GM AT 300 HOURS
V5Ø1	U-235*	40.7	11224 ± 214	27.58
V5Ø2		36.0	10402 ± 280	28.89
V8Ø1	U-238*	37.4	253 ± 4	0.676
V8Ø2		34.1	234 ± 7	0.686
V503	U-235+	40.7	27360 ± 340	67.22
V504		32.5	21803 ± 256	67.08
V803	U-238+	38.3	614 ± 12	1.603
V804		39.3	628 ± 20	1.598

Table 4.4.

Fission Rate Ratio Measurement - Foil Counting Results

* Irradiated in Fission Chamber.

** Standard deviation obtained from fitting decay curve.

\+ Irradiated during a VIPER pulse.

SOURCE	UNCERTAINTY
DETECTOR STABILITY	1%
COMPOSITION OF FOILS	0.7%
IMPURITY FISSIONS	0.5%
RADIOCHEMICAL YIELDS	3%
STATISTICS	2%
FOIL MASSES	1%
TOTAL R.M.S. ERROR	4%

Table 4.5.

Fission Rate Ratio (Foil Measurements)

Sources of Error

4.8. Calibration Irradiation - Experimental Results

The results of the calibration irradiations are summarised in Table 4.6. These results were interpreted in terms of the gross foil count rate produced by a given number of fissions in the foil major constituent isotope, i.e. in the case of U-235 foils, the observed count rate from a foil per fission in U-235. This interpretation allows for easy calculation of the fission rate, and since the fission rate ratios of the impurity isotopes relative to the major constituent are constant does not introduce any systematic error. The calculated results are given in Table 4.7, and possible sources of error in Table 4.8. The values obtained from the calibration were:

1) $U\text{-}235$
$5.38 \pm 0.15 \times 10^{-11}$ gross foil counts sec^{-1} per U-235 fission

2) $U\text{-}238$
$5.92 \pm 0.23 \times 10^{-11}$ gross foil counts sec^{-1} per U-238 fission

FOIL		COUNTS PER SEC PER GM AT 300 HOURS	FISSION CHAMBER DEPOSIT	TOTAL CORRECTED COUNT *
V501	U-235	27.58	1.12	41 107 600
V502		28.89		
V505		40.02	1.12	59 447 900
V506				
V801	U-238	0.676	3.5	74 058 000
V802		0.686		

Table 4.6

Results of Calibration Irradiations

* Corrected for dead time, zero bias and foil thickness (See Section 5)

CALIBRATION	GROSS FOIL COUNTS PER SEC PER FISSION*
U-235 (a)	5.45×10^{-11}
U-235 (b)	5.31×10^{-11}
U-238	5.92×10^{-11}

Table 4.7

Results of Calibration Irradiations.

* Gross foil counts per second per fission in major constituent isotope.

SOURCE	UNCERTAINTY U-235	UNCERTAINTY U-238
FISSION CHAMBER DEPOSIT MASS	0.7%	1%
FOIL MASSES	1%	1%
GAMMA COUNTING STATISTICS	2%	3%
DETECTOR STABILITY	1%	1%
IMPURITY FISSIONS	0.5%	1.3%
FISSION COUNTING STATISTICS	NEGLIGIBLE	NEGLIGIBLE
FISSION CHAMBER CORRECTIONS	1%	1%
FOIL COMPOSITIONS	0.7%	.7%
TOTAL R.M.S. ERROR	2.8%	3.9%

Table 4.8

Fission Calibration Measurements - Sources of Error

4.9. References

Covell 1959 - Covell, D.F.
Analytical Chemistry, 31, 1785 (1959).

McCormick 1971 - McCormick, W.
Private Communication.

Yule 1969 - Yule, H.P.
Modern Trends in Activation Analysis
Nat. Bur. Stand (U.S.) Special Publication
312, Vol. 2, 1969.

	DIAMETER	THICKNESS/ LENGTH
FISSION COUNTING FOILS	$0.297^{+0}_{-.003}$ in	.002 to .003 in
SAMPLE SLUGS	$0.39 \pm .01$ cm	$1.00 \pm .01$ cm
FISSION CHAMBER DEPOSITS	$1.19 \pm .01$ in	-

TABLE 4.9

Nominal Dimensions of Samples and Fission Counting Foils

5. CALIBRATION OF STANDARD FOIL FOR FISSION MEASUREMENTS

5.1. General

Measurements of the number of fissions produced in the sample by a VIPER pulse were made by gamma counting foils of the sample material for 1.6 MeV La-140 activity (Section 4). These measurements were made relative to a calibration experiment in which foils were irradiated in a back-to-back fission chamber, one side of which held the foils, the other side being used as a parallel-plate fission chamber.

In order to irradiate the foils to a level comparable with that achieved in a full-sized VIPER pulse, it was necessary to irradiate the chamber in the large irradiation cavity at a power of 600 W for a period of about 5 hours. Operational problems and heating considerations precluded the use of longer times or higher powers.

To monitor the fission rate at such a power it was necessary to use a fission chamber deposit with a total mass of about 100 μgm U-235, or serious dead-time problems would be encountered. No calibrated foil of such a mass suitable for use in a parallel plate demountable chamber existed at A.W.R.E., so it was necessary to assay one. This was performed by two independent methods:

1. Comparison with a known foil in the subcritical assembly PANDA.
2. Low-geometry alpha assay.

5.2. Calibration in PANDA

The subcritical assembly PANDA is a small VERA-type assembly using fuel plates assembled in rods, the composition of which may be readily changed to modify the core constituents. 14 MeV neutrons may be injected into the assembly by means of an accelerator using the D-D reaction.

For the calibration a back-to-back demountable fission chamber containing the foil to be calibrated (labelled 1.12), and a blank platinum backing foil

was installed on the central plane of a dummy fuel element situated near the core centre of PANDA assembly 1B. The filling and operation of the fission chamber was as described in Section 4. The alignment and position of the fission chamber were carefully noted.

The assembly was then injected with 14-MeV neutrons and the count-rate from the unknown foil compared with that from a monitor fission chamber permanently located in PANDA.

The chamber was then replaced with a similar one containing an assayed foil and the comparison repeated.

In order to check any inaccuracy in the positioning of the two chambers, the first chamber was subsequently replaced and the experiment repeated. The results are shown in Table 5.1.

5.2(1) Fission Chamber Corrections

5.2(1)(i) Zero Bias Correction.

The pulse-height distribution from the two chambers was measured using a multi-channel analyser. A typical spectrum for foil 1.12 is shown in Figure 5.1. The correction was determined by extrapolating the differential bias curve to zero energy, and estimating the fractional loss below the discriminator bias level.

The corrections were found to be:

Foil 1.12	0.7%
Foil T4	0.7%

with an estimated accuracy of $\pm$ 0.2%. As these corrections were identical, no correction was made to the figures in calculating the ratios shown in Table 5.2.

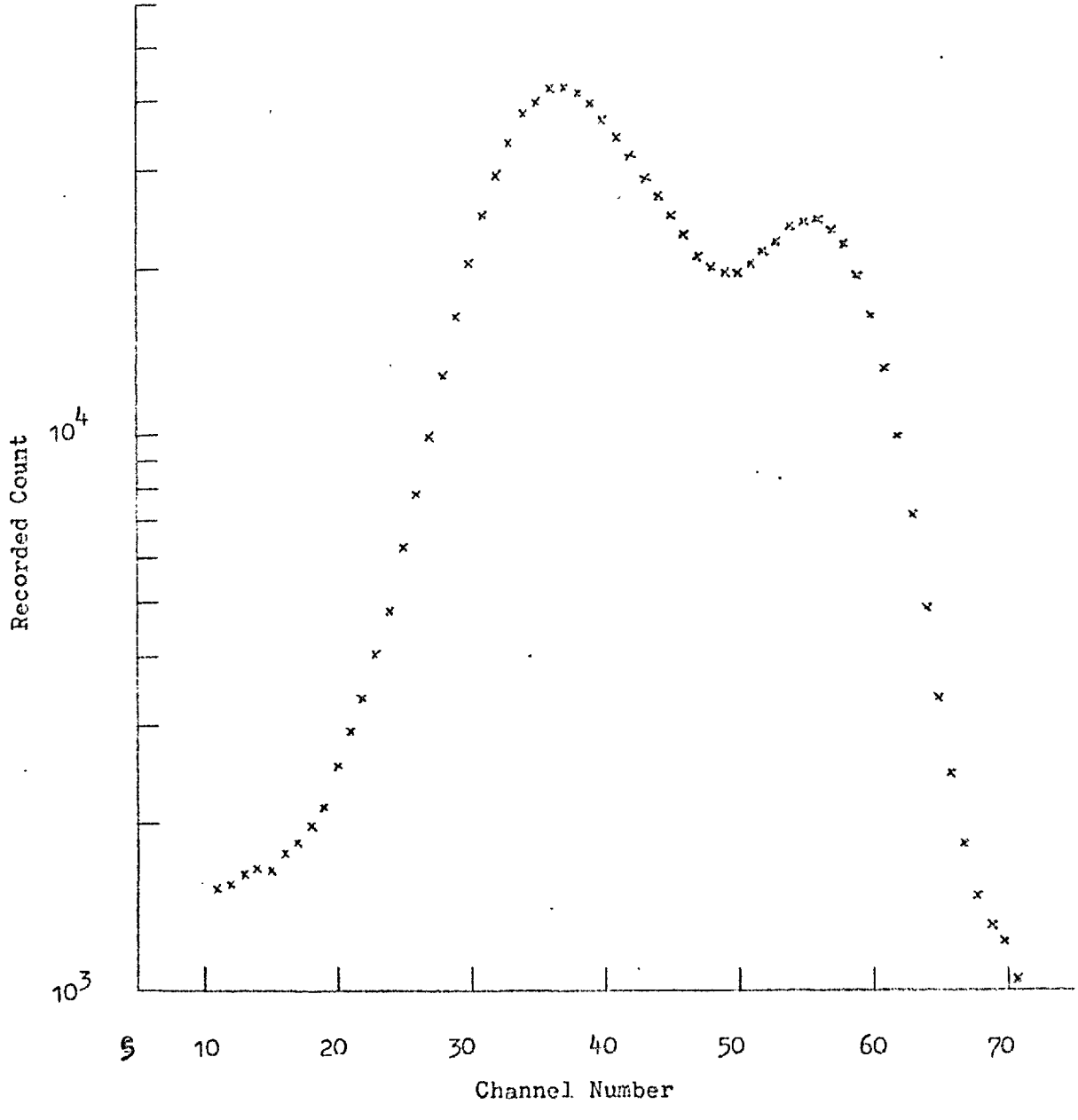

Figure 5.1

Fission Chamber Spectrum - Foil 1.12

5.2(1)(ii) Foil Thickness Correction

The correction for counting loss due to non-escape of fission fragments from the foil has been shown to be described by:

$$E(B) = 1 - \frac{t}{2[R_o - R(B)]} \qquad (5.1)$$

[Rossi and Staub 1949], where

E(B) is the counter efficiency at the bias B

t is the thickness of the foil

R_o is the range of the fission fragments

R(B) is the range of a fragment which leaves it with just enough energy to be detected at the bias B (both ranges measured in the foil material)

White [White 1969] has pointed out that the surface roughness of the foil should be taken into account when estimating the foil thickness t.

In order to estimate the foil thickness correction it has been assumed that an approximately linear range-energy relationship holds for the fission fragments. This is a reasonable assumption over a limited energy range [Bohr et al 1940]. The following values have been used:

R_o = 12.6 mgm cm^{-2} [Rossi and Staub 1949]

B = 0.2 x average fragment energy

then

$E \doteq 1 - 0.0005$

for a foil of density 10 μgm cm^{-2}.

This correction is therefore negligible for the foil 1.12.

5.2(1)(iii) Dead-Time Corrections

The maximum count rates observed during the calibration were:

Foil 1.12 84.9 counts sec^{-1}

Foil T4 161.4 counts sec^{-1}

1.12	MONITOR	BLANK
8344	157581	47
8476	160838	22
8359	161165	16
8493	159576	15
8427	160503	18
T4	MONITOR	
66171	160953	
65775	161208	
66674	161641	
65435	159006	
64530	158143	
64528	157702	
1.12	MONITOR	BLANK
7674	147200	19
7784	148412	18
7856	146719	14
7944	147239	15
7662	147605	19
7792	146632	14

Table 5.1

Results of 100 second counts comparing the count rates of the unknown foil 1.12 and the standard foil T4 with a PANDA monitor chamber.

The dead-time of the counting channels had been determined [M. Mullender] to be 0.4 μsec. The counting loss due to dead time in the calibration was therefore negligible.

5.2(2) Error due to Counter Position

The good agreement obtained between the ratios observed for the first and second installations of the chamber containing foil 1.12 indicates that the errors introduced by the variation in position of the chambers is negligible (Table 5.2). The chambers were situated at the PANDA core centre, where the flux gradient was a minimum.

5.2(3) Error due to Isotopic Composition of the Foils

Both foils had been prepared at A.W.R.E. from the same batch of 93% enriched U-235 [White]. No errors should therefore have been introduced by differences in the isotopic composition of the two foils.

5.2(4) Mass of Standard Foil T4

The foil T4 had been calibrated by two independent methods. By alpha particle assay [White] and by absolute calibration in a 14-MeV neutron beam [McCormick 1971]. This latter method gave an effective mass, which included the foil thickness correction.

The values obtained were:

1. Alpha assay 613 ± 6 μgm U235
2. 14-MeV neutron beam 614 ± 6 μgm U235

The thickness correction for the foil was calculated to be 1.1% (5.1), and thus the effective mass of the foil, as determined by alpha assay was:

607 ± 6 μgm U235

The final value for the effective mass of U-235 in the foil T4 was taken to be the mean of these values:

610 ± 6 μgm U235

RATIO	VALUE	ERROR*
$\frac{1.12}{\text{MONITOR}}$ (a)	0.0526	0.0002
$\frac{T4}{\text{MONITOR}}$	0.410	0.002
$\frac{1.12}{\text{MONITOR}}$ (b)	0.0525	0.0002

Table 5.2

Mean Counting Rate Ratios Observed in the Calibration Experiment

* One standard deviation

5.2(5) Results

The calculated ratios of the count rates observed in the experiment are shown in Table 5.2.

From these ratios the mass of U-235 in the foil 1.12 (equivalent to the 'effective mass', since the foil thickness correction is negligible) was found to be:

78.18 ± 0.91 µgm U-235

5.3. Calibration by Alpha Assay

The method of low - or medium - geometry alpha counting has long been used for the accurate assay of active deposits, and relative measurements may be made to accuracies of 0.1% [Bambynek 1966, White 1969].

Although the correction required for the geometry factor is large, it can be measured very accurately, and other corrections, e.g. backscattering and absorption are usually very small for alpha particles of energy greater than a few MeV.

The foil 1.12 was assayed in two alpha counters, one at A.W.R.E., and one at Imperial College. Figure 5.2 shows the Imperial College alpha counter, which was very similar to the one used at A.W.R.E.

The counter comprises an evacuated chamber, enclosing a surface barrier semiconductor detector supported above an aperture defining the solid angle over which alpha particles may be detected. A baffle reduces the effect of alpha particles scattered from the counter walls. The geometry-defining aperture is bevelled to reduce the effect of scattering at the aperture edge [Lerch and Spernol 1965].

5.3(1) Geometry Calculations

The geometry factor was calculated by a formula due to Curtis et al [Curtis 1955]. A review of geometry calculations has been given by Lerch and Spernol [Lerch and Spernol 1955].

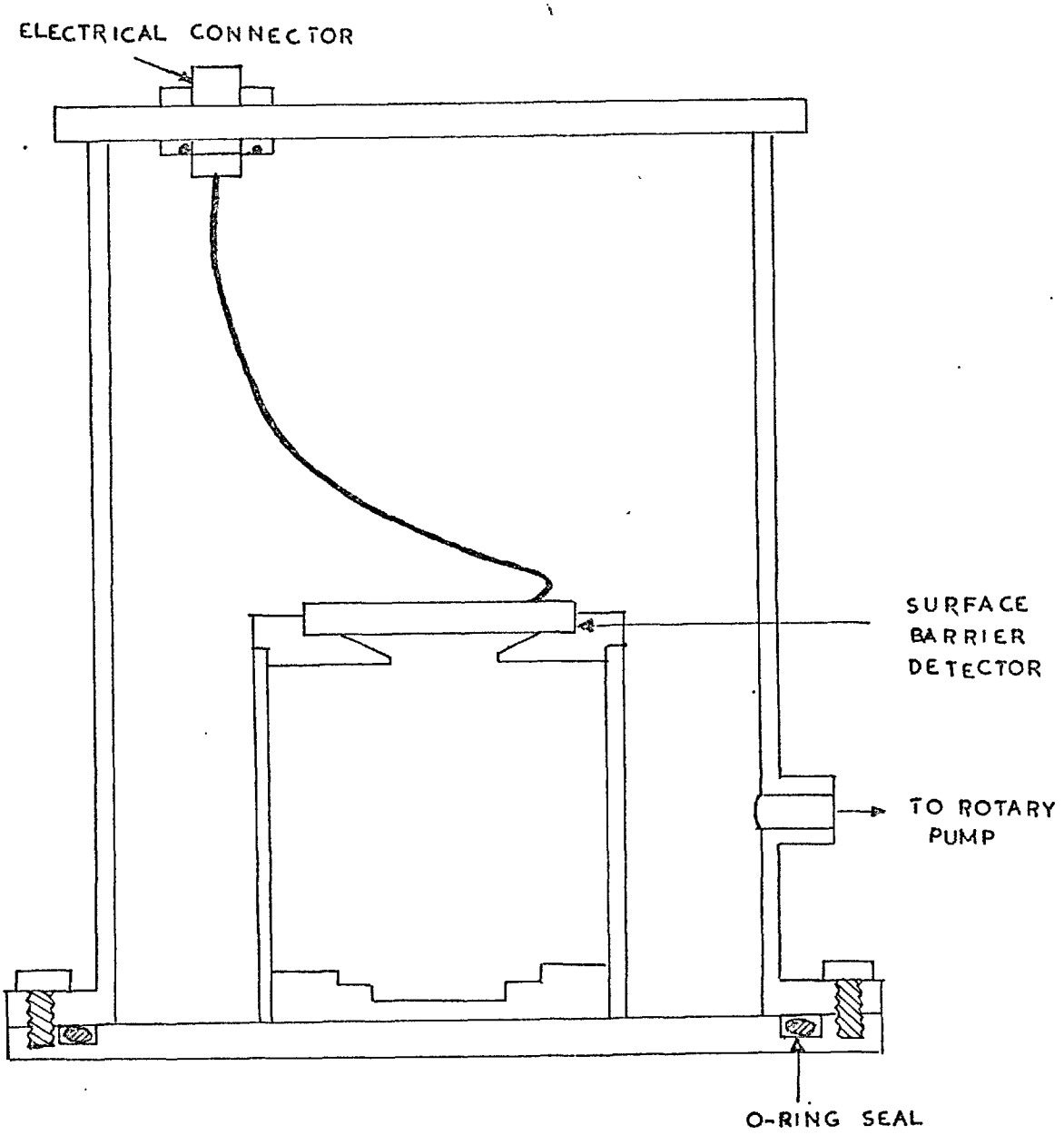

FIGURE 5.2

LOW GEOMETRY ALPHA COUNTER

$$G = \frac{2}{b^2} \int_0^b G_p \rho \, d\rho \qquad (5.2)$$

$$G_p = \frac{a^2}{4z^2} \left[1 - \frac{3}{4} \frac{a^2 + 2\rho^2}{z^2} + \frac{5}{8} \frac{a^4 + 3\rho^4 + 6a^2\rho^2}{z^4} - \frac{35}{64} \frac{a^6 + 4\rho^6 + 12a^4\rho^2 + 18a^2\rho^4 + \ldots\ldots}{z^6} \right] \qquad (5.3)$$

See Figure 5.3 for an explanation of the symbols.

In the case of the A.W.R.E. counter, the dimensions were well known, the counter having been in use for a period of years. The Imperial College counter had only been used once before and the geometry factor was therefore recalculated, and checked with a calibrated Am-241 alpha source.

The dimensions of the counters and the calculated geometry factors are given in Table 5.3. As the equations (5.2) and (5.3) are not amenable to differentiation, the error in the geometry factor was calculated using estimates for the partial derivatives used in the "chain rule" obtained numerically (Table 5.4)

5.3(2) Scattering Effects

Small-angle backscattering from the foil and backing material may be ignored in low-geometry work, since such events give rise only to particles with tragectories almost parallel to the foil surface.

Corrections for large-angle backscattering due to Coulomb scattering by the atomic nuclei have been calculated by P. White [White 1965] to be about 0.2% for a relatively thick foil (0.5 mgm cm^{-2}).

Bambynek [Bambynek 1966] has shown that scattering from the walls of the counting chamber contributes an error of about 0.05% for a favourable geometry, and that scattering from the residual gas in the counter may be ignored for alpha particles of sufficient energy.

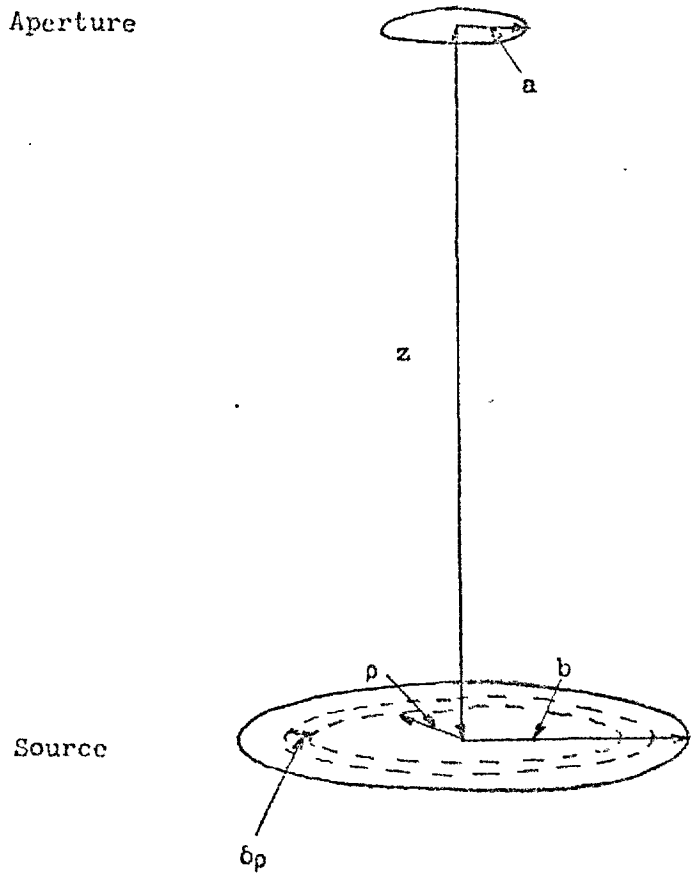

a - Detector Aperture Radius

b - Source Radius

z - Axial Displacement of Source from Detector Aperture

$\delta\rho$ - Element of Radius at radius ρ

Figure 5.3

Alpha Counter Geometry Calculation Symbols

DIMENSION	a	b	z
I.C. (INS) FOIL 1.12	0.2500 ±0.0005	0.594 ±0.001	1.538 ± 0.003
I.C. (INS) Am-241 SOURCE	0.2500 ±0.0005	0.137 ±0.001	1.539 ± 0.003
A.W.R.E. (CM)	0.5053 ±0.0005	1.508 ±0.001	9.56 ± 0.01

COUNTER	G
I.C. FOIL 1.12	$0.5862 \cdot 10^{-2}$ $\pm 4.0\ 10^{-5}$
I.C. Am-241 SOURCE	$0.6445\ 10^{-2}$ $\pm 5.0\ 10^{-5}$
A.W.R.E. FOIL 1.12	$0.6856\ 10^{-3}$ $\pm 5.0\ 10^{-6}$

Tables 5.3

Calculation of geometry factor. For explanation of symbols see Figure 5.3.

a	b	Z	G
0.250	0.594	1.538	0.005863
0.255	0.594	1.538	0.006096
0.250	0.599	1.538	0.005853
0.250	0.594	1.543	0.005829

Hence:

$$\left.\frac{\Delta G}{\Delta a}\right|_{b,z} \doteq + 0.047$$

$$\left.\frac{\Delta G}{\Delta b}\right|_{a,z} \doteq - 0.002$$

$$\left.\frac{\Delta G}{\Delta Z}\right|_{a,b} \doteq - 0.007$$

Table 5.4

Estimation of the dependence of G on uncertainties in a, b and z.

For an explanation of the symbols see Figure 5.3.

ISOTOPE	ATOMIC %
U-234	1.19
U-235	92.95
U-236	0.18
U-238	5.68

Table 5.5

Mass spectrometric data for the composition of foils 1.12 and T4.

Accuracy $\pm$ 0.7% of quoted value.

ISOTOPE	ALPHA HALF-LIFE
U-234	$2.475 \pm 0.016 \times 10^5$ *
U-235	$7.13 \pm 0.16 \times 10^8$ *
U-236	$2.391 \pm 0.018 \times 10^7$ *
U-238	4.51×10^9

Table 5.6

Alpha Half-Life Data

* Fleming, Ghiorso and Cunningham. Phys. Rev. 88, 642, (1952).

Am-241	VALUE (D.P.S.)
ALPHA ASSAY	$6.00 \pm 0.10 \times 10^3$
AMERSHAM VALUE	$5.92 \pm 0.10 \times 10^3$

Table 5.7

Comparison of the alpha assay and Amersham values for the Am-241 source strength.

The correction for absorption of alpha particles in the foil material may be calculated in a way analogous to that used for fission fragments (5.1). The correction is negligible for a foil such as 1.12.

5.3(3) Results

Foil masses were calculated from the known isotopic composition of the foil (Table 5.5) and the half-life data shown in Table 5.6.

The results obtained from the calibrated Am-241 source are shown in Table 5.7. The value obtained by alpha counting is in good agreement with the value quoted by Amersham.

The values obtained for the mass of foil 1.12 were:

1. A.W.R.E. 79.52 $\pm$ .92 µgm U-235
2. I.C. 78.82 $\pm$ .91 µgm U-235

5.4. Mass of Calibrated Foil

The final value adopted for the mass of U-235 in the foil 1.12 was the weighted mean of the three measurements, namely:

78.84 $\pm$.52 µgm U-235

5.5. References

Bambynek 1966 - Precise Solid-Angle Counting.
W.B. Bambynek.
Standardisation of Raio nuclcles.
Proceedings of a Symposium.
I.A.E.A. Vienna. 1967.

Bohr et al 1940 - Bohr, Boeggild, Brostroem and Lauritsen
Phys. Rev. 58, 839 (1940).

Curtis 1955 - Curtis, Heyd, Olt and Eichelberger.
Nucleonics 13 (5) 38 (1955).

Lerch and Spernol 1965 - Geometry Factors in Low and Medium Geometry Solid Angle Counting.
Lerch and Spernol.
Round Table on High Precision Mass Spectrometry and Alpha Counting.
EANDC 53 "S" (1965).

McCormick 1971 - W.B. McCormick and D.L.E. Smith.
Private Communication.

Mullender - M.L. Mullender.
Private Communication.

White - P. White.
Private Communication.

White 1965 - Alpha and Fission Counting of Thin Foils of Fissile Material.
P. White.
Round Table on High Precision Mass Spectrometry and Alpha Counting.
EANDC 53 "S" (1965).

White 1969 - P. White,
Nuclear Instr. and Meth.
79, 1 (1970).

Rossi and Staub 1949 - Ionization Chambers and Counters.
B.B. Rossi and H.H. Staub.
National Nuclear Energy Series:
Division V, Vol. 2.
McGraw Hill (1949).

6. EXPERIMENTAL RESULTS

6.1. General

Because of the very large range of delayed neutron count rates over which it was necessary to make measurements, it was decided to make three irradiations for each isotope, in order to make accurate measurements at short, medium and long times after irradiation. Operational problems with the VIPER reactor made it more desirable to accentuate the longer-lived groups by an intense burst irradiation than by using a saturation irradiation (Section 2). Delayed neutron counts were obtained by this method over periods in excess of 500 seconds after irradiation.

6.2. Reactor Background

Although the neutron detector was shielded from the reactor by a six-foot thick concrete wall, the rabbit tube itself provided a channel through which neutrons and gamma rays could ender the detector. In order to estimate the contribution to the observed delayed neutron count from the reactor, and from any possible activation of the rabbit, an irradiation was performed in which an empty rabbit was fired into the detector. The observed neutron count rate from this irradiation is compared with that from a similar irradiation, in which a foil of U-235 of mass 30 mgm was contained in the rabbit, in Figure 6.1.

It may be seen that the decay of the background contribution from the reactor is much more rapid than the delayed neutron decay, and represents less than 1% of the delayed neutron count rate at times greater than 100 msec after irradiation. This was considered satisfactory, since to provide a great deal more shielding would have proved difficult, and the flight path of the rabbit could not have been shielded from the reactor.

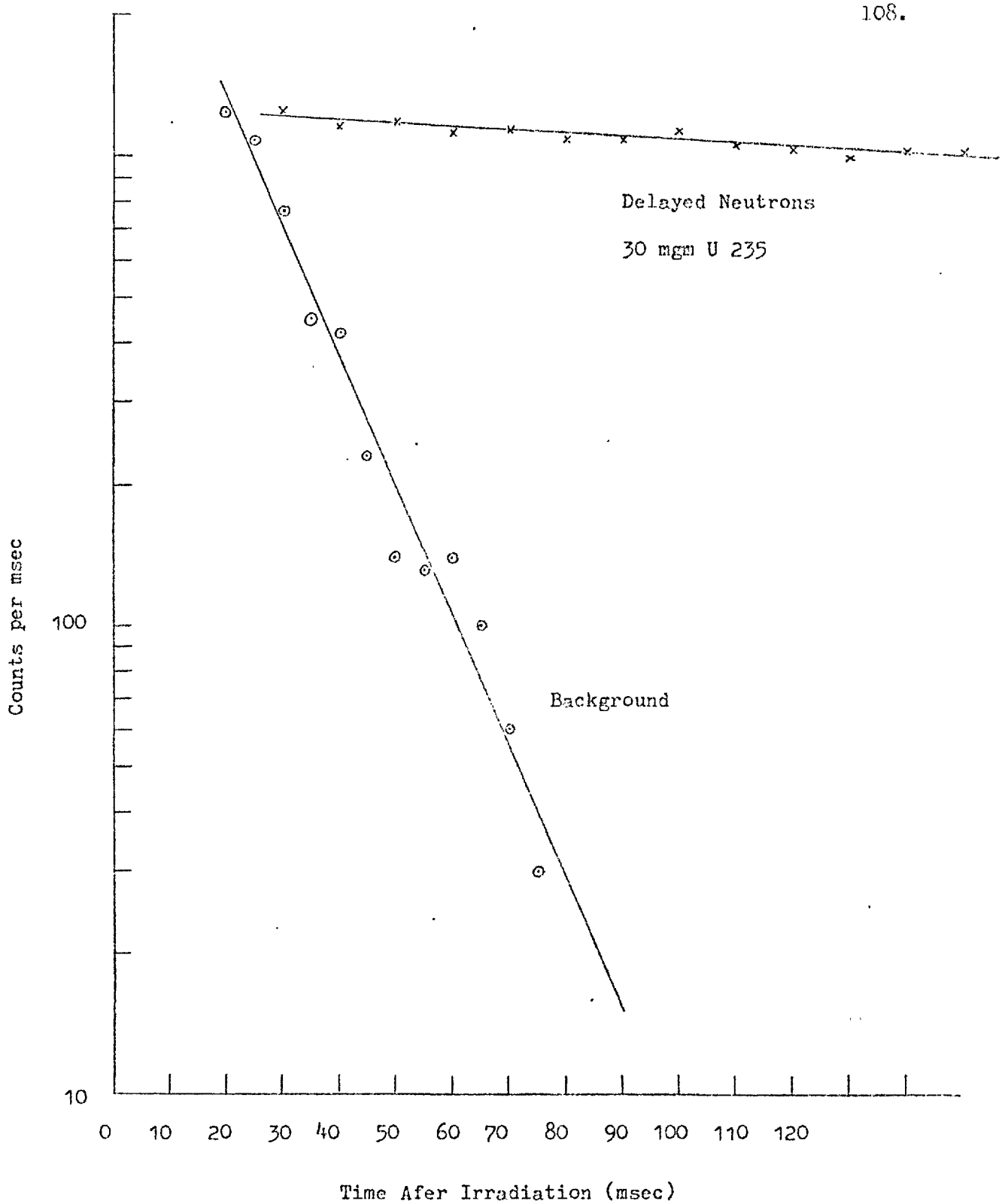

Figure 6.1

Reactor Background

6.3. Dead Time of Data Acquisition System

The real-time data acquisition system using the ARGUS computer operated by reading and clearing 2000-series scalers at prearranged intervals. During the read and clear cycle, the scalers were inhibited from accepting counts from the delayed neutron detector. In order to estimate the dead time of this system, the output from a crystal clock operating at a frequency of 1 MHZ was fed into one of the scalers, and the result multiscaled with an interval of 100 msec. The mean counting loss per time interval from 100 such counts was found to be 70.1 $\pm$ 2 counts, and the dead time per read was therefore 70 $\pm$ 2 μsec. This represented a dead time of 0.7% in the worst case (i.e. 10 msec channels).

6.4. Experimental Results

The procedure adopted for the observation of the delayed neutron count rate from a particular fissile isotope was to make three irradiations to study short, medium and long times. The pulsed reactor VIPER can be predictably controlled over the range of one tenth of a full power pulse to the maximum power pulse. By adjusting the sample mass from one tenth of a gram to ten grammes, it was therefore possible to vary the total sample fissions over three orders of magnitude. The irradiations and sample masses are tabulated, along with the results of the fission foil counting in Tables 6.1.

6.4(1) Timing Measurements

The firing of the rabbit system was initiated by a 10 KW power trip on the reactor. For irradiations made with low power pulses, the slow initial reactor period necessitated the introduction of a 20 msec delay between the 10 KW trip and rabbit firing. The rabbit flight time was measured by gating a clock between the 10 KW signal and one derived from the breaking of

a wire at the arrester end of the rabbit tube. This timing was used solely to monitor the rabbit performance and to predict the rabbit arrival position. A clock was also gated between the 10 KW pulse and the first read signal to the 2000 series scales, this being used to determine the time from which the delayed neutron counting started. The timing of the ARGUS computer was derived from a crystal clock interrupting the execution of the program. The timing measurements associated with each delayed neutron measurement are given in Tables 6.2.

6.4(2) Detector Efficiency Measurements

Prior to each measurement, a Pu-240 spontaneous fission source was counted in a reproducable position with respect to the delayed neutron detector and rabbit tube. The detector was then moved to a position such that the rabbit should arrive at the position of peak detector efficiency (this being the region of minimum rate of change of efficiency with sample displacement). The detector background was then observed, and after the pulse the rabbit penetration measured. These readings are given in Tables 6.2.

6.5. Analysis of Group Structure

The observed delayed neutron counts were corrected for detector efficiency, dead time and delayed neutrons from impurity isotopes using Keepins data [Keepin 1956]. The results of the three irradiations were normalised (in each case the runs did not differ by more than the estimated error where joined), and plotted for initial exponential peeling by hand. The estimates for the group yields and decay constants obtained by this method were then used as initial parameters for an iterative least squares fit by computer.

In order to simplify the fitting procedure, the half-life of the longest-lived delayed neutron group was held fixed at the radiochemically

PULSE NO.	PULSE SIZE	SAMPLE MASS (GM)	TOTAL FISSION FOIL MASS (GM)	TOTAL FOIL COUNT SEC^{-1}	TOTAL SAMPLE FISSIONS*
319	$\frac{1}{10}$	0.0372	0.0372	$0.374 \pm .005$	6.89×10^{9}
320	MAX	0.1086	0.1086	$4.118 \pm .094$	7.66×10^{10}
321	MAX	8.3015	0.1018	$6.374 \pm .063$	9.66×10^{12}

Table 6.1(a)

U-235 Irradiations

* not corrected for self-multiplication of fissions in the sample (Total U-235 fissions)

PULSE NO.	PULSE SIZE	SAMPLE MASS (GM)	TOTAL FISSION FOIL MASS (GM)	TOTAL FOIL COUNT SEC^{-1}	TOTAL SAMPLE FISSION*
333	MAX	0.1100	0.1100	$0.0916 \pm .0007$	1.54×10^{9}
335	MAX	1.1193	0.1123	$0.1002 \pm .0030$	1.69×10^{10}
336	MAX	8.4522	0.1107	$0.0837 \pm .002$	1.08×10^{11}

Table 6.1(b)

U-238 Irradiations

* not corrected for self-multiplication of fissions in the sample (Total U-238 fissions)

PULSE 319

REFERENCE SOURCE COUNT RATE		10.45 ± 0.12 COUNTS sec^{-1}
DETECTOR POSITION		45.0 cm
PENETRATION		24.6 cm
TIME CHANNELS	1 mS	300
	10 mS	300
	100 mS	300
	1S	300
DELAY BEFORE FIRST READ PULSE		111 mS
NEUTRON CHANNEL BACKGROUND		3.72 COUNTS sec^{-1}
GAMMA CHANNEL BACKGROUND		0.44 COUNTS sec^{-1}

PULSE 320

REFERENCE SOURCE COUNT RATE		14.78 ± 0.14 COUNTS sec^{-1}
DETECTOR POSITION		45.0 cm
PENETRATION		25.4 cm
TIME CHANNELS	1 mS	0
	10 mS	0
	100 mS	300
	1S	500
DELAY BEFORE FIRST READ PULSE		84.5 mS
NEUTRON CHANNEL BACKGROUND		4.03 COUNTS sec^{-1}
GAMMA CHANNEL BACKGROUND		0.31 COUNTS sec^{-1}

PULSE 321

REFERENCE SOURCE COUNT RATE		14.04 ± 0.14 COUNTS sec^{-1}
DETECTOR POSITION		46 cm
PENETRATION		35.3 cm
TIME CHANNELS	1 mS	0
	10 mS	0
	100 mS	0
	1S	1000
DELAY BEFORE FIRST READ PULSE		120 mS
NEUTRON CHANNEL BACKGROUND		3.57 COUNTS sec^{-1}
GAMMA CHANNEL BACKGROUND		0.42 COUNTS sec^{-1}

Table 6.2(a)

Efficiency and Timing Measurements - U-235

PULSE 333

REFERENCE SOURCE COUNT RATE		12.74 ± .12 c.p.s.
DETECTOR POSITION		50.0 cm
PENETRATION		27.3 cm
TIME CHANNELS	1 mS	0
	10 mS	100
	100 mS	300
	1S	300
DELAY BEFORE FIRST READ PULSE		31.0 mS
NEUTRON CHANNEL BACKGROUND		1.63 c.p.s.
GAMMA CHANNEL BACKGROUND		0.39 c.p.s.

PULSE 335

REFERENCE SOURCE COUNT RATE		12.86 ± .12 c.p.s.
DETECTOR POSITION		45.0 cm
PENETRATION		29.3 cm
TIME CHANNELS	1 mS	0
	10 mS	0
	100 mS	300
	1S	300
DELAY BEFORE FIRST READ PULSE		113.0 mS
NEUTRON CHANNEL BACKGROUND		1.59 c.p.s.
GAMMA CHANNEL BACKGROUND		0.42 c.p.s.

PULSE 336

REFERENCE SOURCE COUNT RATE		12.27 ± .12 c.p.s.
DETECTOR POSITION		42.0 cm
PENETRATION		38.7 cm
TIME CHANNELS	1 mS	0
	10 mS	0
	100 mS	0
	1S	500
DELAY BEFORE FIRST READ PULSE		557 mS
NEUTRON CHANNEL BACKGROUND		1.50 c.p.s.
GAMMA CHANNEL BACKGROUND		0.38 c.p.s.

Table 6.2(b)

Efficiency and Timing Measurements - U-238

determined value for Br^{87}, which has been shown [Coryell 1963] to be the major component (> 95%) of the longest-lived group. The fitting procedure due to Powell [Powell] was used.

In neither case was it found possible to represent the decay curve by a sensible 6-group structure. Only five groups could be fitted, increasing the number of groups produced non-significant or negative amplitudes. The 5-group representations obtained are given in Tables 6.3.

6.6. Absolute Yield Measurements

The absolute yield of delayed neutrons for each isotope was determined from the observed delayed neutron counts and the measured fission rate. Corrections were applied for the counting loss during rabbit flight time reactor background contribution to the observed count, the presence of delayed-neutron producing impurities in the sample, detector and data-acquisition system dead times and self-multiplication of fissions in the samples.

6.6(1) Correction for counts due to sample gamma emission

The problem of the detection of gamma rays from the sample proved to be less critical than had been expected. At no time during the measurements was the observed count rate in the gamma monitor not wholly attributable to its small neutron efficiency. No correction was therefore made to the observed delayed neutron counts for scintillations caused by gamma rays from the sample.

6.6(2) Counting loss during rabbit flight time

The counting loss during the sample transfer was estimated by extrapolating the fitted decay curve to zero time. This is almost certainly an overestimate, since growth-and-decay effects are probably present. No information, however, is available on these effects. The corrections applied were of order 4%.

a_i	λ_i sec^{-1}
0.0311 ± 0.0002	0.0127
0.246 ± 0.001	0.0281 ± 0.0001
0.108 ± 0.003	0.113 ± 0.001
0.527 ± 0.002	0.299 ± 0.001
0.088 ± 0.030	3.37 ± 0.14

$X^2 = 794$ $\nu = 950$ $p \doteq 0.5$

Table 6.3(a)

Results of a 5-group bit to the U-235 Delayed Neutron Decay

a_i	λ_i sec^{-1}
0.0078 ± 0.0005	0.0127
0.138 ± 0.002	0.0278 ± 0.0003
0.198 ± 0.011	0.146 ± 0.002
0.351 ± 0.010	0.399 ± 0.007
0.305 ± 0.007	3.79 ± 0.09

$X^2 = 371$ $\nu = 420$ $p \doteq 0.5$

Table 6.3(b)

Results of a 5-group bit to the U-238 Delayed Neutron Decay

6.6(3) Reactor Background Contribution

The contribution to the observed delayed neutron counts from the reactor pulse was estimated from Figure 6.1. This contribution was only important for the measurements made at short times, and was estimated, using the known fission rate ratios for U-238, and the sample masses used in the measurements to be less than 0.1% of the total delayed neutron count for U-235, and about 0.4% for U-238.

6.6(4) Delayed neutrons from impurities in the sample

Corrections were made to the data for delayed neutrons emitted from sample impurities, using Keepin's data [Keepin 1956], and the measured fission rate ratio. This represented a correction of about 0.3% to the total delayed neutron count in the case of U-235, and 5% in the case of U-238.

6.6(5) Dead time corrections

Because of the large range of delayed neutron count rates observed from the sample after irradiation, it was inevitable that, at some times, relatively large dead time corrections would have to be made to the data. The only alternative would have been to have made a very large number of irradiations, which was not economically feasible. The data acquired in the three irradiations performed for each measurement were joined at times chosen as a compromise between adequate statistical accuracy and workable dead time corrections. The maximum dead time corrections which were applied are shown in Table 6.4. The overall dead time correction including that from the data acquisition system dead time was less than 1.5% of the total observed delayed neutron count.

6.6(6) Self-multiplication of fissions in the sample

Delayed neutrons born in a small fissile sample have a small probability of causing a fission before escaping. The effect of this is to increase the number of neutrons observed from the sample (since $\nu > 1$), and to increase the number of fissions observed in the sample.

It may be shown [see for example Keepin 1956] that the true delayed neutron yield is related to the observed delayed neutron yield approximately by the relationship:

$$Y_{true} = Y_{obs} (1 - [\bar{\nu}-1-\alpha] \Sigma_f \, lo) \qquad (6.1)$$

This correction is only significant for the largest samples used in the current experiments, and represents a correction of about 3% for the largest U-235 sample. However, the contribution of this irradiation to the overall delayed neutron decay is small, since most of the delayed neutrons are emitted at short times. The overall correction to the absolute yield from this source was less than 0.03% for U-235 and was even smaller for U-238.

6.7. Absolute Yield Values

The magnitudes of the corrections applied to the absolute yield values, and the estimated uncertainties in them are shown in Tables 6.5 and the uncertainties due to these corrections and the fission and detector efficiency measurements combined in Tables 6.6.

The neutron detector efficiency to delayed neutrons was calculated from the calibration curve (Figure 3.15) and the reported delayed neutron spectra [Batchelor 1956]. Keepin's delayed neutron yields [Keepin 1956] were used to determine the overall delayed neutron spectra at different times after irradiation, the spectrum reported for group 4 being assigned to groups 4, 5 and 6. The departure of the detector response from a true "flat response" necessitated a correction of 11%, to which was assigned an uncertainty of

U-235 TIME AT JOIN DEAD TIME CORRECTION	RABBIT ARRIVAL 5%	10 SEC 2%	200 SEC 2%
U-238 TIME AT JOIN DEAD TIME CORRECTION	RABBIT ARRIVAL 2%	2 SEC 2%	80 SEC 0.4%

Table 6.4

Maximum Corrections Applied for Dead Time Counting Loss

CORRECTION	MAGNITUDE	ESTIMATED ACCURACY OF CORRECTION	UNCERTAINTY
COUNTING LOSS DURING RABBIT FLIGHT TIME	3.9%	± 10%*	0.4%
REACTOR BACKGROUND	0.1%	± 100%	0.1%
DELAYED NEUTRONS FROM IMPURITIES	0.3%	± 10%	0.03%
DEAD TIMES	1.5%	± 5%	0.07%
SELF-MULTIPLICATION OF FISSIONS	0.03%	± 50%	0.02%
DETECTOR SPECTRAL RESPONSE	11%	± 10%	1.1%
		TOTAL R.M.S. UNCERTAINTY	1.2%

Table 6.5(a)

Corrections Applied to Delayed Neutron Yield Measurements U-235

CORRECTION	MAGNITUDE	ESTIMATED ACCURACY OF CORRECTION	UNCERTAINTY
COUNTING LOSS DURING RABBIT FLIGHT TIME	3.6%	± 10%	0.4%
REACTOR BACKGROUND	0.4%	± 100%	0.4%
DELAYED NEUTRONS FROM IMPURITIES	5.0%	± 10%	0.5%
DEAD TIMES	1%	± 5%	0.05%
SELF-MULTIPLICATION OF FISSIONS	NEGLIGIBLE		
DETECTOR SPECTRAL RESPONSE	11%	± 10%	1.1%
		TOTAL R.M.S. UNCERTAINTY	1.4%

Table 6.5(b)

Corrections Applied to Delayed Neutron Yield Measurements - U-238

SOURCE		UNCERTAINTY
FISSION MEASUREMENTS	FISSION CALIBRATION FOIL COUNTING STATISTICS DETECTOR DRIFT	2.8% 1.5% 1%
DETECTOR EFFICIENCY MEASUREMENTS	ABSOLUTE CALIBRATION EFFICIENCY STANDARDISATION SAMPLE ARREST POSITION CORRECTION	2.5% 1% 1%
SAMPLE MASSES		1%
CORRECTIONS TO RAW DATA		1.2%
TOTAL R.M.S. UNCERTAINTY		4.7%

Table 6.6(a)

Uncertainty in Absolute Yield Measurements - U-235

SOURCE		UNCERTAINTY
FISSION MEASUREMENTS	FISSION CALIBRATION FOIL COUNTING STATISTICS DETECTOR DRIFT	3.9% 2% 1%
DETECTOR EFFICIENCY MEASUREMENTS	ABSOLUTE CALIBRATION EFFICIENCY STANDARDISATION SAMPLE ARREST POSITION CORRECTION	2.5% 1% 1%
SAMPLE MASSES		1%
CORRECTIONS TO RAW DATA		1.4%
	TOTAL R.M.S. UNCERTAINTY	5.2%

Table 6.6(b)

Uncertainty in Yield Measurements - U-238

$\pm$ 10%, from the reported uncertainty in the spectrum measurements. The variation of detector efficiency to delayed neutrons with time was very small (less than 0.1%).

The total number of counts accrued for the yield measurements was of order 10^6 in the case of U-235 and 5×10^5 in the case of U-238, statistical errors on the delayed neutron counting were therefore negligible.

The values obtained for the absolute delayed neutron yields were:

U-235 0.0174 $\pm$ 0.0008 delayed neutrons per fission.

U-238 0.0492 $\pm$ 0.0025 delayed neutrons per fission.

6.8. Symbols

a_i The relative amplitude of the i' th delayed neutron group.

α Ratio of capture to fission cross-sections.

l_o The mean path length of a neutron in the sample.

λ_i The decay constant of the i'th delayed neutron group.

Σ_f Macroscopic fission cross-section.

ν Mean number of neutrons emitted per fission.

Y_{true} The true delayed neutron yield.

Y_{obs} The observed neutron yield.

6.9. References

Batchelor 1956 - Batchelor, R; Hyder, H.R. McK.
J. Nuclear Energy 3 7 (1956).

Coryell 1963 - Coryell, C.D.; Williams, E.T.
Private Communication to G.R. Keepin.

Keepin 1957 - Keepin, G.R.; Wimett, T.F.; Zeigler, R.K.
J. Nuclear Energy 6 1 (1957).

Powell - Powell, J.; Unpublished.

7. THE THEORY OF DELAYED NEUTRON EMISSION

7.1. General

Of the neutrons emitted in the fission process, a small proportion (about 1%) are not emitted at the instant of scission, or emitted promptly from the fission fragments, but are delayed by times long compared with the duration of the fission process. The mechanism of delayed neutron emission was first explained by Bohr and Wheeler [Bohr 1939] in terms of the liquid drop model. Fission fragments formed far from the region of beta stability undergo beta transitions along an isobaric sequence until a stable nuclide is reached. The energy release in beta-decay is in certain cases sufficiently great to leave the product nucleus in a state of sufficiently high excitation for neutron emission to occur.

7.2. Qualitative Discussion

Figure 7.1 shows a level scheme by which a precursor nuclide (Z, N) undergoes beta-decay to an excited state of the nuclide (Z + 1, N-1). If the excitation of the emitter nuclide is less than the binding energy of the last neutron then de-excitation by gamma emission only is possible. If, however, the level populated by beta-decay has an energy greater than the binding energy of the last neutron, then neutron - and gamma - emission compete for the de-excitation process.

As the neutron binding energy is generally about 5 to 8 MeV, nuclides which are expected to be precursors must exhibit relatively high beta decay energies. The neutron binding energy decreases with displacement from the nuclear stability line (this is the general trend, if even-odd and shell effects are ignored), on the neutron-rich side, and is particularly low just above a closed neutron shell. An unpaired particle has a lower binding energy than a paired one, and therefore delayed neutron emitters with N = magic number + 1, 3 will lie closer to the stability line than other emitters.

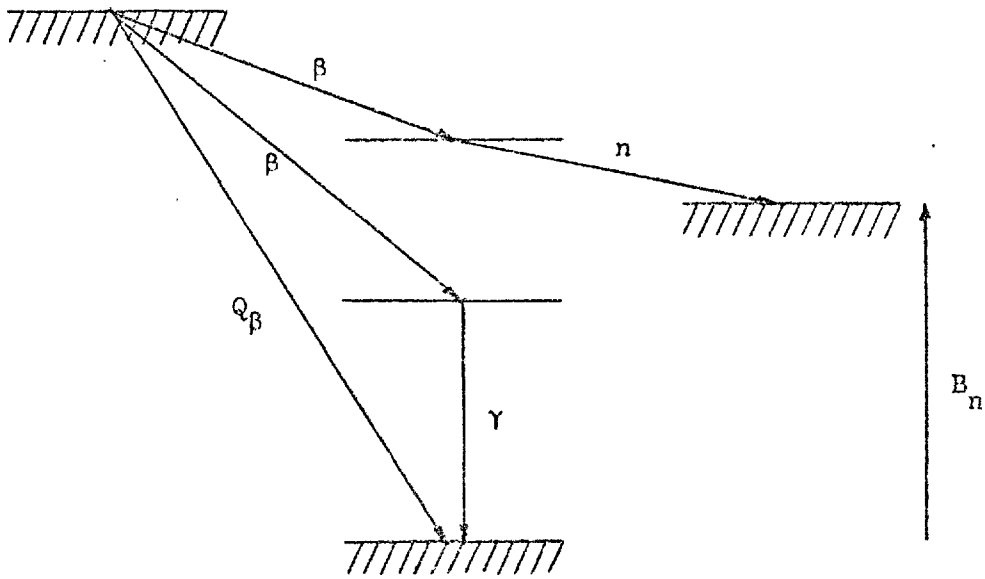

Precursor	Emitter	Final Nuclide
(Z,N)	(Z+1,N-1)	(Z+1,N-2)

Figure 7.1

Delayed neutron decay scheme

A displacement from the stability line of about three charge units on the neutron-rich side is consistent with sufficiently high beta-decay energies for delayed neutron emission.

Delayed neutron precursors which lie fairly close to the stability line are of greatest interest in the fission process since only these are produced with appreciable yield.

7.3. Delayed Neutron Emission

The probability of delayed neutron emission by the scheme of Figure 7.2 is given by the product of the probability of beta decay to a level above the binding energy of the last neutron in the emitter nuclide, and the ratio of neutron-and-gamma-emission from this level.

According to Fermi beta-decay theory, the probability of populating the level E, $J_e^{\pi e}$ from the state $J_i^{\pi i}$ (Figure 7.2) is given by:

$$\lambda\,(W_o) = \int_1^{W_o} C\,.\,/\,M_{if}\,/^2\,.\,F\,(Z_e,\,W)(W^2-1)^{\frac{1}{2}}.(W_o-W)^2.WdW \qquad (7.1)$$

with

$$W_o = \frac{Q_\beta - E}{m_e c^2} + 1 \qquad (7.2)$$

Since the matrix element M_{if} is, in general, a factor of ten smaller for first forbidden transitions than for allowed transitions, only the latter would be expected to give rise to appreciable delayed neutron activities. Considering only allowed transitions, the matrix element may be replaced by a constant, as it is known to be independent of energy.

Thus

$$\lambda\,(Wo) = k\,f\,(Z_e,\,W_o) \qquad (7.3.)$$

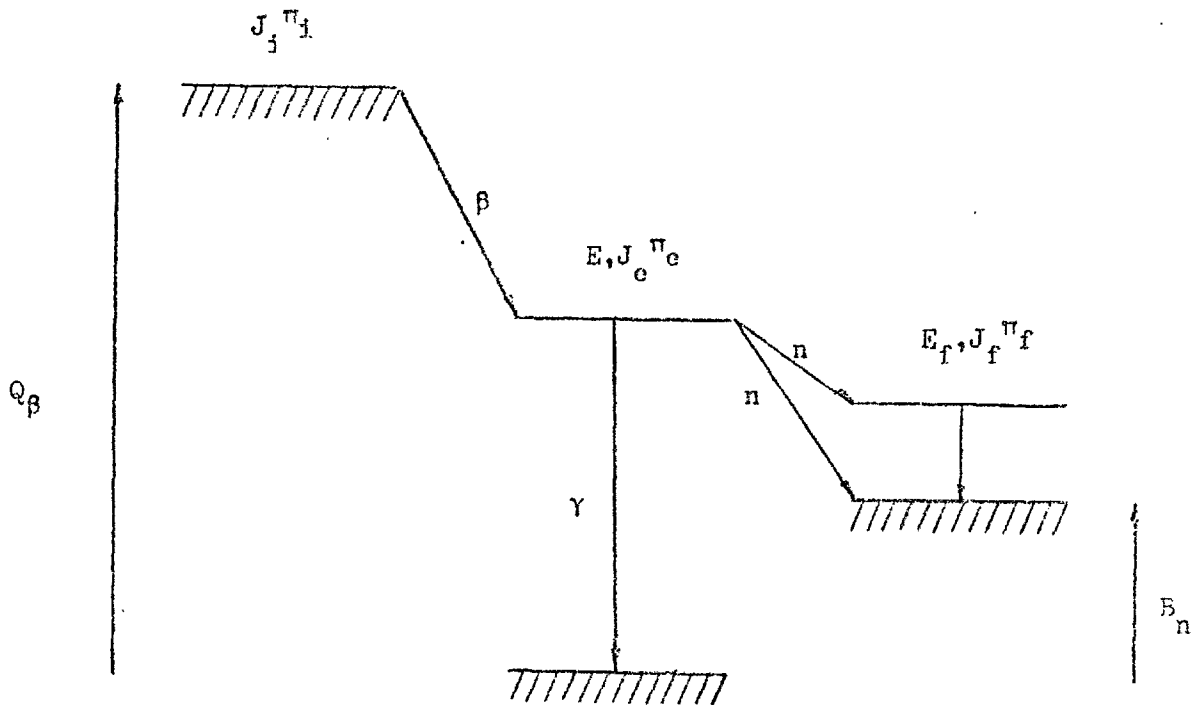

Figure 7.2

Delayed Neutron Decay Scheme

Where

$$f(Z_e, W_o) = \int_1^{W_o} (W^2-1)^{\frac{1}{2}} F(Z_e, W)(W_o-W)^2 . W . dW \qquad (7.4)$$

Selection rules require

$$\Delta J = 0, \pm 1 \; ; \; \Delta \pi = 0 \qquad (7.5)$$

In order to obtain the population probabilities of the states of the emitter, it is necessary to multiply the transition probability obtained above by the probability of finding a level of suitable spin and parity at the energy E, i.e. by the density of accessible states of the emitter nuclide.

The density of states of spin J_e at energy E is given by the Fermi gas model as:

$$\Omega (E, J_e) = w(E) \frac{2J_e + 1}{2(2\pi)^{\frac{1}{2}}\sigma^3} \exp\left(-\frac{(J_e + \frac{1}{2})^2}{2\sigma^2}\right) \qquad (7.6)$$

Where

$$w(E) = \frac{\pi^{\frac{1}{2}}}{12} \quad \frac{1}{a^{\frac{1}{4}} \; U^{\frac{5}{4}}} \quad \exp\left(2\sqrt{aV}\right) \qquad (7.7)$$

The energy U in equation (7.7) is an effective excitation energy, and is usually taken to be the actual excitation energy less the pairing energy, i.e. it is measured from the ground state of the corresponding odd-odd nuclide.

$$U = E - \delta \qquad (7.8)$$

Below this energy of the level density is often considered to be constant, in order to account for the increased level separation at low excitation energies [Keepin 1956].

The population probability of the level E, J_e is therefore:

$$P_\beta = \frac{\lambda\,(Q_\beta - E) \cdot \sum_{J_e} \Omega\,(E, J_e^{\pi e})}{\int_0^{Q_\beta} \lambda\,(Q_\beta - E) \sum_{J_e} \Omega\,(E, J_e^{\pi e})} \qquad (7.9)$$

The probability of de-excitation of the level E, $J_e^{\pi e}$ by neutron emission to a level E_f $J_f^{\pi f}$ is given by:

$$P_n\,(E_n, J_e^{\pi e} J_f^{\pi f}) = \frac{\sum_{jn} \Gamma_n^{jn}\,(E_n)}{\gamma + \sum_{J_f} \sum_{j_n} \Gamma_n^{jn}(E_n)} \qquad (7.10)$$

Where

$$\left|J_e - J_f\right| \leq j_n \leq J_e + J_f \qquad (7.11)$$

and

$$j_n = l_n \pm \tfrac{1}{2} \qquad (7.12)$$

The delayed neutron emission spectrum is therefore given by:

$$P(E_n) = \sum_{J_e} \sum_{J_f} \sum_{j_n} P_\beta\,(E, J_i^{\pi i}, J_e^{\pi e})\ \frac{\Gamma_n^{jn}\,(E_n)}{\gamma + \sum_{J_f} \sum_{j_n} \Gamma_n^{jn}(E_n)} \qquad (7.13)$$

and the delayed neutron emission probability by:

$$P_n^1 = \int_0^{Q_\beta - B_n} P\,(E_n)\ dE_n \qquad (7.14)$$

7.4. Estimation of Nuclear Parameters

7.4(1) Beta Decay and Neutron Binding Energies

It has been pointed out that delayed neutron precursors lie, in general, about three or more charge units from the line of nuclear stability. Very few measurements have been made on such nuclei, and it is therefore necessary to resort to the use of mass formulae to obtain estimates of these energies. These formulae do not give very good results for such nuclei, since they have been fitted to a large number of masses near the stability line. Systematics of delayed neutron precursors have been calculated on the basis of various mass formulae, notably by Keepin [Keepin 1956] and Pappas and Rudstam [Pappas 1960]. Since the estimates of beta decay energies and neutron binding energies may be in error by 0.5 MeV or more, these systematics are of dubious value, except in indicating areas for experimental verification.

7.4(2) Level Densities

The level density parameter a in the statistical model formula (7.7) is obtained by fitting data from slow neutron resonance measurements to the formula. The general trend is for the parameter a to increase linearly with A, but the curve of a versus A shows marked dips at the magic numbers (Figure 7.3). [Facchini 1968].

The spin cut-off parameter σ is given by [Facchini 1968]:

$$\sigma^2 = \langle m_j^2 \rangle gt \qquad (7.15)$$

where the expectation value of m_j^2 is taken over states around the Fermi level. An empirical expression for σ is given by Facchini and Saetta - Menichella [Facchini 1968].

$$\sigma^2 = 0.24\, A^{\frac{2}{3}}\, gt \qquad (7.16)$$

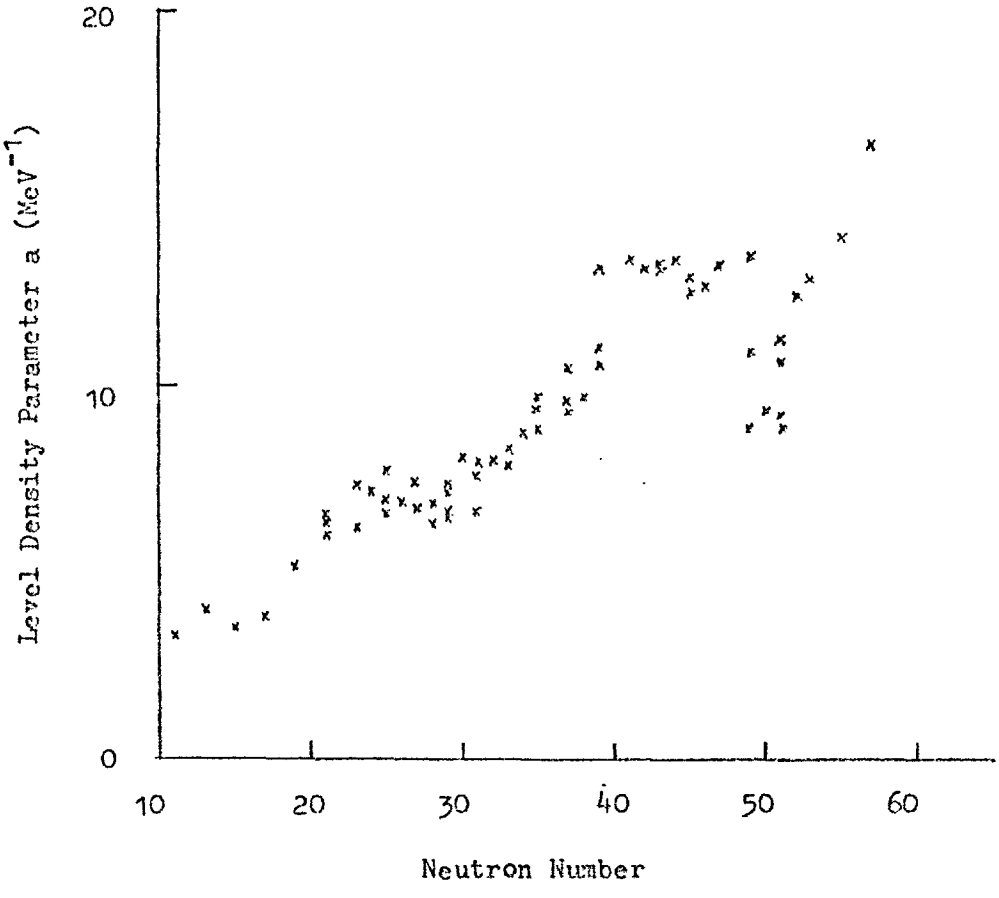

Figure 7.3

Variation of Level Density Parameter a with Neutron Number

7.4(3) Neutron Emission Widths

An expression for the neutron emission widths may be obtained from the statistical model of the nucleus. In terms of transmission coefficients, the widths Γ_n^{jn} are given by [Blatt 1952].

$$\Gamma_n^{jn} = T_n^{jn} \frac{D}{2\pi} \qquad (7.17)$$

where T_n^{jn} is the transmission coefficient for neutrons of angular momentum jn, and D is an energy which is expected to be of the order of the level spacing.

7.4(4) Radiation Widths

Radiation widths are small compared with neutron widths for $E_n > 100$ KeV, and vary only slowly with A [Blatt 1952].

Typical values of radiation widths lie in the range 0.1 to 30 eV [Blatt 1952].

7.5. Theoretical Predictions

The application of equations (7.13) and (7.14) to the prediction of delayed neutron spectra and emission probabilities is hindered by the fact that few of the nuclear parameters appearing in these equations are known to any great accuracy. Confirmation of theoretical predictions is also difficult, since measurements of delayed neutron emission probabilities are rare, and the only detailed measurement of delayed neutron spectra to date [Batchelor 1956] is of the group spectra, rather than the spectra of individual precursors.

Only in the cases of Br^{87}, which contributes probably 90% or more of the delayed neutron activity of group 1, and Br^{88} and I^{137} which together make up the greater part of group 2 is it possible to check the theoretical predictions against experiment.

A program PRESPEC was written to evaluate equations (7.13) and (7.14), and the predictions for Br^{87}, Br^{88} and I^{137} are shown in Figures 7.4-7.6, for various

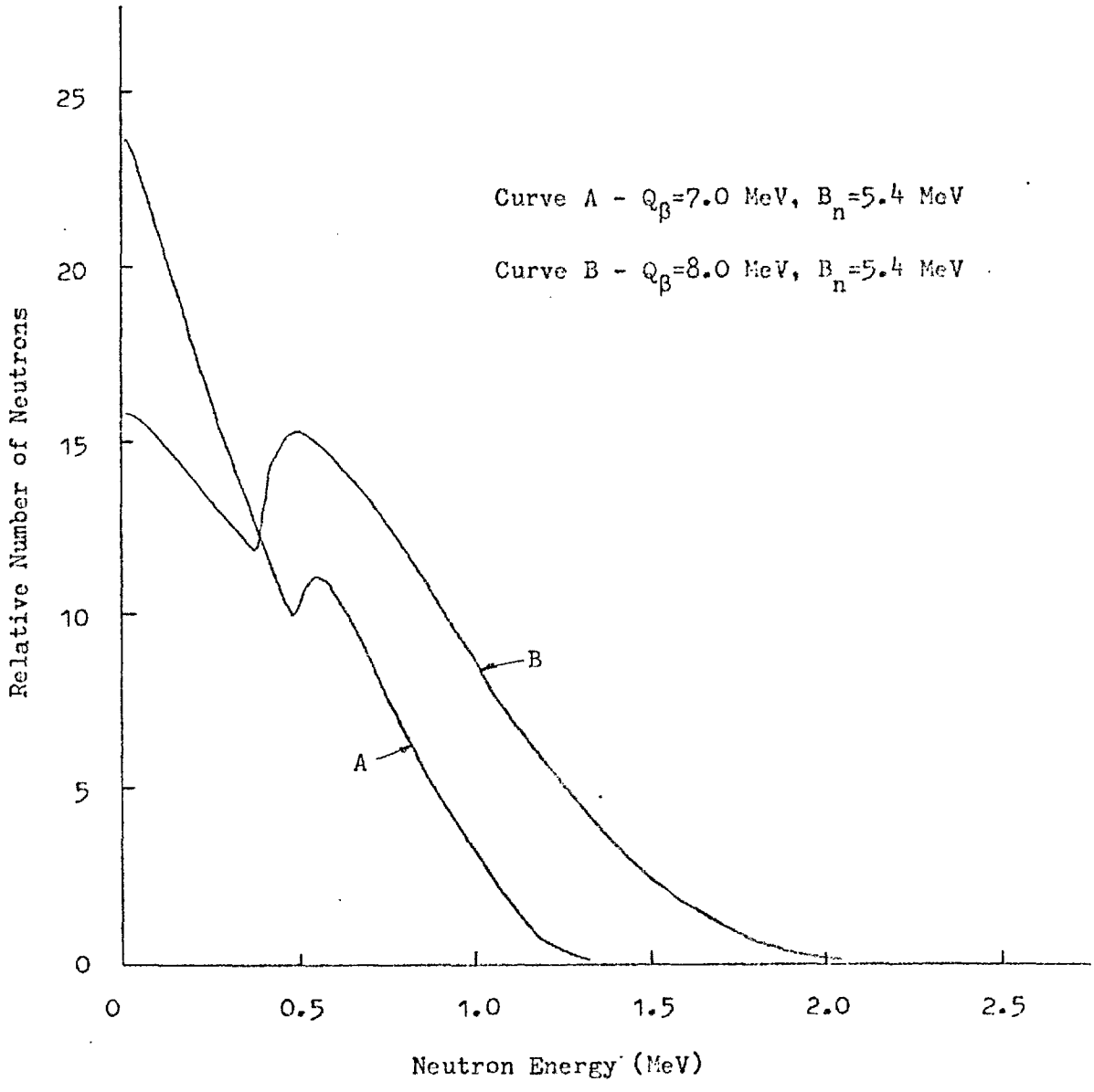

Figure 7.4

Bromine 87 Calculated Delayed Neutron Spectra

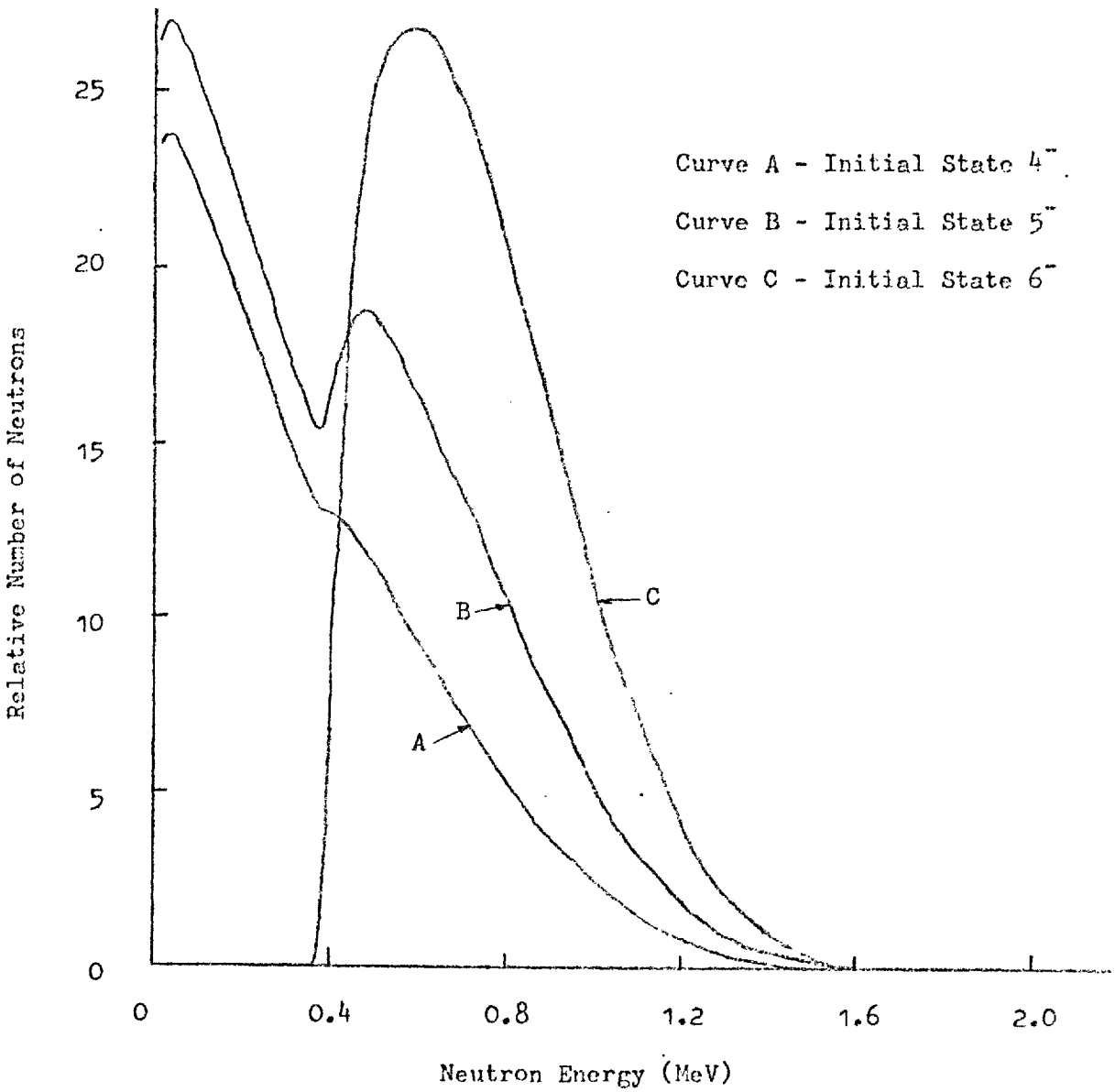

Figure 7.5

Bromine 88 Calculated Delayed Neutron Spectra

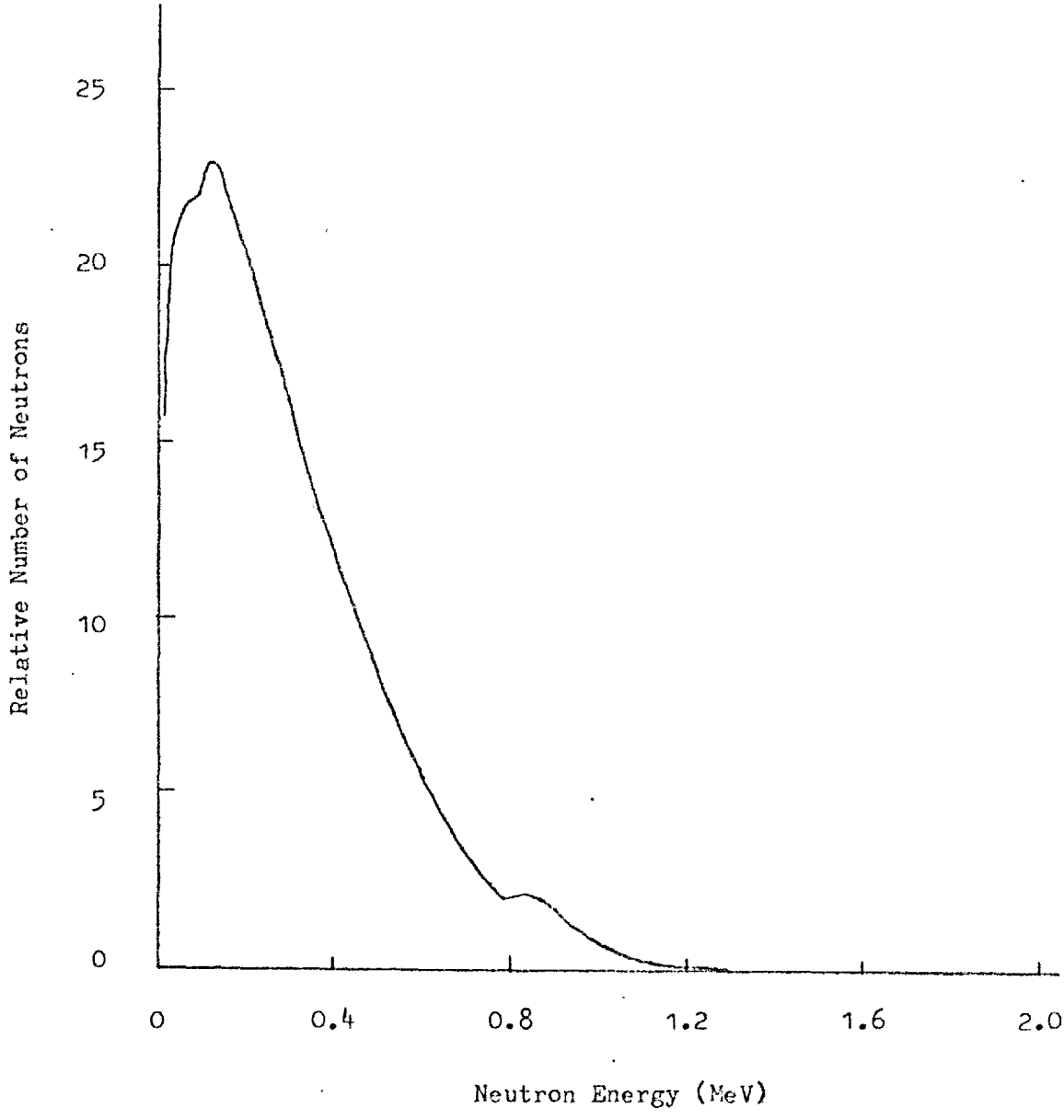

Figure 7.6

Iodine 137 Calculated Delayed Neutron Spectrum

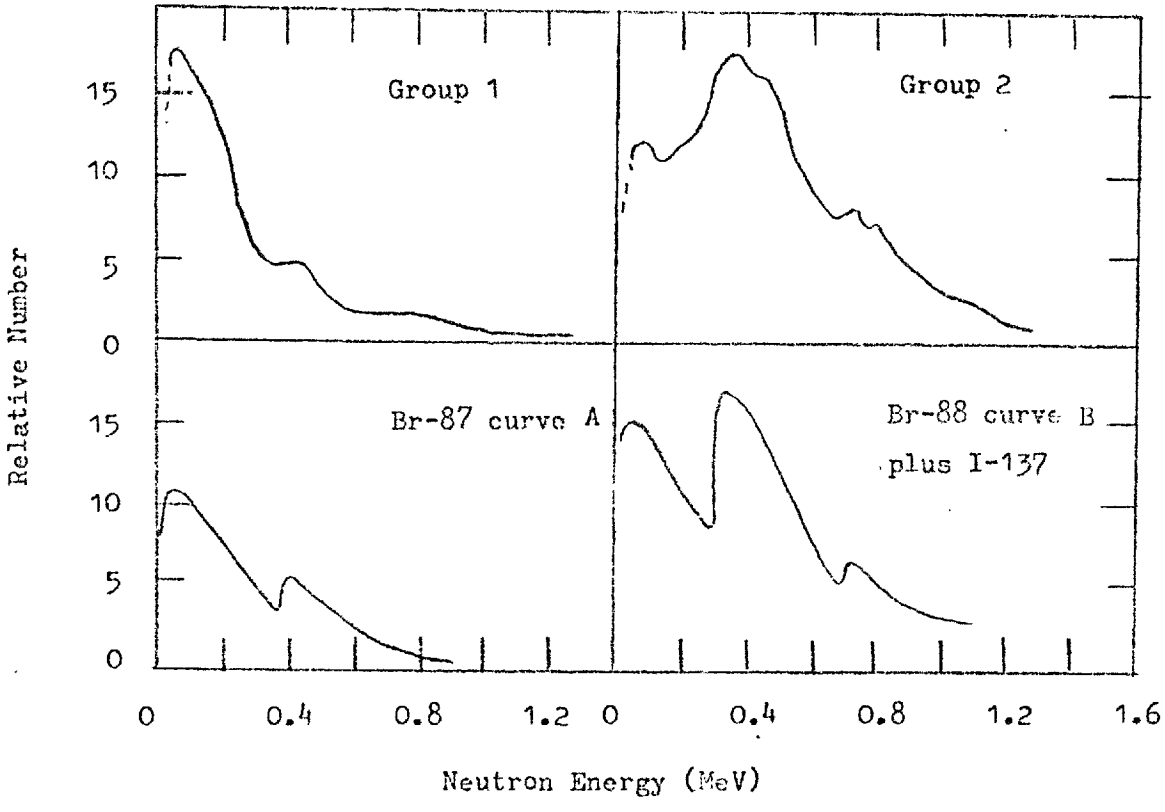

Figure 7.7

Batchelor & Hyder Spectra for Groups 1 & 2 Compared with Theoretical Predictions

estimates of the nuclear parameters involved. The experimental spectra for groups 1 and 2 [Batchelor 1956] are shown in Figure 7.7, and it can be seen that the general features of the observed spectra are correctly predicted.

The calculated values of delayed neutron emission probability are compared with experimental values in Table 7.1. Agreement with the observed values is poor, as would be expected considering the number of poorly-known parameters in equation (7.13).

NUCLIDE	P_n CALCULATED+ THIS WORK (%)	P_n CALCULATED* (%)	P_n MEASURED* (%)
Br-87	4.1	1.9 ± 1.4	2.5 ± 0.5
Br-88	2.0	3.5 ± 2.7	4.0 ± 1.0
I-137	1.7	2.2 ± 1.7	4.8 ± 1.3

Table 7.1

Comparison of Calculated and Experimental Delayed Neutron Emission Probabilities

* Taken from [Amiel 1969].

+ These values are based on the most likely assignment of nuclear parameters in the light of the predicted spectral shape. No attempt has been made to estimate the accuracy of these predictions.

7.6. Symbols

a	Level density parameter
B_n	Neutron binding energy of the emitter nuclide
c	Velocity of light
C	Constant incorporating the Fermi coupling constant
E	Excitation energy of the emitting level
E_n	Energy of emitted energy
F	Fermi function
J_e	Total angular momentum of the emitting state
J_i	Total angular momentum of the initial state
j_n	Total angular momentum of the emitted neutron
l_n	Orbital angular momentum of the emitted neutron
M_{if}	Matrix element in Fermi theory of beta decay
m_e	Rest mass of an electron
P	Population probability of level E, J_e
P_n	De-excitation probability
P'_n	Delayed neutron emission probability
$P(E_n)$	Probability of emission of a neutron of energy E_n
Q_β	Beta decay energy of precursor
U	Effective excitation energy
W	Energy of emitted electron in units of $m_e c^2$
W_o	Energy available for beta decay in units of $m_e c^2$
Z_e	Atomic number of emitter nuclide
∂	Pairing energy
π_e	Parity of emitting state
π_i	Parity of initial state

$\lambda(W_o)$	Probability of a beta transition of energy W_o
$W(E)$	Density of states
$\Omega(E,J_e)$	Density of states of angular momentum J_e
σ	Spin cut - off parameter
Γ_n^{in}	Width for emission of neutrons of angular momentum j_n
Γ_γ	Radiation width
g	Single particle level density
t	Nuclear temperature
T	Transmission coefficient
D	Energy of the order of the level spacing

7.7. References

Amiel 1969 - Amiel, S.
Delayed Neutrons in Fission
2nd I.A.E.A. Symposium on Pnysics and Chemistry of Fission. July 1969.

Batchelor 1956 - Batchelor, R; Hyder, H.R. McK.
J. Nuclear Energy, 3, 7 (1956).

Blatt 1952 - Blatt, J; Weisskopf, V.F.
Theoretical Nuclear Physics.
John Wiley 1952.

Bohr 1939 - Bohr, N; Wheeler, J.A.
The Mechanism of Nuclear Fission.
Phys. Rev., 56, 426 (1939).

Facchini 1968 - Facchini, U; Saetta-Menuchella, E.
Level Density Parameter Values from Neutron and Proton Resources.
Energia Nucleara, 15, 54 (1968).

Keepin 1956 - Keepin, G.R; Wimett, T.F; Zeigler, R.K.
J. Nuclear Energy, 6, 1 (1957).

Pappas 1960 - Pappas, A.C; Rudstam, G.
Nucl. Phys., 21, 353 (1960).

8. DISCUSSION

8.1. General

The absolute yields of delayed neutrons in fast fission were found to be higher (though in the case of U-235 not significantly so) than the values reported by Keepin [Keepin 1957]. This is in agreement with the bulk of recent measurements [Tomlinson 1971]. The yield of delayed neutrons from U-238 fission was found to be about 20% higher than that reported by Keepin, which is in agreement with theoretical predictions from observed sample worth discrepancies [Codd]. However, the observed shape of the delayed neutron decay differs substantially from that reported by Keepin.

8.2. Period-Reactivity Relationships

Period-reactivity relationships calculated for pure-isotope systems from the fitted decay parameters differ significantly from those given by Keepin [Keepin 1965]. The values obtained from the present measurements and those reported by Keepin are compared in Figure 8.1 for U-235 systems, and the hypothetical relationship for U-238 in Figure 8.2. In order to verify that the discrepancies were not due to faults in the least-squares fitting procedure, the relationship was also obtained by direct Laplace transform of the observed delayed neutron decay data [Keepin 1964]. This showed the discrepancy to be a real one.

The period reactivity relationships obtained indicate a discrepancy of up to 10% in reactivity for a given stable period, compared with Keepin's values. It is extremely difficult to estimate the error on the period-reactivity relationships calculated from the fitted a_i's and λ_i's since they are correlated but the error on the Laplace transform curve may be estimated from the statistical accuracy of the observed counts, since the relationship

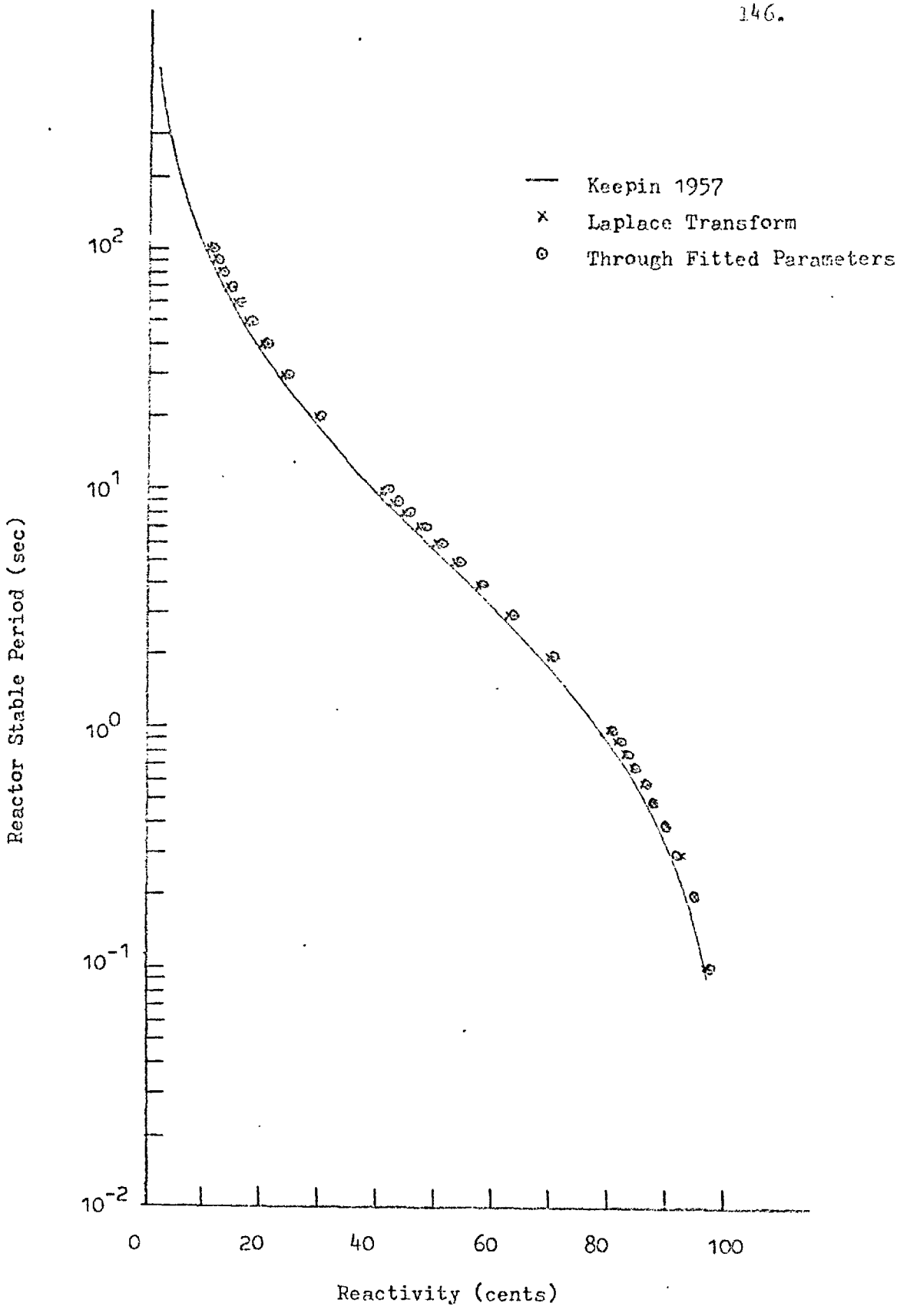

Figure 8.1

Period-Reactivity Relationship U-235

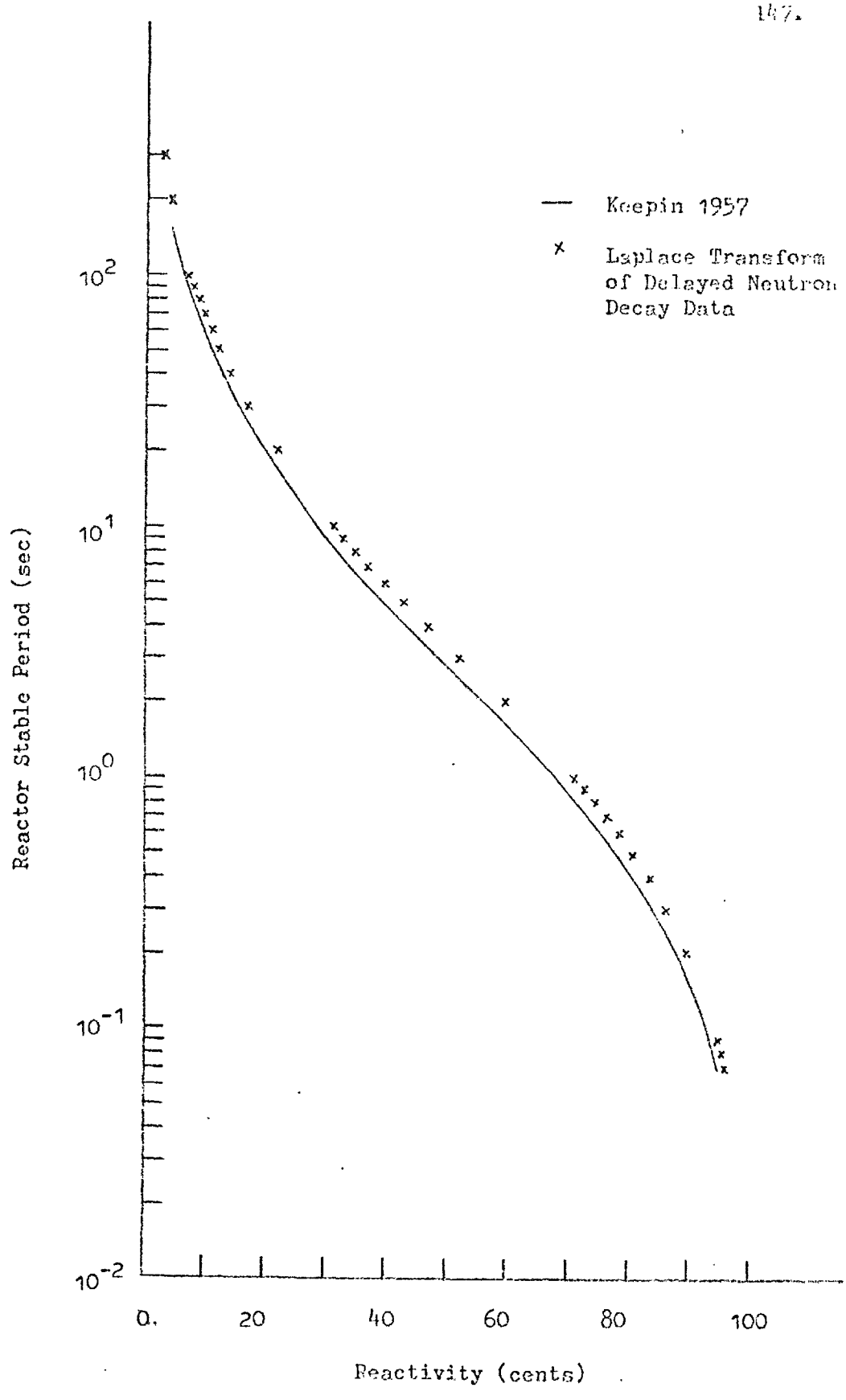

Figure 8.2

Period-Reactivity Relationship U-238

is merely a numerical integration of these values. As the integration tends to smooth the statistical variation on the individual channels, the accuracy of the Laplace transform - derived relationship should be better than the errors assigned to individual channels. Typically, the statistical accuracy of the individual counts was about 3%, so the disagreement between Keepin's curve and the one derived from the present work is certainly a significant one.

It seems highly unlikely that such a large discrepancy could have gone unnoticed, but in order to assess sample worth measurements in the light of these results it will be necessary to survey not only the observed worths, but also the methods by which reactivity scales were established for these measurements.

8.3. Group Structure

The five-group fitted periods and relative abundances obtained give a good representation of the observed shape of the delayed neutron decay (see X^2 values, Tables 6.3). However, adequate information for a detailed analysis into groups associated with identifiable precursors has not yet been obtained. In particular, the periods observed for the third and fourth delayed neutron groups (Tables 6.3) are in poor agreement, indicating that these groups contain contributions from more than one main precursor.

8.4. Future Work

The absolute yields of delayed neutrons in the fast fission of U-235 and U-238 have been measured to an accuracy which is unlikely to be improved significantly with current techniques. More work, however, is necessary to obtain detailed information on the group structure of the delayed neutron

emission, and to clarify the anomalous period-reactivity relationships predicted by the present work. It is also of importance to survey the methods of determining reactivity scales in current use together with the sample worth measurements reported by Codd.[Codd].

8.5. References

Codd - Codd, J.
A.E.E. Winfrith. Unpublished.

Keepin 1957 - Keepin, G.R.; Wimett, T.F.; Zeigler, R.K.
J. Nuclear Energy 6 1 1957.

Keepin 1965 - Keepin, G.R.
Physics of Nuclear Kinetics.
Addison Wesley 1965.

Tomlinson 1971 - Tomlinson, L.
A.E.R.E. Harwell. Unpublished.